Appendix of the Doctoral Thesis

This appendix consists of following publications which are presented as part of the doctoral thesis:

Kubínová Z, Janáček J, Lhotáková Z, Kubínová L, Albrechtová J. 2014. Unbiased estimation of chloroplast number in mesophyll cells: advantage of a genuine three-dimensional approach. *Journal of Experimental Botany* 65, 609–620.

Kubínová Z, Janáček J, Lhotáková Z, Šprtová M, Kubínová L, Albrechtová J. 2018. Norway spruce needle size and cross section shape variability induced by irradiance on a macro- and microscale and CO_2 concentration. *Trees* 32(1), 231–244.

Kubínová Z, Glanc N, Radochová B, Lhotáková Z, Janáček J, Kubínová L, Albrechtová J. 2019. Unbiased estimation of Norway spruce (*Picea abies* L. Karst.) chloroplast structure: Heterogeneity within needle mesophyll under different irradiance and [CO_2]. *Image Analysis & Stereology* 38(1), 83–94.

Kubínová L, Radochová B, Lhotáková Z, Kubínová Z, Albrechtová J. 2017. Stereology, an unbiased methodological approach to study plant anatomy and cytology: past, present and future. *Image Analysis & Stereology* 36(3), 187–205.

Journal of Experimental Botany, Vol. 65, No. 2, pp. 609–620, 2014
doi:10.1093/jxb/ert407 Advance Access publication 11 December, 2013
This paper is available online free of all access charges (see http://jxb.oxfordjournals.org/open_access.html for further details)

Journal of Experimental Botany
www.jxb.oxfordjournals.org

RESEARCH PAPER

Unbiased estimation of chloroplast number in mesophyll cells: advantage of a genuine three-dimensional approach

Zuzana Kubínová[1]*, Jiří Janáček[2], Zuzana Lhotáková[1], Lucie Kubínová[2] and Jana Albrechtová[1]

[1] Charles University in Prague, Faculty of Science, Department of Experimental Plant Biology, Viničná 5, 128 44 Prague 2, Czech Republic
[2] Institute of Physiology, Academy of Sciences of the Czech Republic, v.v.i., Vídeňská 1083, 142 20 Prague 4, Czech Republic

* To whom correspondence should be addressed. E-mail: kubinova@natur.cuni.cz

Received 31 July 2013; Revised 6 November 2013; Accepted 8 November 2013

Abstract

Chloroplast number per cell is a frequently examined quantitative anatomical parameter, often estimated by counting chloroplast profiles in two-dimensional (2D) sections of mesophyll cells. However, a mesophyll cell is a three-dimensional (3D) structure and this has to be taken into account when quantifying its internal structure. We compared 2D and 3D approaches to chloroplast counting from different points of view: (i) in practical measurements of mesophyll cells of Norway spruce needles, (ii) in a 3D model of a mesophyll cell with chloroplasts, and (iii) using a theoretical analysis. We applied, for the first time, the stereological method of an optical disector based on counting chloroplasts in stacks of spruce needle optical cross-sections acquired by confocal laser-scanning microscopy. This estimate was compared with counting chloroplast profiles in 2D sections from the same stacks of sections. Comparing practical measurements of mesophyll cells, calculations performed in a 3D model of a cell with chloroplasts as well as a theoretical analysis showed that the 2D approach yielded biased results, while the underestimation could be up to 10-fold. We proved that the frequently used method for counting chloroplasts in a mesophyll cell by counting their profiles in 2D sections did not give correct results. We concluded that the present disector method can be efficiently used for unbiased estimation of chloroplast number per mesophyll cell. This should be the method of choice, especially in coniferous needles and leaves with mesophyll cells with lignified cell walls where maceration methods are difficult or impossible to use.

Keywords: Chloroplast counting, confocal microscopy, disector method, mesophyll, coniferous needle structure, Norway spruce (*Picea abies* L. Karst.), profile counting, stereology.

Introduction

Chloroplasts are important organelles of plant photosynthesizing cells as loci where the photosynthetic processes take place. In mesophyll cells, chloroplasts are usually located next to the cytoplasmic membrane adjacent to intercellular spaces to decrease the resistance to CO_2 diffusion (Terashima *et al.*, 2011). The chloroplast number per cell represents a frequently examined quantitative anatomical parameter, reflecting various leaf internal and external conditions. It can be influenced by internal factors, such as ploidy (Mochizuki and Sueoka, 1955) and environmental factors, e.g. CO_2 concentration (Wang *et al.*, 2004; Teng *et al.*, 2006). Well-established methods for estimation of the chloroplast number per cell previously used in two-dimensional (2D) space are based on: (i) counting chloroplasts in stomatal guard cells in epidermal peels, (ii) determining the number of chloroplasts in flattened mesophyll cells after maceration, and (iii) counting profiles of chloroplasts in leaf sections.

Abbreviations: 2D, two-dimensional; 3D, three-dimensional; SUR, systematic uniform random.

Chloroplast counting in guard cells of epidermal peels using a light microscope is not problematic, enabling counting of chloroplasts contained in one cell in one focal plane; this has been applied to various plants, e. g. *Beta vulgaris* L. (Mochizuki and Sueoka, 1955), *Solanum tuberosum* L. (Frandsen, 1968), and *Citrullus lanatus* (Thunb.) Matsum. and Nakai. (Sari *et al.*, 1999).

One of the most frequently used methods for estimation of chloroplast number per mesophyll cell in herbaceous plants in 2D is counting chloroplasts in separated mesophyll cells obtained by maceration procedures, as described by Possingham and Saurer (1969). Fixation and maceration of *Spinacia oleracea* L. leaves enabled the separation of mesophyll cells, which were then flattened into a single plane of focus, allowing the chloroplasts to be viewed in a single layer and thus to be easily counted under phase contrast in an optical microscope with an eyepiece graticule. Methods based on these principles were then improved (Possingham and Smith, 1972), and modified protocols have been widely used, e.g. for *Triticum aestivum* L. (Boffey *et al.*, 1979), *Spinacia oleracea* L. (Chaly *et al.*, 1980), *Pisum sativum* L. (Lamppa *et al.*, 1980), *Medicago sativa* L. (Molin *et al.*, 1982), *B. vulgaris* L. (Tymms *et al.*, 1983), and *Chenopodium album* L. (Yamasaki *et al.*, 1996). The maceration process was further adapted and applied to *Arabidopsis thaliana* L. and counting was accomplished after chloroplast thresholding using an image analysis program (Pyke and Leech, 1991; Marrison *et al.*, 1999; Stettler *et al.*, 2009). Sung and Chen (1989) extracted chloroplasts from macerated leaves of *Glycine max* L. Merrill and counted chloroplasts per leaf using a haemocytometer—a special microscope slide with an engraved graticule. To our knowledge, a method for chloroplast counting using maceration has not yet been applied to leaves with thick, lignified cell walls, such as coniferous needles.

Another method frequently used for the estimation of chloroplast number per mesophyll cell in 2D is based on counting chloroplast profiles in semi-thin (1–4 μm thick) physical sections of a leaf using transmission electron and light microscopy (Boffey *et al.*, 1979; Zechmann *et al.*, 2003; Wang *et al.*, 2004; Jin *et al.*, 2011; Simon *et al.*, 2013). This method is frequently used, but its practical application including sampling design is often insufficiently described (Sam *et al.*, 2003; Hayashida *et al.*, 2005; Teng *et al.*, 2006; Gopi *et al.*, 2008). Moreover, in many recent studies, the chloroplast and/or cell profiles in 2D were counted to get an estimation of chloroplast number in 3D, which is a theoretically incorrect approach. For example, the number of chloroplasts per unit of leaf area was estimated from the number of chloroplast profiles in a 0.8 μm thick section observed by light microscopy (Miyazawa and Terashima, 2001; Oguchi *et al.*, 2005) and the number of mesophyll cells per leaf area was determined from the number of cell profiles in 5 μm thick sections (Adachi *et al.*, 2013).

Some further methods have involved analysis of several optical sections from the same specimen, enabling the counting of chloroplasts in 3D directly—either during focusing through the whole thick physical section by a light microscope (e.g. for *T. aestivum* L. and *Triticum monococcum* L.; Ellis and Leech, 1985), focusing through protoplasts in a cell suspension of *Marchantia polymorpha* L. (Bockers *et al.*, 1997), or in a 3D reconstruction created from images of series of optical sections acquired by confocal microscopy. The latter approach was used for determining the chloroplast number per stomatal guard cell in leaves of potato *S. tuberosum* L. (Mozafari *et al.*, 1997), *A. thaliana* L. (Dinkins *et al.*, 2001), *Eucalyptus saligna* Sm. (Xu *et al.*, 2012), and *Glycine dolichocarpa* Tateishi and H. Ohashi (Coate *et al.*, 2012). Chloroplasts in mesophyll cells of *Oryza sativa* L. were counted after comparing photographs from three planes of focus located inside one cell (Hassan and Wazuddin, 2000).

The importance of using a proper method for counting/sampling chloroplasts is obvious, because incorrect approaches can lead to serious bias in the chloroplast number estimation. However, in many studies, the sampling method is not well specified. In general, it is important to note that an unbiased method for sampling/counting particles must sample any of the particles with the same probability (Sterio, 1984). It should be stressed that profiles of particles in a 2D section of a specimen do not represent an unbiased sample of the particles, as the larger particles are sampled (i.e. sectioned) with a higher probability. Moreover, it is known that anatomical parameters often exhibit gradients along the leaf blade (e.g. Pazourek, 1966; Possingham and Saurer, 1969). Thus, a proper design of sampling leaf segments for an analysis is crucial to obtain unbiased results.

For an unbiased estimation of the number of particles in 3D with no assumption about particle shape and size, the optical disector method based on 3D unbiased sampling probe was developed (Sterio, 1984; Gundersen, 1986). This method enables particles of varying shape, such as chloroplasts in a cell and cells within a tissue, to be sampled interactively and counted in an unbiased way. This method has already been used successfully for estimation of mesophyll cell number (Albrechtová and Kubínová, 1991; Kubínová, 1991, 1993, 1994; Kubínová *et al.*, 2002; Albrechtová *et al.* 2007), but to our knowledge it has never been used for chloroplast number estimation.

We hypothesised that the number of chloroplast profiles counted in cell sections in 2D would be different from the number of chloroplasts counted by an unbiased method in 3D. To verify our hypothesis, we compared 2D and 3D approaches to chloroplast counting (i) in practical measurements of mesophyll cells of Norway spruce needles, (ii) in a 3D model of a mesophyll cell with chloroplasts, and (iii) by a theoretical analysis.

Materials and methods

Norway spruce (*Picea abies* L. Karst.) current-year needles were collected from crowns of 18-year-old trees planted on an experimental site of the Global Change Research Centre, Academy of Sciences, Czech Republic, the Bílý Kříž in Moravskoslezské Beskydy mountains, in 2004 (Urban *et al.*, 2001). Spruce needles were collected from south- and south-west-facing branches from the middle crown part and were stored in a deep freeze until processing (Lhotáková *et al.*, 2008). The images were captured during 2009 and analysed during 2009–2012.

Sampling of 0.2 mm thick needle cross-sections cut off using a hand microtome and placed into a drop of water was done in a systematic uniform random (SUR) way at intervals of 3 mm (Fig. 1).

The images of the spruce needle cross-sections were captured using a Leica SP2 AOBS confocal laser-scanning microscope (Leica Microsystems, Wetzlar, Germany) with Ar laser excitation of 488 nm; phenolics autofluorescence was detected in the green channel (494–577 nm) and autofluorescence of chlorophyll in chloroplasts was detected in the red channel (625–710 nm) (Fig. 2A). The acquired images were analysed using Ellipse software (ViDiTo, Košice, Slovakia, http://www.ellipse.sk/, last accessed 21 November 2013), which offers special modules for stereological measurements.

The Ellipse Disector module (Tomori *et al.*, 2001) enables application of a virtual 3D probe to the stack of serial optical sections. It is possible to browse through the successive optical sections and to mark the selected particles (Figs. 3B–D). The optical disector probe (Sterio, 1984, Gundersen, 1986) represents a virtual 3D block with three exclusion planes (Fig. 3A). The bottom look-up plane belongs to exclusion planes together with two side planes. The reference plane on the top does not belong to the exclusion planes. Particles lying within this block or intersecting its planes, except the exclusion ones, are counted (Fig. 3). The particles are sampled without bias if each particle has the same probability of being sampled, i.e. if the 3D space is filled in by the spatial mosaic of the shifted copies of the disector probe and each particle in the space is sampled by one and only one shifted copy of the 3D sampling probe (Fig. 4).

At first, the image of an entire cross-section was captured using a dry plan apochromatic 10× objective [numeric aperture (NA) 0.4] with resolution 1024 × 1024 pixels (1500 × 1500 µm). From these images, the areas of needle cross-sections and the proportions of mesophyll were estimated by the point counting method (Weibel, 1979) using the Ellipse Point Grid software module (Fig. 2E). The spruce needle volume was estimated by Cavalieri principle (Gundersen and Jensen, 1987): the mean of the areas of cross-sections was multiplied by the length of the needle.

For mesophyll cell counting, 30 µm thick stacks comprising 16 serial optical sections 2 µm apart were acquired by using a plan apochromatic 20× water-immersion objective (NA 0.7) with resolution 2048 × 2048 pixels (750 × 750 µm) (Fig. 2F, Supplementary Videos S1 and S2, at *JXB* online). Several stacks were acquired in each cross-section to cover its whole area; altogether, 157 stacks were acquired. The height of the disector probe was 10 µm, placed in the middle of captured stacks, i.e. within a substack of six optical sections 2 µm apart, the size of the sampling frame was adjusted to cover the whole cross-section area. A double disector (Gundersen, 1986) was used: the probe was used in both directions, i.e. at first, cells were counted by the disector with the reference plane and look-up planes in the positions shown in Fig. 3A, and then additional cells were counted by the disector with the reference plane set to the position of the former look-up plane and vice versa. Thus, the total height of the probe was twice its real height (20 µm, in this case). The needle volume in the stack was determined by multiplying the height of the double disector and the needle area estimated from the cross-section captured by a 10× objective. The mesophyll cell density (number of cells per needle volume) was estimated by the formula (Sterio, 1984; Gundersen, 1986):

$$estN_{Vneedle}(cell) = \frac{\sum_{i=1}^{n} Q_i^-(cell)}{\sum_{i=1}^{n} P_i} \cdot \frac{p}{a \cdot h}$$

where $estN_{Vneedle}(cell)$ is the estimated number of mesophyll cells per needle volume, $Q_i^-(cell)$ is the sum of all sampled cells in all disector probes within a needle, $\sum P_i$ is the sum of all points falling within a needle in all disector probes (for calculation needle volume in each probe) used for cell counting, p is the number of test points in a grid in a sampling frame used for cell counting, a is the area of the disector sampling frame (the base plane of the 3D probe) used for cell counting, and h is the height of the disector probe used for cell counting

For chloroplast counting, the positions of captured stacks were selected by random application of rectangle grid in the Rectangles module of the Ellipse software (ViDiTo, Košice, SR) (Fig. 2C) on the images captured by a 10× objective, while the size of the rectangles was set equal to the size of the field of view and the distance between the rectangles was set to capture on average 24 stacks of optical sections per spruce needle. In each position, 20 µm thick stacks comprising 41 serial optical sections 0.5 µm apart were acquired using a plan apochromatic 63× water-immersion objective (NA 1.2) with zoom 2× and resolution 512 × 512 pixels (119 × 119 µm) (Fig. 2D). Altogether, 464 stacks were acquired and used for counting chloroplasts by applying the disector method.

The dimensions of the disector sampling frame for chloroplast counting in the middle of the stack were set to 500 × 500 pixels (116 × 116 µm) and the height of the probe was 5.5 µm, as there were 12 optical sections included, 0.5 µm apart. To estimate the volume of the spruce needle within each disector probe, the needle area in the middle image of the stack was determined by the point-grid method and multiplied by the disector height. The chloroplast density (number of chloroplasts per needle volume) was estimated by the formula (Sterio, 1984; Gundersen, 1986):

$$estN_{Vneedle}(chl) = \frac{\sum_{i=1}^{n} Q_i^-(chl)}{\sum_{i=1}^{n} P_i'} \cdot \frac{p'}{a' \cdot h'}$$

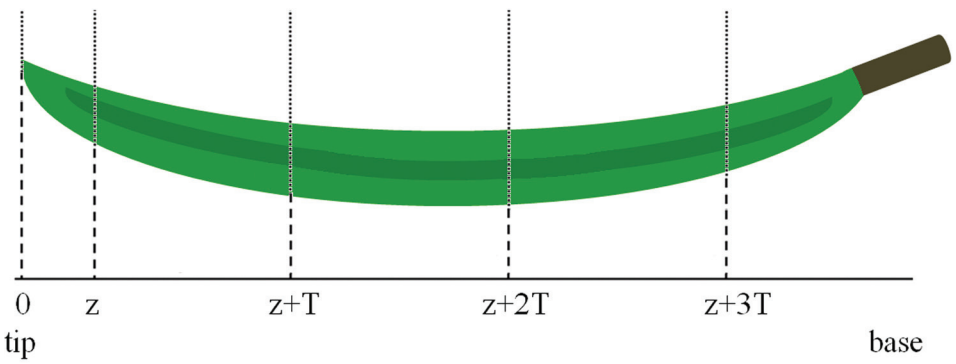

Fig. 1. Systematic uniform random (SUR) sampling of positions of cross-sections along the needle. 0, tip; z, position of the first cross-section: a random integer from an interval 0–5 was chosen using a table of random numbers; this number determined the position of the first cross-section (z) in the needle (0 corresponded to 0.5 mm from the tip and 1 corresponded to 1 mm, up to 5, which corresponded to 3 mm from the tip), T=3 mm (the interval between subsequent cross-sections). (This figure is available in colour at *JXBV* online.)

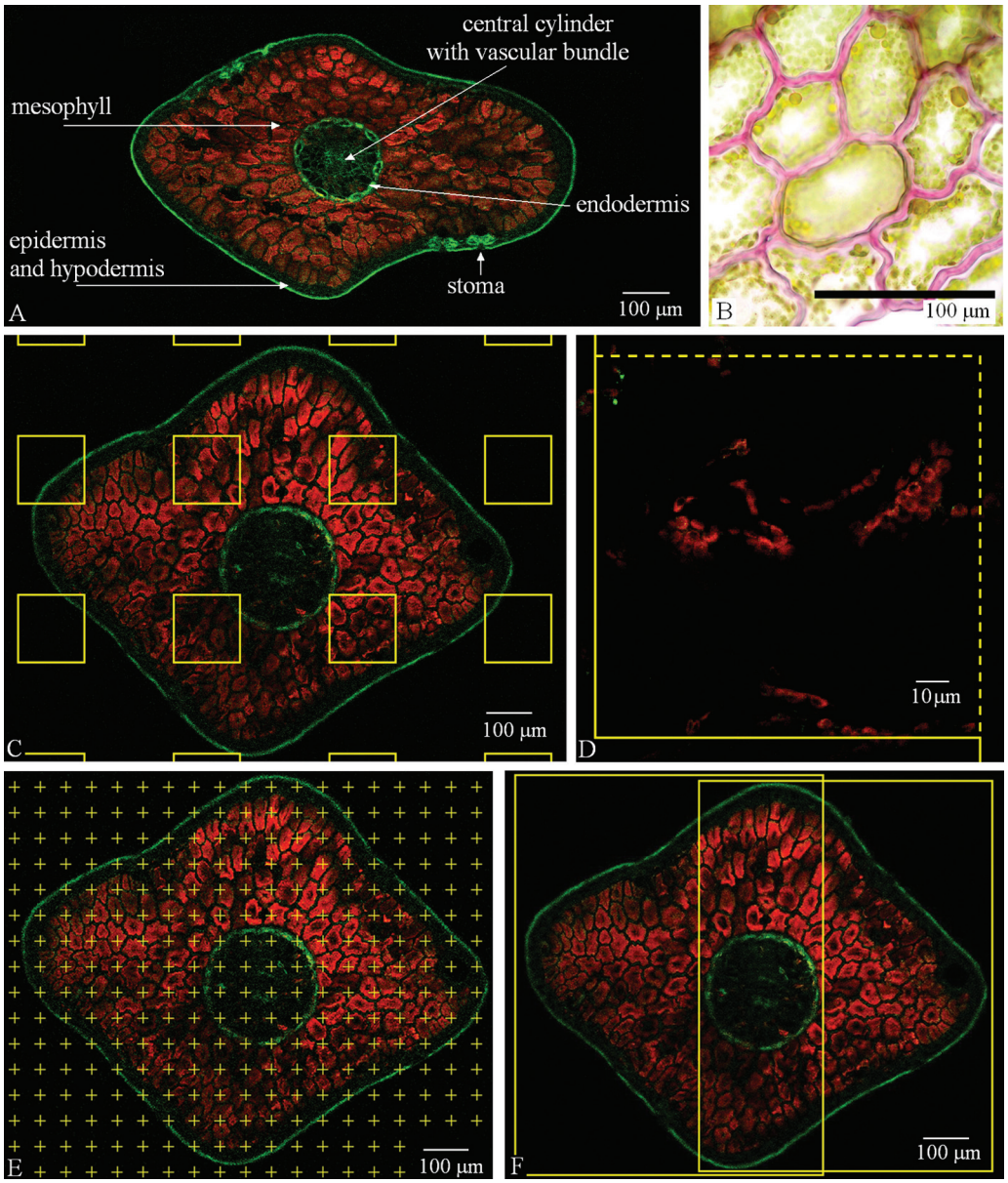

Fig. 2. Norway spruce needle cross-section: image acquisition, sampling, and processing. (A) Anatomical structure of a Norway spruce needle in a cross-section. Autofluorescence of chlorophyll in chloroplasts was detected in the red channel and autofluorescence of phenolics was detected in the green channel. (B) Histochemical lignin detection in cell walls (pink) of mesophyll cells using a phloroglucinol/HCl test (O'Brian and McCully, 1981). (C) Sampling frames were superimposed on a needle transverse section using the Rectangles module in Ellipse software. (D) Stacks of optical sections were acquired at the positions of rectangles in (C) with higher resolution. (E) Estimation of needle cross-sectional area by a point counting method using the Point Grid module in Ellipse software (F) Two frames showing the subsequent acquisition of series for counting mesophyll cells. (A, C–F), confocal microscopy: (B) bright-field light microscopy.

where $estN_{Vneedle}(chl)$ is the estimated number of chloroplasts per needle volume, $Q_i^-(chl)$ is the sum of all sampled chloroplasts in all disector probes within a needle, $\Sigma P'_i$ is the sum of all points falling within a needle in all 3D probes (for calculation of needle volume in each probe) used for chloroplast counting, p' is the number of test points in a grid in a sampling frame used for chloroplast counting, a' is the area of the disector sampling frame (the base plane of the 3D probe) used for chloroplast counting, and h' is the height of the disector probe used for chloroplast counting.

The estimated number of chloroplasts per mesophyll cell was calculated by the ratio of the chloroplast number and the mesophyll cell number per needle volume:

$$estN_{Ncell}(chl) = \frac{estN_{Vneedle}(chl)}{estN_{Vneedle}(cell)}$$

where $estN_{Ncell}(chl)$ is the estimated number of chloroplasts per mesophyll cell, $estN_{Vneedle}(cell)$ is the estimated number of mesophyll cells per needle volume, and $estN_{Vneedle}(chl)$ is the estimated number of chloroplasts per needle volume.

The profiles of chloroplasts and cells in 2D images were counted in the same stacks as those used for 3D measurements in the middle optical sections using the 2D unbiased sampling frame (Gundersen, 1977) (Fig. 2D). The number of chloroplasts per cell was calculated

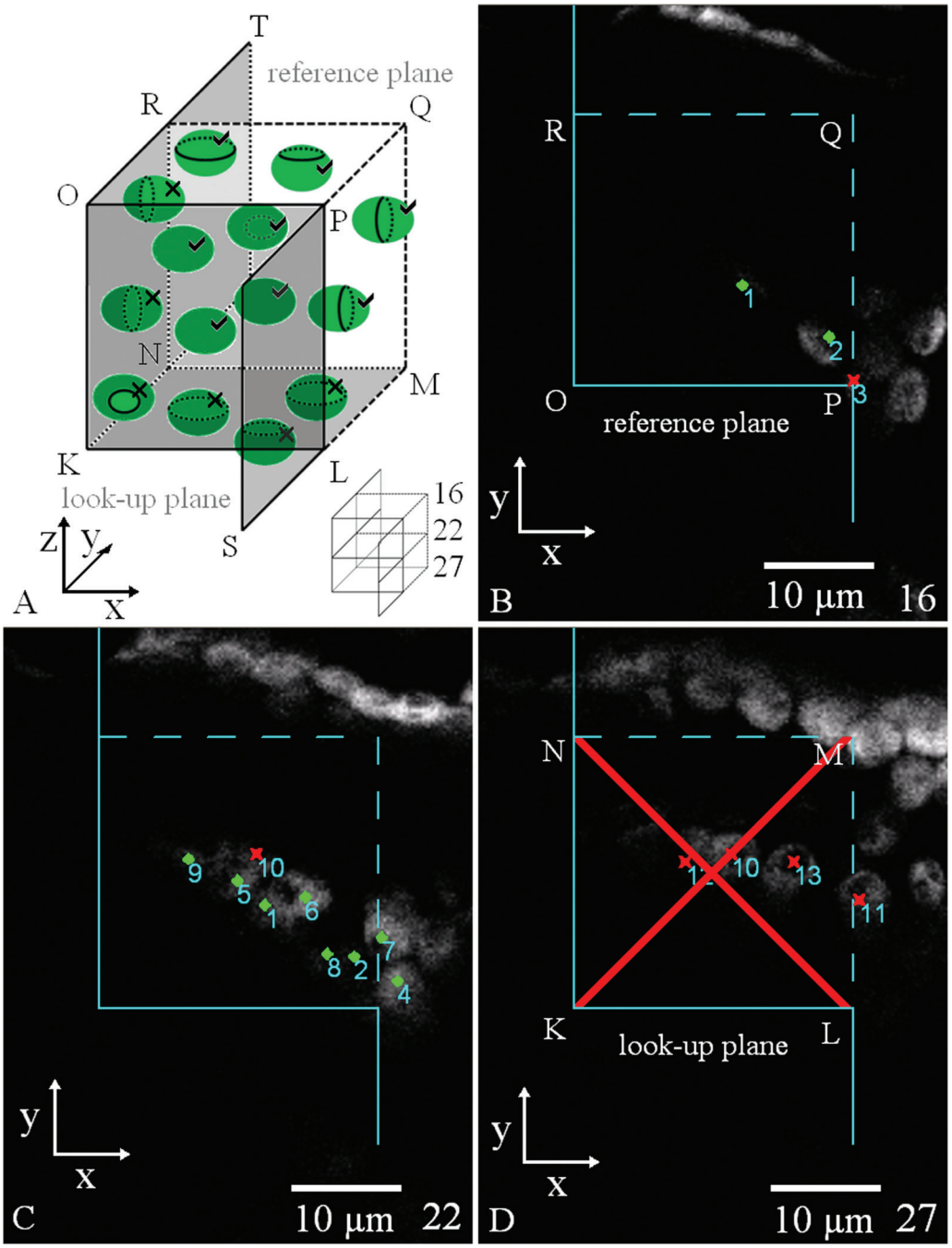

Fig. 3. Chloroplast counting using the virtual 3D disector probe. (A) Scheme of the disector probe with chloroplasts. The disector probe is a 3D block. Chloroplasts lying within this block or intersecting its planes are counted, except those intersecting the exclusion planes. The exclusion planes in this scheme are represented by the dark planes and the transparent front plane (all bordered by a full line): the bottom KLMN (so-called look-up plane), KNRO, KLPO, and half-planes PLS and RNT. The top rectangle OPQR is called the reference plane and does not belong to the exclusion planes. Chloroplasts that lie fully inside the probe are always counted. In this scheme, eight chloroplasts are counted (ticked) and six chloroplasts are not counted (crossed). (B–D) Three optical sections of the stack of real serial optical sections acquired by confocal microscopy. Within section numbers 16–27, the disector probe was placed using the Disector module in the Ellipse software, section 16 being the reference plane of the probe (B), section 22 inside the disector probe (C), and section 27 the look-up plane of the disector probe (D). Counted particles are those within the probe not intersecting the exclusion planes: point, counted particle; cross, particle is not counted. In this example, eight chloroplasts were counted (chloroplasts numbers 3 and 10–13 are intersecting the exclusion planes). (This figure is available in colour at *JXB* online.)

as the ratio of the chloroplast profile number per needle area to the cell profile number per needle area, while the needle area was estimated previously by the point counting method (Weibel, 1979).

In order to obtain comparable results by 2D and 3D methods, we calculated the chloroplast number per cell in each needle cross-section (68 in total) by both methods. In the 3D method, we summed

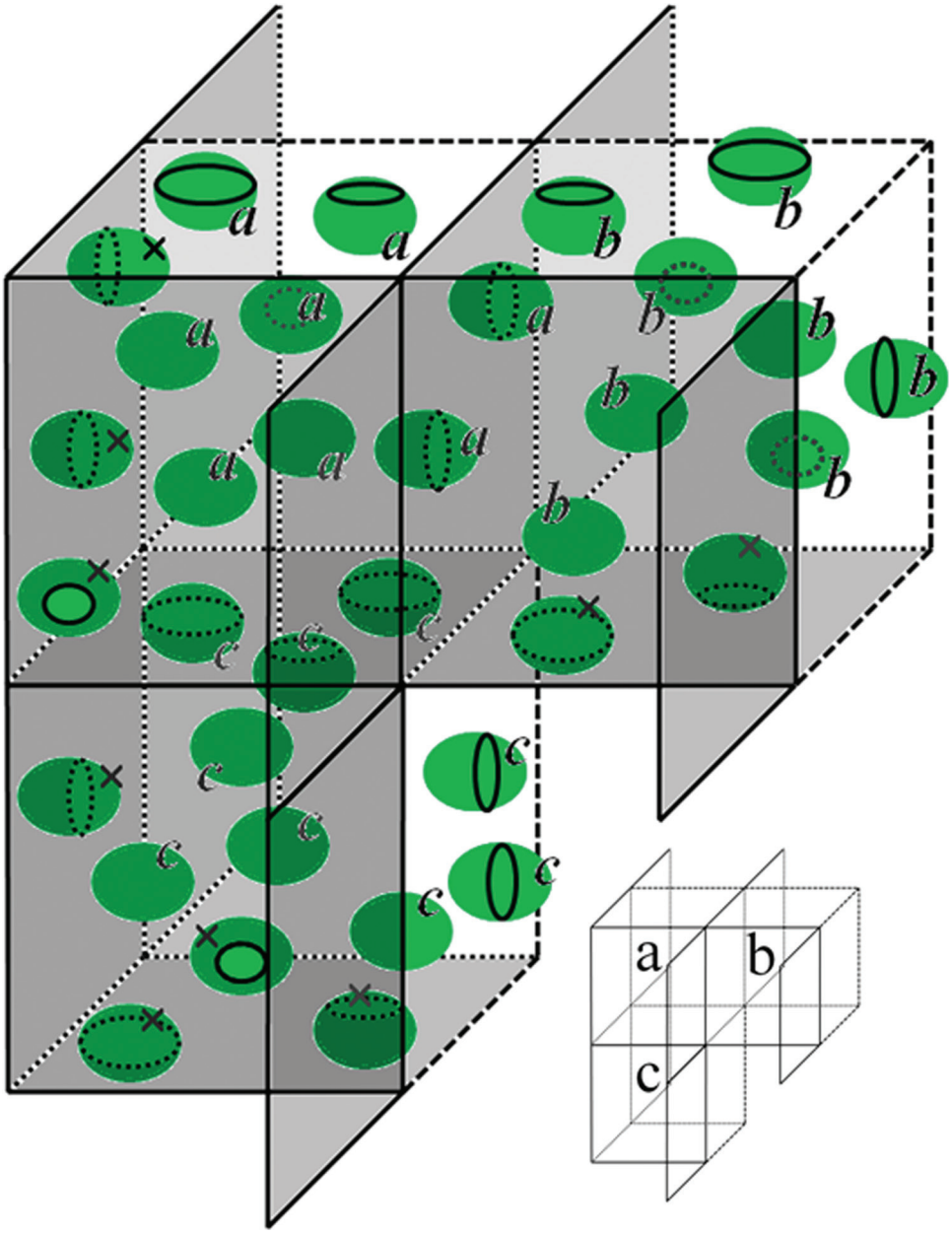

Fig. 4. Scheme of the hypothetic spatial mosaic of 3D disector sampling probes illustrating that particles are unambiguously sampled by only one disector sampling probe. The probes a, b, and c are located next to each other. The exclusion planes in this scheme are represented by grey planes. Particles are labelled according to the label of the probe they are counted in. In this scheme, in probe *a* eight chloroplasts are counted (labelled *a*), in probe *b* eight chloroplasts are counted (labelled *b*), and in probe *c* nine chloroplasts are counted (labelled *c*). Chloroplasts labelled by crosses are not counted by any of the three probes shown here, but they would be unambiguously sampled by adjacent hypothetical probes. (This figure is available in colour at *JXB* online.)

the number of chloroplasts per volume as estimated by the disector method in each cross-section and divided it by the sum of the estimated number of cells in each cross-section. In the 2D profile counting method, we summed the estimated number of chloroplasts per area in each cross-section and divided it by the sum of the estimated number of cells in each cross-section. Acquired values were compared using statistical analysis (paired *t*-test) in NCSS 2000 program (Number Cruncher Statistical Systems, Kaysville, Utah, USA).

For visualization of mesophyll cell surface (Fig. 5A–E) and 3D chloroplast arrangement in a mesophyll cell (Fig. 5G), the 3D reconstructions were created based on processing series of optical sections 2 µm apart acquired by a confocal microscope using a 20× objective. A model of a simplified mesophyll cell with 210 chloroplasts was made in the Cortona software (Fig. 5F, H, Supplementary Video S3 at *JXB* online) in order to demonstrate comparison of the 3D disector and the 2D profile counting methods.

For maceration of needle mesophyll samples, in order to count chloroplasts directly in separated cells, different methods were tested: a 1 M aqueous solution of HCl (Possingham and Saurer, 1969); a 3.5% aqueous solution of glutaraldehyde and 0.1 M aqueous solution of Na_2EDTA (Boffey *et al.*, 1979); and a solution of 10% aqueous CrO_3 and 10% aqueous HNO_3 (O'Brian and McCully, 1981). A phloroglucinol/HCl test (O'Brian and McCully, 1981) was applied to demonstrate lignification of mesophyll cell walls (Fig. 2B).

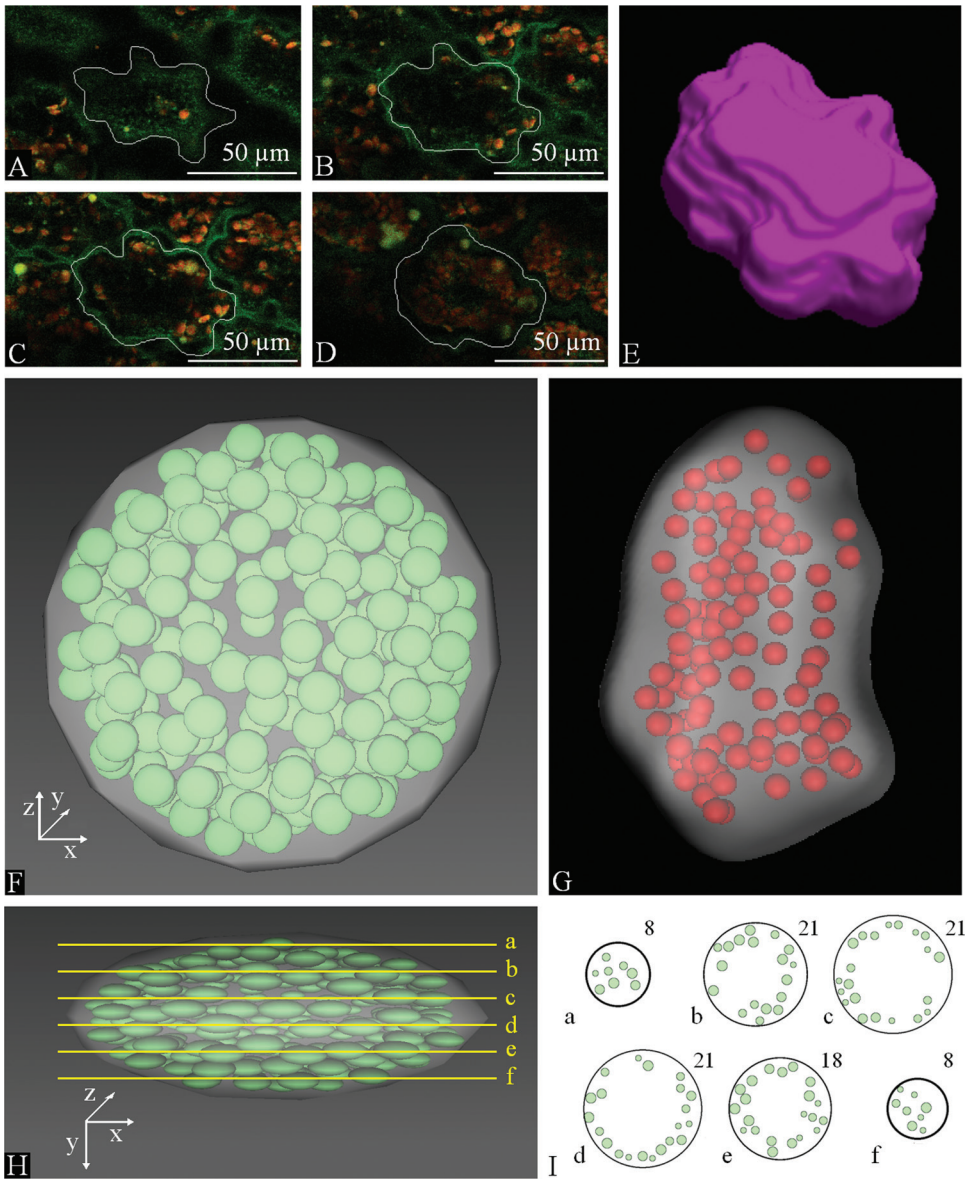

Fig. 5. 3D reconstruction and 3D model of a Norway spruce mesophyll cell. (A–D) Different optical sections of a mesophyll cell in a stack of images captured by a confocal microscope by using an objective 20×. (E) 3D reconstruction of the surface of the mesophyll cell from the confocal image stack shown in (A)–(D) using Ellipse software. (F) Face view of a model of a mesophyll cell with 210 chloroplasts made in Cortona 3D software. (G) 3D reconstruction of the mesophyll cell with chloroplasts from a stack of optical sections from confocal microscopy using Ellipse software. The positions of chloroplasts do not correspond to the *in vivo* state. (H) Side view of the model from (F) with six lines indicating planes of cross-sections. (I) 2D sections through the model cell shown in (F) and (H). Letters indicate the position of section planes in (H). Numbers indicate the number of chloroplast profiles in each of these sections.

Results

The Norway spruce needle structure (Fig. 2A) is composed of a one-cell-layer epidermis with highly cutinized periclinal cell walls on the needle surface; below the epidermis, there is one-cell layer of sclerenchymatic hypodermis not present below the stomata, followed by mesophyll and a central cylinder with a vascular bundle surrounded by transfusion tissue. Mesophyll cells contain chloroplasts and have an irregular shape with lobed anticlinal cell walls and are prolonged in the direction perpendicular to the needle surface (Fig. 5E), forming layers of tightly connected mesophyll cells surrounded by intercellular spaces (Supplementary Videos S1 and S2, Supplementary Fig. S1 at *JXB* online).

Numerous maceration methods were tested in order to count chloroplasts directly in separated spruce mesophyll cells. However, the spruce mesophyll cells kept connected together by the middle lamella and cell walls. We concluded that maceration methods were unsuccessful due to lignification of mesophyll cell walls detected histochemically (Fig. 2B) and observed regularly in our previous study (Soukupová *et al.*, 2000).

The average Norway spruce needle volume was $8.17 \pm 1.00\,mm^3$ ([mean ± standard error (SE)] and the

proportion of mesophyll in the needle volume was 72.0 ± 0.8 %. The average number of chloroplasts per mesophyll cell estimated by profile counting in 2D was 20.92 ± 1.32, while the average number of chloroplasts estimated by the disector probe in 3D was 10 times higher, i.e. 209.65 ± 17.44 (Fig. 6). Unsurprisingly, statistical analysis showed a significant difference between results obtained in 2D and 3D. The methods of chloroplast counting in 2D and 3D thus yielded estimates of the chloroplast number per mesophyll cell that were different by one order of magnitude.

To visualize differences in the results yielded by both methods, we used the 3D model of a mesophyll cell (Fig. 5F, H, I, Supplementary Video S3). We made 111 sections through the cell model and counted profiles in each section. The mean number of particle profiles per section was 17.23 ± 0.69 (mean±SE). However, there were 210 particles in the model cell. Our test showed that the average number of chloroplasts estimated by profile counting was more than 10 times underestimated in comparison with the real number of chloroplasts in the model. This is clearly demonstrated in Fig. 6.

The difference between both estimators tested can be also explained theoretically as shown below. The number of chloroplasts per mesophyll cell can be calculated by:

$$estN_{Ncell}(chl) = \frac{estN_{Vneedle}(chl)}{estN_{Vneedle}(cell)}$$

Instead of direct counting of N, it could be estimated by estimations of densities N_V:

$$\hat{N}_V = \frac{\hat{N}_V(chl)}{\hat{N}_V(cell)}$$

obtained by stereological methods. $\hat{N}_V(cell)$ should be estimated with a small error, $CV < \frac{1}{4}$, because it is not possible to divide by zero, and $\hat{N}_V(chl)$ with an error of about $CV < \frac{2}{5}$ (Marsaglia, 2006). The number of chloroplasts cannot be directly estimated by counting profiles in the section, because the areal density of profiles is related not only to density N_v but also to height h: $N_A = h \cdot N_V$. If we count the ratio of estimations,

$$\frac{\hat{N}_A(chl)}{\hat{N}_A(cell)}$$

we get close to the value

$$\frac{h(chl)}{h(cell)} \cdot \frac{N_V(chl)}{N_V(cell)}$$

which is different from the desired value by the ratio of the height of chloroplasts to the height of mesophyll cells:

$$\frac{h(chl)}{h(cell)}$$

The chloroplasts are much smaller than mesophyll cells (chloroplast mean height is approximately 4 µm, while the cell mean height is approximately 40–60 µm); therefore, the theoretically expected difference is high, also of one order of magnitude.

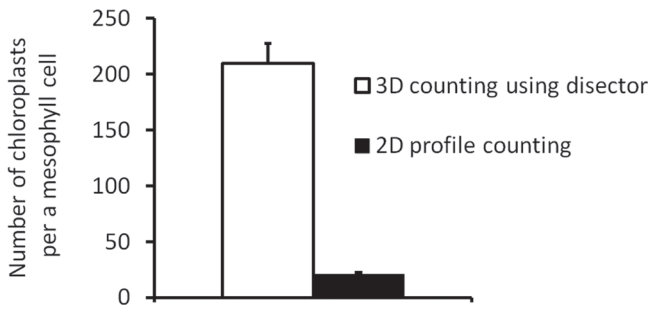

Fig. 6. Comparison of 3D- and 2D-based methods for chloroplast number estimation. The mean number of chloroplasts per mesophyll cell in Norway spruce needle estimated by 3D disector was 209.65 ± 17.44 (mean±SE) (open column), and by profile counting in 2D (filled column) was 20.92 ± 1.32. This result was statistically significantly different (P<0.001).

Discussion

Counting chloroplast profiles in 2D yielded values of chloroplast number per cell that were 10 times underestimated in comparison with the mean number of chloroplasts estimated by the unbiased disector method in 3D. We determined that the systematic shift in an estimated value is inversely related to the ratio of the height of chloroplasts to the height of mesophyll cells. The 3D model also showed that neglecting the 3D appearance of the cell led to the underestimation of the number of chloroplasts (Fig. 6). All our practical and theoretical tests thus clearly showed that the frequently used method for chloroplast number estimation by counting profiles of particles from 2D sections (e. g. Boffey *et al.*, 1979; Sam *et al.*, 2003; Wang *et al.*, 2004; Hayashida *et al.*, 2005; Teng *et al.*, 2006; Gopi *et al.*, 2008) yielded biased estimates and that the results may be one order of magnitude different from the real chloroplast numbers.

A review of the previously reported results on the number of chloroplasts per mesophyll cell with focus on the method used is presented in Supplementary Table S1 at *JXB* online. The studies were conducted on various plant species, considering herbaceous species in the majority of cases. For example, the extreme variability can be seen in the number of chloroplasts in *Arabidopsis* mesophyll cells estimated by various methods. The number of chloroplasts varied from eight to 10 chloroplasts per cell, based on counting chloroplast profiles in thin sections (Teng *et al.*, 2006; Jin *et al.*, 2011), to more than 100 chloroplasts per cell if the number was determined by the maceration method (Pyke and Leech, 1992; Marrison *et al.*, 1999), or even more than 200 (Meyer *et al.*, 2006).

It is generally known that the number of chloroplasts depends on plant internal factors—developmental stage, age, and species genotype (reviewed by Possingham, 1980)—or environmental factors, although the methodical bias could

conceal effects of these factors. Authors often do not describe the sampling design and the method used for chloroplast counting. Nevertheless, sampling design is crucial for yielding unbiased results, as anatomical gradients within a leaf blade were demonstrated also for the number of chloroplasts per cell (Dean and Leech, 1982). Gradients in leaf anatomical parameters, e.g. the number of chloroplasts per cell, also exist in dependence on distance of a leaf from the root system (Possingham and Saurer, 1969).

The chloroplast number per cell in conifers was estimated by profile counting to be six to 16 chloroplasts per cell in different species sampled in August (Maslova *et al.*, 2009) (Supplementary Table S1). These numbers seem to be very low and may not reflect the real chloroplast number in a mesophyll cell. For example, the number of chloroplasts per pair of stomatal guard cells in epidermal peels varies between 10 and 20 (Mochizuki and Sueoka, 1955; Frandsen, 1968; Nicholson, 1981; Qin and Rotino, 1995; Sari *et al.*, 1999) and the mesophyll cells are obviously larger than guard cells. In flat cells, such as the stomatal guard cells, it is possible to observe the chloroplasts practically in one optical section and to count them correctly in contrary to the mesophyll cells, which are larger and thicker, so it is unlikely that profiles of all of the chloroplasts within a cell would be present in a single optical section.

Chloroplast counting in separated mesophyll cells after leaf maceration (e.g. Possingham and Saurer, 1969; Stettler *et al.*, 2009) is appropriate in the case when the chloroplasts in the specimen are not overlapping. Counting of chloroplasts in a solution from the macerated leaf segments (Sung and Chen, 1989) does not enable the determination of chloroplast number per cell as the number of mesophyll cells, from which the chloroplasts present in a solution are released, is not known. Applying the maceration method to coniferous needles is problematic or even impossible, as shown in our study, as they contain phenolic compounds and lignin in cell walls (Fig. 2B), as proved in a histochemical study by Soukupová *et al.* (2000).

Counting chloroplasts in cells directly during focusing through the specimen using conventional light microscopy (Ellis and Leech, 1985; Bockers *et al.*, 1997) can be applied if entire cells can be focused through and the chloroplasts are sparsely distributed in cells; however, chloroplasts usually tend to be densely packed along the cytoplasmic membrane. Determining the chloroplast number per cell in 3D reconstructions made from a series of confocal microscope images (Mozafari *et al.*, 1997; Dinkins *et al.*, 2001; Coate *et al.*, 2012; Xu *et al.*, 2012) can yield an unbiased estimate if SUR sampling is applied and a sufficient number of cells is analysed. However, this is a much more time-consuming approach than application of the disector method.

In order to get unbiased results, it is also important to apply unbiased sampling of locations within the leaf where the measurement is performed. Many authors of previous studies reporting the chloroplast number per mesophyll cell do not explain the sampling design in a sufficient detail. However, a SUR sampling, along with both assumptions—the unbiased method for counting particles and the sufficient number of measurements—are essential for getting unbiased and accurate results (Sterio, 1984).

In the present study, sample preparation and image acquisition were carefully designed according to the principle of SUR sampling (Gundersen and Jensen, 1987). Needles collected from Norway spruce trees were stored frozen before processing; freezing of needles does not influence various geometrical parameters of mesophyll (Lhotáková *et al.*, 2008). Similarly, the number of mesophyll cells and the number of chloroplasts cannot change during the needle storage. Norway spruce chloroplasts kept their chlorophyll fluorescence activity, even after 5 years of storage in a freezer, and were perfectly suitable for confocal microscopy. To eliminate the possible shrinkage of a tissue caused by cutting, the dry stem pith of *Sambucus nigra* L. was used to fix the sample during cutting. It was found that some cells might have been pulled out of the specimen during cutting (Lhotáková *et al.*, 2008), and this is why the disector probe was placed in the middle of a stack.

In general, plant mesophyll cells contain a large central vacuole and, *in vivo*, chloroplasts are usually located in the peripheral cytoplasm, close to the cell wall. However, the spatial distribution of organelles may be disrupted by freezing. Therefore, we are aware that our 3D models of mesophyll cells (Fig. 5) do not correspond to *in vivo* chloroplast arrangement; however, they illustrate well the size of Norway spruce mesophyll cells, their variable and irregular shape, as well as the number and size of chloroplasts within a cell. The particular mesophyll cell chosen for 3D reconstruction was a smaller one, so that it was possible to focus through the entire cell. Most mesophyll cells were too high to be focused through; therefore, a method based on direct counting of chloroplasts within the entire cell could not be used. The present 3D model of mesophyll cell (Fig. 5F, H, I) was constructed such that it contained the mean number of chloroplasts obtained in our study.

Conclusions

Based on the above-presented lines of evidence, we conclude that the presented optical disector method for chloroplast counting, using stacks of confocal microscopic images acquired from thick tissue sections accompanied by SUR sampling, is a very efficient method for estimating chloroplast number per mesophyll cell. While using the optical disector method for chloroplast counting, an important consideration that a mesophyll cell is a 3D structure is taken into account. We propose this method as a universal unbiased one. It should be the method of choice, especially in conifers or other xeromorphic leaves with mesophyll cells with lignified walls, where maceration methods are difficult or impossible to apply.

Supplementary data

Supplementary data are available at JXB online.

Supplementary Figure S1. Norway spruce needle longitudinal median section by confocal microscopy using 20× objective.

Supplementary Table S1. Review of studies with results on the number of chloroplasts per mesophyll cell of different plant species (most studied plant species: families *Brassicaceae*, *Fabaceae*, *Chenopodiaceae*, and *Poaceae*, and other families; coniferous species) with focus on the method used.

Supplementary Video S1. 3D stack of 16 serial optical cross-sections 2 µm apart acquired by confocal microscopy using a 20× objective.

Supplementary Video S2. 3D reconstruction of the mesophyll arrangement created by volume rendering from images of 16 serial optical sections rotating in 3D space.

Supplementary Video S3. 3D model of a simplified mesophyll cell with 210 chloroplasts (modelled by surfaces of oblate ellipsoids) made in IRIS Explorer (NAG, UK).

Acknowledgements

We are grateful to Drahomíra Bartáková for technical assistance, Barbora Radochová for assistance with confocal microscopy, and Marianna Dubánková for help with sample collection. This work was supported by the Czech Science Foundation (P501/10/0340), funds provided by the Academy of Sciences of the Czech Republic (AV0Z50110509 and RVO:67985823), and by the Charles University in Prague (SVV 265203).

References

Adachi S, Nakae T, Uchida M, *et al.* 2013. The mesophyll anatomy enhancing CO_2 diffusion is a key trait for improving rice photosynthesis. *Journal of Experimental Botany* **64,** 1061–1072.

Albrechtová J, Kubínová L. 1991. Quantitative analysis of the structure of etiolated barley leaf using stereological methods. *Journal of Experimental Botany* **42,** 1311–1314.

Albrechtová J, Janáček J, Lhotáková Z, Radochová B, Kubínová L. 2007. Novel efficient methods for measuring mesophyll anatomical characteristics from fresh thick sections using stereology and confocal microscopy: application on acid rain-treated Norway spruce needles. *Journal of Experimental Botany* **58,** 1451–1461.

Bockers M, Čapková V, Tichá I, Schafer C. 1997. Growth at high CO_2 affects the chloroplast number but not the photosynthetic efficiency of photoautotrophic *Marchantia polymorpha* culture cells. *Plant Cell Tissue and Organ Culture* **48,** 103–110.

Boffey SA, Ellis JR, Sellden G, Leech RM. 1979. Chloroplast division and DNA synthesis in light-grown wheat leaves. *Plant Physiology* **64,** 502–505.

Chaly N, Possingham JV, Thomson WW. 1980. Chloroplast division in spinach leaves examined by scanning electron-microscopy and freeze-etching. *Journal of Cell Science* **46,** 87–96.

Coate JE, Luciano AK, Seralathan V, Minchew KJ, Owens TG, Doyle JJ. 2012. Anatomical, biochemical, and photosynthetic responses to recent allopolyploidy in *Glycine dolichocarpa* (Fabaceae). *American Journal of Botany* **99,** 55–67.

Dean C, Leech RM. 1982. Genome expression during normal leaf development.1. Cellular and chloroplast numbers and DNA, RNA, and protein-levels in tissues of different ages within a 7-day-old wheat leaf. *Plant Physiology* **69,** 904–910.

Dinkins R., Srinivasa Reddy MS, Leng M, Collins GB. 2001. Overexpression of the *Arabidopsis thaliana MinD1* gene alters chloroplast size and number in transgenic tobacco plants. *Planta* **214,** 180–188.

Ellis JR, Leech RM. 1985. Cell-size and chloroplast size in relation to chloroplast replication in light-grown wheat leaves. *Planta* **165,** 120–125.

Frandsen N. 1968. Die Plastidenzahl als Merkmal bei der Kartoffel. *Theoretical and Applied Genetics* **38,** 153–167.

Gopi R, Jaleel CA, Panneerselvam R. 2008. Leaf anatomical responses of *Amorphophallus campanulatus* to triazoles fungicides. *EurAsian Journal of BioSciences* **2,** 46–52.

Gundersen HJG. 1986. Stereology of arbitrary particles—a review of unbiased number and size estimators and the presentation of some new ones, in memory of Thompson, William, R. *Journal of Microscopy* **143,** 3–45.

Gundersen HJG, Jensen EB. 1987. The efficiency of systematic sampling in stereology and its prediction. *Journal of Microscopy* **147,** 229–263.

Gundersen HJG. 1977. Notes on the estimation of the numerical density of arbitrary profiles: the edge effect. *Journal of Microscopy* **111,** 219–223.

Hassan L, Wazuddin M. 2000. Colchicine-induced variation of cell size and chloroplast number in leaf mesophyll of rice. *Plant Breeding* **119,** 531–533.

Hayashida A, Takechi K, Sugiyama M, Kubo M, Itoh RD, Takio S, Fujita T, Hiwatashi Y, Hasebe M, Takano H. 2005. Isolation of mutant lines with decreased numbers of chloroplasts per cell from a tagged mutant library of the moss *Physcomitrella patens*. *Plant Biology* **7,** 300–306.

Jin B, Wang L, Wang J, Jiang KZ, Wang Y, Jiang XX, Ni CY, Wang YL, Teng NJ. 2011. The effect of experimental warming on leaf functional traits, leaf structure and leaf biochemistry in *Arabidopsis thaliana*. *BMC Plant Biology* **11,** 10.

Kubínová L. 1991. Stomata and mesophyll characteristics of barley leaf as affected by light—stereological analysis. *Journal of Experimental Botany* **42,** 995–1001.

Kubínová L. 1993. Recent stereological methods for the measurement of leaf anatomical characteristics: estimation of volume density, volume and surface area. *Journal of Experimental Botany* **44,** 165–173.

Kubínová L. 1994. Recent stereological methods for measuring leaf anatomical characteristics: estimation of the number and sizes of stomata and mesophyll cells. *Journal of Experimental Botany* **45,** 119–127.

Kubínová L, Janáček J, Krekule I. 2002. Stereological methods for estimating geometrical parameters of microscopical structure studied by three-dimensional microscopical techniques. In: Diaspro A, ed. *Confocal and two-photon microscopy*, New York: Wiley-Liss.

Lamppa GK, Elliot LV, Bendich AJ. 1980. Changes in chloroplast number during pea leaf development—an analysis of a protoplast population. *Planta* **148,** 437–443.

Lhotáková Z, Albrechtová J, Janáček J, Kubínová L. 2008. Advantages and pitfalls of using free-hand sections of frozen needles for three-dimensional analysis of mesophyll by stereology and confocal microscopy. *Journal of Microscopy* **232,** 56–63.

Marrison JL, Rutherford SM, Robertson EJ, Lister C, Dean C, Leech RM. 1999. The distinctive roles of five different ARC genes in the chloroplast division process in Arabidopsis. *Plant Journal* **18,** 651–662.

Marsaglia G. 2006. Ratios of normal variables. *Journal of Statistical Software* **16,** 1–10.

Maslova TG, Mamushina NS, Sherstneva OA, Bubolo LS, Zubkova EK. 2009. Seasonal structural and functional changes in the photosynthetic apparatus of evergreen conifers. *Russian Journal of Plant Physiology* **56,** 607–615.

Meyer R, Yuan J, Afzal J, Iqbal MJ, Zhu MX, Garvey G, Lightfoot DA. 2006. Identification of Gsr1 in *Arabidopsis thaliana*: a locus inferred to regulate gene expression in response to exogenous glutamine. *Euphytica* **151,** 291–302.

Miyazawa SI, Terashima I. 2001. Slow development of leaf photosynthesis in an evergreen broad-leaved tree, *Castanopsis sieboldii*: relationships between leaf anatomical characteristics and photosynthetic rate. *Plant, Cell & Environment* **24,** 279–291.

Mochizuki A, Sueoka N. 1955. Genetic studies on the number of plastid in stomata. I. Effect of autopolyploidy in sugar beets. *Cytologia* **20,** 358–366.

Molin WT, Meyers SP, Baer GR, Schrader LE. 1982. Ploidy effects in isogenic populations of alfalfa. 2. Photosynthesis, chloroplast number, ribulose-1,5-bisphosphate carboxylase, chlorophyll, and DNA in protoplasts. *Plant Physiology* **70,** 1710–1714.

Mozafari J, Wolyn DJ, AliKhan ST. 1997. Chromosome doubling via tuber disc culture in dihaploid potato as determined by confocal microscopy. *Plant Cell Reports* **16,** 329–333.

Nicholson GG. 1981. The use of chloroplast numbers in guard cells as a means of distinguishing the chromosome races of *Ranunculus ficaria* L. *Annals of Botany* **48,** 909–913.

O'Brian TP, McCully ME. 1981. *The study of plant structure: principles and selected methods* . Melbourne, Australia: Termarcarphi Pty Ltd.

Oguchi R, Hikosaka K, Hirose T. 2005. Leaf anatomy as a constraint for photosynthetic acclimation: differential responses in leaf anatomy to increasing growth irradiance among three deciduous trees. *Plant, Cell & Environment* **28,** 916–927.

Pazourek J. 1966. Anatomical gradients. *Acta Universitatis Carolinae—Biologica* , Suppl. 1/2, 19–25.

Possingham JV, Saurer W. 1969. Changes in chloroplast number per cell during leaf development in spinach (*Spinacea oleracea*). *Planta* **86,** 186–194.

Possingham JV, Smith JW. 1972. Factors affecting chloroplast replication in spinach. *Journal of Experimental Botany* **23,** 1050–1059.

Possingham JV. 1980. Plastid replication and development in the life-cycle of higher-plants. *Annual Review of Plant Physiology and Plant Molecular Biology* **31,** 113–129.

Pyke KA, Leech RM. 1991. Rapid image analysis screening procedure for identifying chloroplast number mutants in mesophyll cells of *Arabidopsis thaliana* (L.) Heynh. *Plant Physiology* **96,** 1193–1195.

Pyke KA, Leech RM. 1992. Chloroplast division and expansion is radically altered by nuclear mutations in *Arabidopsis thaliana*. *Plant Physiology* **99,** 1005–1008.

Qin X, Rotino GL. 1995. Chloroplast number in guard cells as ploidy indicator of *in vitro*-grown androgenic pepper plantlets. *Plant Cell Tissue and Organ Culture* **41,** 145–149.

Sam O, Ramirez C, Coronado MJ, Testillano PS, Risueno MC. 2003. Changes in tomato leaves induced by NaCl stress: leaf organization and cell ultrastructure. *Biologia Plantarum* **47,** 361–366.

Sari N, Abak K, Pitrat M. 1999. Comparison of ploidy level screening methods in watermelon: *Citrullus lanatus* (Thunb.) Matsum. and Nakai. *Scientia Horticulturae* **82,** 265–277.

Simon UK, Polanschütz LM, Koffler BE, Zechmann B. 2013. High resolution imaging of temporal and spatial changes of subcellular ascorbate, glutathione and H_2O_2 Distribution during *Botrytis cinerea* infection in Arabidopsis. *PLoS ONE* **8,** 1–11.

Soukupová J, Cvikrová M, Albrechtová J, Rock BN, Eder J. 2000. Histochemical and biochemical approaches to the study of phenolic compounds and peroxidases in needles of Norway spruce (*Picea abies*). *New Phytologist* **146,** 403–414.

Sterio DC. 1984. The unbiased estimation of number and sizes of arbitrary particles using the disector. *Journal of Microscopy* **134,** 127–136.

Stettler M, Eicke S, Mettler T, Messerli G, Hortensteiner S, Zeeman SC. 2009. Blocking the metabolism of starch breakdown products in Arabidopsis leaves triggers chloroplast degradation. *Molecular Plant* **2,** 1233–1246.

Sung FJM, Chen JJ. 1989. Changes in photosynthesis and other chloroplast traits in lanceolate leaflet isoline of soybean. *Plant Physiology* **90,** 773–777.

Teng NJ, Wang J, Chen T, Wu XQ, Wang YH, Lin JX. 2006. Elevated CO_2 induces physiological, biochemical and structural changes in leaves of *Arabidopsis thaliana*. *New Phytologist* **172,** 92–103.

Terashima I, Hanba YT, Tholen D, Niinemets U. 2011. Leaf functional anatomy in relation to photosynthesis. *Plant Physiology* **155,** 108–116.

Tomori Z, Krekule I, Kubínová L. 2001. DISECTOR program for unbiased estimation of particle number, numerical density and mean volume. *Image Analysis & Stereology* **20,** 119–130.

Tymms MJ, Scott NS, Possingham JV. 1983. DNA content of *Beta vulgaris* chloroplasts during leaf cell expansion. *Plant Physiology* **71,** 785–788.

Urban O, Janouš D, Pokorný R, Marková I, Pavelka M, Fojtík Z, Šprtová M, Kalina J, Marek MV. 2001. Glass domes with adjustable windows: a novel technique for exposing juvenile forest stands to elevated CO_2 concentration. *Photosynthetica* **39,** 395–401.

Wang XZ, Anderson OR, Griffin KL. 2004. Chloroplast numbers, mitochondrion numbers and carbon assimilation physiology of *Nicotiana sylvestris* as affected by CO_2 concentration. *Environmental and Experimental Botany* **51,** 21–31.

Weibel ER. 1979. Practical methods for biological morphometry. In: *Stereological methods* , vol. **1**. New York: Academic Press, 1–415.

Xu CY, Salih A, Ghannoum O, Tissue DT. 2012. Leaf structural characteristics are less important than leaf chemical properties in determining the response of leaf mass per area and photosynthesis of *Eucalyptus saligna* to industrial-age changes in [CO_2] and temperature. *Journal of Experimental Botany* **63,** 5829–5841.

Yamasaki T, Kudoh T, Kamimura Y, Katoh S. 1996. A vertical gradient of the chloroplast abundance among leaves of *Chenopodium album*. *Plant and Cell Physiology* **37,** 43–48.

Zechmann B, Müller M, Zellnig G. 2003. Cytological modifications in zucchini yellow mosaic virus (ZYMV)-infected Styrian pumpkin plants. *Archives of Virology* **148,** 1119–1133.

Trees (2018) 32:231–244
DOI 10.1007/s00468-017-1626-3

ORIGINAL ARTICLE

Norway spruce needle size and cross section shape variability induced by irradiance on a macro- and microscale and CO_2 concentration

Zuzana Kubínová[1] · Jiří Janáček[2] · Zuzana Lhotáková[1] · Miroslava Šprtová[3] · Lucie Kubínová[2] · Jana Albrechtová[1,4]

Received: 17 March 2017 / Accepted: 11 October 2017 / Published online: 20 October 2017

Abstract

Key message **Needle cross-section parameters differ according to needle orientation on a shoot corresponding to irradiance microgradient. Irradiance is a stronger morphogenic factor determining needle size and shape than CO_2 concentration.**

Abstract We investigated the effects of irradiance on macroscale and microscale, elevated CO_2 concentration [CO_2], and their interaction on Norway spruce (*Picea abies* L. Karst.) needles. The irradiance macroscale was represented by sun and shade shoots from two vertical positions in a crown and the irradiance microscale corresponded to spatial orientation of individual needles on a shoot (upper, side, and lower needles relative to the shoot axis). Determination of needle cross section shape using generalized Procrustes analysis and principal component analysis provided a novel approach for evaluating needle morphometry. As expected, shade needles on the irradiance macrogradient were flatter and had less cross-sectional area and smaller volume than did sun needles. The irradiance microgradient was detected within both sun and shade shoots, being steeper in sun shoots than shade shoots. On the microscale, the irradiance gradient induced changes in needle size and cross section shape according to needles' orientation on a shoot. Due to a more favourable light environment the traits of the upper needles within both sun and shade shoots resembled more the sun needle traits. The sun needle volume was significantly larger in the case of elevated [CO_2] as compared to ambient [CO_2]. Irradiance was a stronger morphogenic factor determining needle size and cross section shape compared to CO_2 concentration. We demonstrated that generalized Procrustes analysis can be a very powerful tool in ecophysiological studies for evaluating small-scale, subtle leaf shape changes on an intraspecific level caused by environmental factors.

Keywords Coniferous needle morphology · Elevated CO_2 concentration · Generalized Procrustes analysis · Geometric morphometry · Irradiance gradient · Leaf shape

Communicated by G. Piovesan.

Electronic supplementary material The online version of this article (doi:10.1007/s00468-017-1626-3) contains supplementary material, which is available to authorized users.

✉ Jana Albrechtová
albrecht@natur.cuni.cz

[1] Department of Experimental Plant Biology, Faculty of Science, Charles University, Viničná 5, 128 44 Prague 2, Czech Republic

[2] Institute of Physiology, The Czech Academy of Sciences, v.v.i., Vídeňská 1083, 142 20 Prague 4, Czech Republic

[3] Global Change Research Institute, The Czech Academy of Sciences, v.v.i., Bělidla 986/4a, 603 00 Brno, Czech Republic

[4] Institute of Botany, The Czech Academy of Sciences, v.v.i., Zámek 1, 252 43 Průhonice, Czech Republic

Introduction

In the extended canopy, and particularly in forest trees, shading reduces irradiance, thereby impacting the irradiance gradient and thus the development of sun and shade leaves (Stahl 1883; Kim et al. 2005). In species with dorsiventral leaves, sun leaves are thicker compared to shade leaves, this greater thickness being accompanied by more layers of palisade mesophyll (Wylie 1949; Hanba et al. 2002; Kim et al. 2005; Niinemets 2007) and larger internal mesophyll surface area (Terashima 2005). Some conifer species also show needle differentiation between sun and shade ecotypes, but the

differences are not as apparent as in leaves of broadleaved trees. Sun needles may have a higher volume-to-surface ratio and a thicker mesophyll layer (Niinemets 2007) or a circular shape in cross section that is in contrast with laterally flatter shade needles (Cescatti and Zorer 2003).

Because the leaves and branches overlap and shade one another, the irradiance gradient within a spruce canopy can be very steep. Photosynthetic photon flux density may thereby be reduced by as much as two thirds from top to bottom within a tree crown (Reiter et al. 2005). Moreover, the quality of light changes along the crown's vertical gradient, as absorption of light for photosynthesis by leaves of higher vertical position in a crown change the spectral composition of photosynthetically active radiation (Navrátil et al. 2007). Provided that incident irradiance may be limiting for photosynthesis, different light conditions within a mature tree crown could affect the carbon gain. As shown by Reiter et al. (2005) for Norway spruce, shade branches may display low or negative carbon balance.

Downscaling to the shoot microscale, the photosynthetic photon flux density at the leaf surface and the daily amounts of intercepted light within a branch vary not only among vertical canopy layers (Iio et al. 2009) but depend also upon leaf inclination angle in broadleaved trees (Fleck et al. 2003). The influence of the light gradient within the conifer crown is also manifested in needle arrangement on shoots. The shoot architecture determined by the needle arrangement on a shoot has been studied together with needle surface area and described by the parameter $STAR_{max}$ (maximum ratio of shoot silhouette area to total needle surface area). $STAR_{max}$ is a measure of light interception efficiency per unit needle area of a shoot when the shoot axis is perpendicular to the direction of irradiance (Carter and Smith 1985; Stenberg 1996). Shade shoots of *Pinus* and *Picea* have been shown to have higher $STAR_{max}$ than did sun shoots (Stenberg 1996). Shade shoots are usually more flat and with fewer needles, which grow more horizontally than vertically to intercept more light, while in the case of sun shoots the needles grow all around the shoot axis (Stenberg 1996; Cescatti and Zorer 2003; Ishii et al. 2012). Carter and Smith (1985) modified sun and shade conifer shoots in *Picea engelmannii* Parry ex Engelm. by cutting selected needles to eliminate self-shading. Then they compared modified shoots with intact ones and found that needle removal resulted in an increase in $STAR_{max}$. Although the arrangement of sun and shade shoots thus seems to be well understood, it remains unclear how the characteristics of individual needles are influenced by their orientation on a shoot. Despite the fact that needle self-shading has been considered in many studies, to our knowledge, within-shoot light gradients have not yet been examined in conifers.

While the influence of irradiance on needle morphology is fairly predictable, such is not the case of carbon dioxide concentration in the air ($[CO_2]$). Changes in needle anatomy and morphology under elevated $[CO_2]$ have been studied and observed in different conifer species, but the findings are ambiguous. *Pinus taeda* L. and *Pinus sylvestris* L. needles in elevated $[CO_2]$ have been observed to be thicker, mainly due to an increase of mesophyll thickness (Thomas and Harvey 1983; Lin et al. 2001), while *Larix kaempferi* (Lamb.) Carr. needles have been reported to retain the same thickness (Eguchi et al. 2004). Moreover, the effects of $[CO_2]$ on needle morphology depend on such aspects of the experimental design as the level of elevated $[CO_2]$, duration of the experiment, and age of the treated plants. Older conifer trees seem to be less responsive to elevated $[CO_2]$ regarding morphological changes in needles. Although Lin et al. (2001) reported that treatment over several years of *P. sylvestris* seedlings in pots with elevated $[CO_2]$ led to an increase in needle thickness, Luomala et al. (2005) observed that similar treatment of 20-year-old trees in a forest caused no change in this parameter. Our previous study of 18-year-old Norway spruce trees after eight years of treatment (Lhotáková et al. 2012) corresponded with the results of Luomala et al. (2005). We observed no significant effect of elevated $[CO_2]$ on needles' anatomical and morphological parameters (needle volume, internal needle surface area, mesophyll volume). The effect of elevated $[CO_2]$ on needle morphology is complex and interacts with other factors. To fully understand the effect of irradiance and elevated $[CO_2]$ on needle morphology and anatomy, it is vital to use a more precise method of needle parameter measurement.

The ratio of needle thickness to needle width is often considered to be a key morphological characteristic (Sellin 2001; Apple et al. 2002; Palmroth et al. 2002; Homolová et al. 2013; Gebauer et al. 2015), but this parameter does not precisely describe the cross section shape. In contrast, generalized Procrustes analysis (GPA), a geometric morphometric method, allows for precise quantitative analysis of plant organ shape. It also enables comparison of needle symmetry and shape independent of the actual needle cross section size. In general, this powerful method for shape description has been used rarely in plant studies, and then mostly for the detection of interspecific differences among plants (Klingenberg 2010; Savriama and Klingenberg 2011; Viscosi and Cardini 2011; Neustupa 2013). We anticipated that GPA would enable us to detect even very subtle differences among needle cross section shapes depending on their positions along the needle axis and spatial orientation on the shoot.

We expected that the needle cross section would become more circular in sun needles and flatter in shade needles, as commonly reported in other studies (e.g. Cescatti and Zorer 2003). We further hypothesized that

H1 Within a shoot there is a microscale gradient in irradiance caused by needle self-shading.

H2 Needle size and cross section shape change similarly as in sun and shade needle ecotypes according to their spatial orientation on a shoot.

H3 Irradiance is a stronger morphogenic factor than is elevated CO_2 concentration.

Our study may help to elucidate the influence of elevated [CO_2] in interaction with different irradiance availability on macro- and microscale on Norway spruce needle morphology.

Materials and methods

Materials

Current-year Norway spruce needles were collected in October 2012 from crowns of 12-year-old trees planted at Bílý Kříž in the Moravskoslezské Beskydy Mountains at the experimental site of the Global Change Research Institute, the Czech Academy of Sciences, Czech Republic (49°30′8.813″ N, 18°32′20.213″ E; 908 m a.s.l.). The trees were growing in a mixed Norway spruce and European beech stand (35 spruce and 60 beech trees in each dome) with spacing of 1.2 m between individual trees within special glass domes either ambient (AC) or elevated (EC; 700 ppm) CO_2 concentration (Urban et al. 2001). The EC treatment was applied for seven growing seasons (since 2005). Whole current-year shoots with needles were collected from south- and south-west-facing branches of five trees in AC and five trees in EC. One sun (third whorl) and one shade (sixth whorl) shoot was cut from each tree, and thus a total of 20 shoots was sampled altogether. The samples were stored in a freezer (− 20 °C) until processing. For morphological analyses, five needles were cut from the middle part of each shoot in each of the three orientations on a shoot—upper, side and lower (Fig. 1a). This means that 15 needles were cut from each shoot and 300 needles in total were analysed. Needle length was determined first, and then free-hand cross sections were made at ¼, ½ and ¾ of needle length using a razor blade (Fig. 1c). These positions along the needle are further described as base, middle, and tip position, respectively. Each of the 900 cross sections was mounted in a drop of tap water and its image was acquired by an Olympus BX50 light microscope equipped with a Nikon digital camera using a dry plan apochromatic 4 × objective (numeric aperture 0.10) and NIS-Elements AR 3.1 software (Nikon Instruments, Tokyo, Japan).

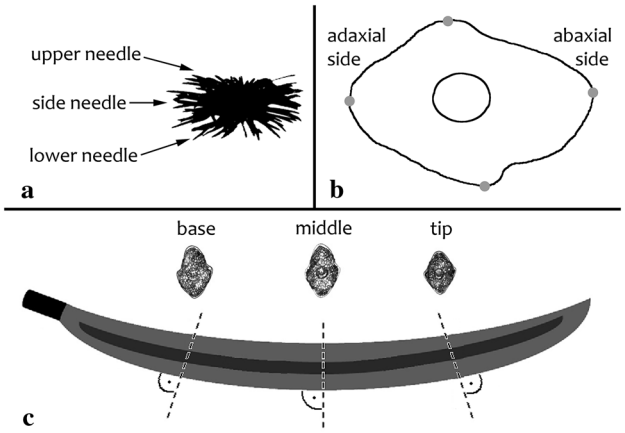

Fig. 1 Scheme of needle sampling design for sampling on a shoot and within a needle. **a** Scheme of needle sampling design demonstrated on a shoot projection along the shoot axis taken from a shoot tip. The shoot tip is oriented towards the observer. Arrows indicate the needle orientation on the shoot in relation to the direction of sun irradiance. **b** Four landmarks placed on abaxial, adaxial, and both lateral extremities of the needle cross section. **c** Scheme of sampling design, taking three cross sections (base, middle, and tip) along the needle

Light microgradient measurements

Measurements of light penetration within sun and shade shoots collected fresh in January 2017 were made with the aim to reveal the presence of a microgradient in irradiance caused by needle self-shading. For this purpose, under artificial laboratory conditions, ten sun and ten shade shoots from trees grown in ambient [CO_2] were examined. The detached shoots were illuminated directly, and therefore the position of the shade shoot within a tree and its shading by other shoots was not simulated in this experiment. The purpose of the measurement, however, was to elucidate how the needle arrangement influences light penetration within the shoot itself. Moreover, artificial illumination of detached shoots is frequently used for revealing effects of the angle of incoming light on photosynthetic rate (Ishii et al. 2012) or optical shoot properties (Oker-Blom et al. 1988; Rautiainen et al. 2012). An AvaSpec-2048 Fiber Optic Spectrometer (Avantes, Apeldoom, the Netherlands) was used in Scope Mode, thus recording real-time analogue-to-digital converter (ADC) values. ADC values correspond to the voltage detected in the sensor generated by photons in visible wavelengths between 400 and 700 nm, and thus reflect the intensity of the light source. A COL-UV/VIS collimating lens (a 6 mm diameter lens with a confocal length of 8.7 mm) mounted at the end of the optic fibre was affixed facing upwards toward the light source. For each sample, the results of ten scans were averaged and the spectrum recorded. The only source of illumination for the shoot consisted of a 5 W LED cool white (colour temperature 6500 K) lamp with an

illumination angle of 5° placed at a distance of 0.5 m from the lens. The objective was to ensure that the shoot was illuminated as precisely as possible from the zenith to avoid light saturation of the sensor.

The lens connected to the sensor was set subsequently to three positions: upper position (U), with needle tips at the same level as the lens; side position (S), with the lens within the side needles on the shoot; and lower position (L), with the needles just above the lens while avoiding shading by a woody twig. Within each shoot, the irradiance was measured at three different places along the shoot in the three vertical positions described above. In total, 180 measurements were recorded. The irradiance (μW cm^{-2}) between 400 and 700 nm for each position within a shoot was expressed as the value of the area under the curve from visible wavelengths for each lens position. The relative light penetration in a shoot side and lower position was then calculated as the ratio of irradiance measured in a shoot side and lower position, respectively, to irradiance measured in an upper position. We compared the irradiance sums within sun and shade shoots using one-way ANOVA and Tukey–Kramer multiple-comparison test in NCSS 9 Statistical Software (NCSS, Kaysville, UT, USA, https://ncss.com/software/ncss).

Computed tomography

To illustrate the general difference in architecture between sun and shade shoots, computed tomography data of two Norway spruce shoots collected fresh in January 2016 were acquired using an Albira μCT/PET scanner (Bruker BioSpin, Billerica, MA, USA; Sanchez et al. 2013) and reconstructed using the Feldkamp, Davis, and Kress (FDK) algorithm in Plastimatch software (Sharp et al. 2007) with voxel size = 125 × 125 × 125 μm^3. Volume rendering utilizing the Amira 5.6 (FEI) program was used to create images and videos.

$STAR_{max}$ measurements

To reveal possible differences between sun and shade shoot arrangements in AC and EC, $STAR_{max}$ (maximum ratio of shoot silhouette area to total needle surface area; Carter and Smith 1985) was determined using an adjusted method from Ishii et al. (2012). The shoot silhouette area (the area projected by the shoot) was measured in the ImageJ (Rasband 1997, https://imagej.nih.gov/ij/) program from images of shoots shot by a perpendicularly placed camera. Total needle area was estimated from projected needle area using a formula described in Homolová et al. (2013):

$$A_L = n \cdot A_P \cdot \mathrm{CF},$$

where A_L is the total needle area, n is the number of needles on a shoot, A_P is the projected needle area, and CF is the correction factor used to estimate the surface area from projected area. The correction factor was calculated using a formula also described in Homolová et al. (2013):

$$\mathrm{CF} = 0.47 \cdot \frac{P_M}{D_{1M}} + 1.31,$$

where P_M is the middle cross section perimeter and D_{1M} is the major diameter of the middle cross section. For additional measurements of $STAR_{max}$ on shoots, for which light penetration was measured, the values of CF from Homolová et al. (2013) were applied as follows: 3.47 for sun shoots and 2.84 for shade shoots.

Chlorophyll content determination

Needles for chlorophyll $a + b$ content and dry mass determinations were collected from sun and shade shoots from two vertical positions within the crown identical to those of needles taken for morphological and photosynthetic analyses. Mixed samples from needles of all orientations on a shoot were used. Chlorophylls *a* and *b* were extracted with *N,N*-dimethylformamide for 7 days at 4 °C under conditions of darkness (Porra et al. 1989). The concentrations of the photosynthetic pigments were measured spectrophotometrically using a Helios-α spectrophotometer (Unicam, Cambridge, UK) according to the equations of Wellburn (1994). The pigment contents were then expressed per unit of leaf dry mass, which was determined after drying the corresponding samples in an oven for 48 h at 80 °C.

Gas exchange measurements

In situ measurements were carried out in mid-September, 2 weeks before sampling the shoots for morphological analyses, on the same spruce trees and at the same vertical levels. Light-saturated rates of CO_2 assimilation (A_{max}) were measured after 10 min exposure to a saturating irradiance (1400 μmol photons $m^{-2}s^{-1}$) and growth CO_2 concentration (i.e. 400 ppm for AC plants and 700 ppm for EC plants) during extended midday hours (10:00–14:00). A_{max} was measured on intact shoots using the 6400-22L Lighted Conifer Chamber (Li-Cor, Lincoln, NE, USA) together with the Li-6400 gas exchange system (Li-Cor, USA) within a range of temperatures from 20 to 23 °C. Relative air humidity within an assimilation chamber was kept at a constant 60%, and the vapour pressure deficit values varied accordingly from 0.9 to 1.1 kPa. Two current-year shoots per tree were evaluated and the average of these two measurements was used for statistical analyses.

Generalized Procrustes analysis application on needles and statistical evaluation

The needle cross sections were analysed using geometric morphometry methods based on the analysis of landmarks (i.e. points located precisely on an analysed shape) to establish a clear one-to-one correspondence between all samples included in the study. Four landmarks were placed on abaxial, adaxial, and both lateral extremities of the perimeter of the cross section images (Fig. 1b) using the Ellipse software (ViDiTo, Košice, Slovakia, http://www.ellipse.sk/). In geometric morphometry, the form of an object means a set of landmarks that are defined by their mutual positions and distances between them. It includes the size of the object but does not depend on landmark absolute positions, which may be influenced, for example, by object rotation. The shape of an object is derived from its form by translation, rotation, and rescaling of landmarks, and it is defined by relative positions of the landmarks not depending on their absolute distance (e.g. all squares have the same shape regardless of their sizes).

The shapes of needle cross sections were analysed using geometric morphometry tools as described by Dryden and Mardia (1998). The calculations were made using the R programing environment for data analysis and graphics (Ihaka and Gentleman 1996) with the R library *shapes* as described in Dryden (2014).The landmark coordinates associated with the categorial data were read from an external file. The generalized Procrustes analysis (GPA) procedure (procGPA) was applied to remove positional and size information and to generate Procrustes shape coordinates used in subsequent shape analyses. GPA applies rescaling, translating, and rotating of the landmark configurations so that the sum of squares of distances between the corresponding points in the configurations is minimized [for an introduction to geometric morphometry, see the excellent monograph by Dryden and Mardia (1998)]. The "plotshape" procedure was used for drawing the Procrustes shape coordinates. Shape differences between groups were tested by Hotelling's T^2 test implemented in the "testmeanshapes" procedure. Principal component analysis (PCA) was applied for visualizing the dispersion of Procrustes shape coordinates using scatter plots of principal components (PC) in the "shapepca" procedure (Online Resource 1).

The area of cross section was estimated as the area of quadrangle with vertices represented by the landmarks. The needle volume was estimated as the average area of the three cross sections multiplied by the needle length. The surface area of the needle was estimated as the mean perimeter of the three cross section quadrangles multiplied by the needle length. The differences in needle volume, cross section area, and length between groups were tested by analysis of variance (ANOVA) in the R programing environment (Ihaka and Gentleman 1996).

Results

The laboratory measurement of light penetration within a shoot revealed the presence of an irradiance microgradient caused by needle self-shading: absolute values (Fig. 2) showed the irradiance gradient. The relative light penetrations (the ratio of side or lower lens positions to an upper position) for sun and shade shoots were 89.45 ± 0.20% (mean ± standard deviation) and 88.1 ± 0.18%, respectively, for a side lens position and 34.29% ± 0.19 and 53.76 ± 0.20%, respectively, for a lower lens position (under the shoot). The light gradient was steeper in sun shoots than in shade shoots, and particularly so between side and lower oriented needles on a shoot. This corresponded to the stronger self-shading in sun shoots as compared to shade shoots, causing a marked light microgradient.

A very distinct needle arrangement of sun and shade shoots investigated in our experiment is demonstrated in Fig. 3 and in online videos (Online Resources 2, 3). $STAR_{max}$ (maximum ratio of shoot silhouette area to total leaf area) was used in our study because it is a well-established measure of needle self-shading within a shoot (Carter and Smith 1985; Ishii et al. 2012). The measurement of $STAR_{max}$ of the shoots used for needle shape and size measurements showed no significant differences between sun and shade

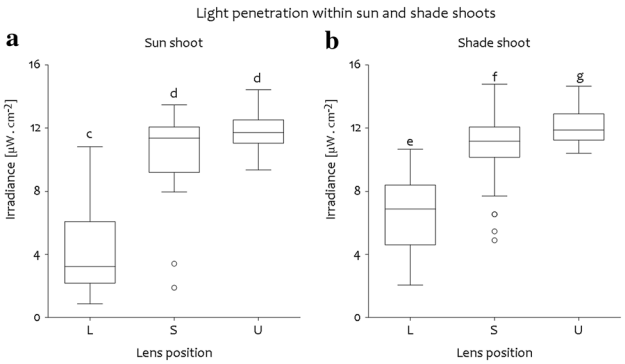

Fig. 2 Light penetration within sun and shade shoots. The irradiance was measured in laboratory conditions using only artificial illumination. The bottom and top edges of the boxes indicate the 25th and 75th percentiles. The lines indicate medians and whiskers extend up to 1.5 times the interquartile range from each box. The circles indicate the outliers. Significant differences were evaluated by the Tukey–Kramer multiple-comparison test. L—lower lens position, with the lower needles above the lens but avoiding shading by the woody twig; S—side lens position, with the lens within the side needles on a shoot; and U—upper lens position, with needle tips of upper needles at the same level as the lens. **a** Sun shoot: the significant differences determined are indicated by letters *c* and *d*. **b** Shade shoot: the significant differences are indicated by letters *e, f* and *g*

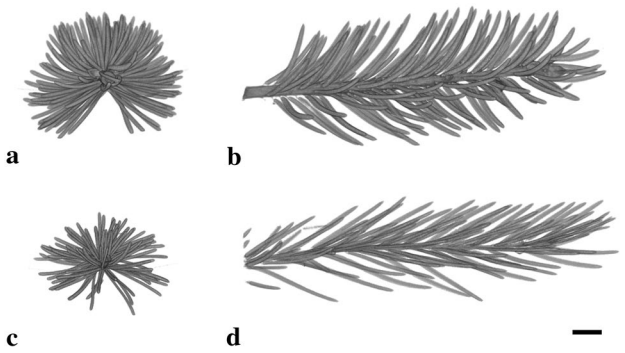

Fig. 3 Typical sun (**a, b**) and shade (**c, d**) needle shoot projections acquired using computed tomography (colours inverted). **a** Sun shoot projection taken from a shoot tip oriented towards the observer. **b** Side view of a sun shoot from the left side. **c** Shade shoot projection taken from a shoot tip oriented towards the observer. **d** Side view of a shade shoot from the left side. Bar corresponds to 5 mm. For 3D view see online videos (Online Resources 2, 3)

shoots in either CO_2 treatment, AC or EC. Sun shoots in AC exhibited a trend towards lower $STAR_{max}$ (0.21 ± 0.08) than did shade shoots (0.31 ± 0.05). In EC, however, the situation was reversed: sun shoots (0.34 ± 0.12) had a tendency to have higher $STAR_{max}$ in EC than did shade shoots (0.30 ± 0.06). The $STAR_{max}$ values in both CO_2 treatments were slightly higher than were the values for Norway spruce shoots presented in Stenberg et al. (1996) (ranging from 0.21 to 0.27). The $STAR_{max}$ of shoots used for the light microgradient measurements grown in AC also exhibited a weak trend towards lower $STAR_{max}$ for sun shoots (0.16 ± 0.03) than shade shoots (0.18 ± 0.02), with no differences being significant.

Irradiance caused lower chlorophyll mass-based contents in sun needles in comparison to shade needles ($p = 0.004$), irrespective of the CO_2 treatment ($p = 0.355$). Chlorophyll $a+b$ content was 5.14 ± 0.70 and 5.95 ± 1.13 mg $g^{-1}$for sun and shade needles, respectively, in AC and 4.70 ± 0.80 and 5.82 ± 1.36 mg $g^{-1}$for sun and shade needles, respectively, in EC.

Strong vertical gradients in irradiance led to significant ($p < 0.01$) within-canopy variation in A_{max} under both CO_2 treatments. Under EC conditions, A_{max} increased in both shoot ecotypes. A significant ($p < 0.01$) increase of 97% was recorded for shade shoots, while sun shoots showed only a 47% increase ($p < 0.05$). A_{max} reached values of 8.7 ± 1.2 and 12.8 ± 1.7 µmol CO_2 m^{-2} s^{-1} in sun shoots from trees grown under AC and EC conditions, respectively. In shade shoots, A_{max} values of 3.6 ± 1.2 and 7.1 ± 2.5 µmol CO_2 m^{-2} s^{-1} were found under AC and EC conditions, respectively.

The first three principal components of the shape covariance matrix manifest themselves in changes in the flatness, lateral asymmetry, and abaxial/adaxial asymmetry of the needle cross sections, respectively (Fig. 4). Complete analysis of section shapes (including three sections along needles) showed that the principal component PC1 corresponded to the flatness of the needle (reflecting the elongation of the cross section along the adaxial–abaxial axis, see Fig. 4) and was responsible for 70% of the total variance. The PC2 corresponded to needle cross section lateral asymmetry and was responsible for 14% of the total variance. The PC3 corresponded to abaxial/adaxial asymmetry and was responsible for only 9% of the total variance. The results of needle cross section shape analysis are visualized in Fig. 4. When only the middle position was analysed, PC1 was responsible for 66%, PC 2 for 17% and PC 3 for 10% of the total variance. Thus, this analysis proved that the change from circular to flatter cross sections, corresponding to changes in needle flatness (PC1), played the most important role in change of the needle cross section shape. For comparison of the mean shape of sections from different positions (i.e. needle base, middle, and tip), generalized Procrustes analysis showed that the tip section's shape differed from the other two sections' shapes according to the Bonferroni-corrected two-group Hotelling's T^2 test (tip–middle: $p < 0.001$, tip–base: $p < 0.001$, base–middle: $p = 0.048$) (Fig. 5a). Besides shape (shape without size) analysis, an analysis of form (shape and size combination) was also conducted (Fig. 5b). The form of the tip section differed from that of the other two sections according to the Bonferroni-corrected two-group Hotelling's T^2 test (tip–middle: $p < 0.001$, tip–base: $p < 0.001$, base–middle: $p = 0.018$). The tip section's distance between adaxial and abaxial edges was less than those of the middle and base sections.

For further analyses, only the middle cross sections were used. The mean shapes of middle sections of sun and shade needles were different according to the Bonferroni-corrected two-group Hotelling's T^2 test (sun–shade: $p < 0.001$, ambient–elevated: $p = 0.032$). They were flatter in shade needles than in sun needles (Fig. 5c). The mean shapes of middle sections of needles in ambient and elevated [CO_2] tended to differ in PC3 (Fig. 5e). The mean shapes of middle sections of upper, side, and lower needles on a shoot were significantly different according to the Bonferroni-corrected two-group Hotelling's T^2 test (upper–lower: $p < 0.001$, side–lower: $p = 0.56$, side–upper: $p = 0.033$) in PC1. Upper needles were less flat than side needles, while lower needles were flatter than side needles (Fig. 5d). The difference between upper and lower needles on a shoot was highly significant (Fig. 6). The upper needles were less flat in both CO_2 experimental conditions irrespective of irradiance according to the two-group Hotelling's T^2 test (sun and AC: $p = 0.002$, sun and EC: $p = 0.02$, shade and AC: $p = 0.023$, shade and EC: $p < 0.001$).

Needle orientation on a shoot, needle cross section position, [CO_2], irradiance on macroscale separately, and interaction of irradiance with all other factors had significant

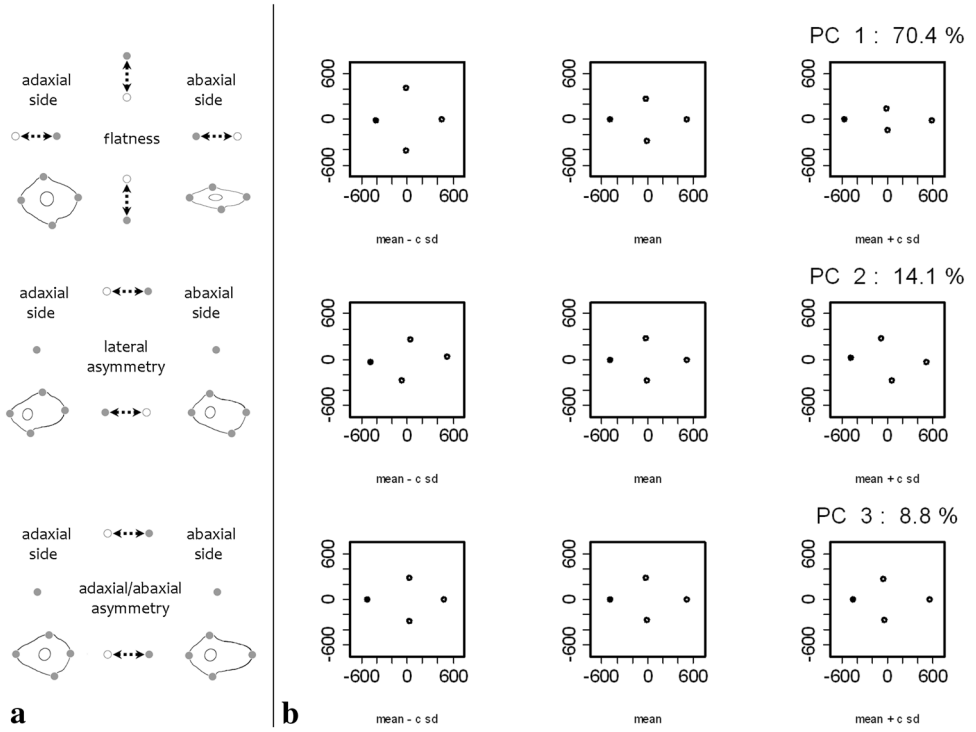

Fig. 4 Results of needle cross section shape analysis. The landmark configurations form a cloud in data space and the principal components show orthogonal directions in the cloud, along which the most pronounced changes in the configurations occur. The character of the changes in the landmark configuration (and the leaf cross section as well) with the position in the data cloud along the principal directions are plotted in the graphs. **a** Scheme of the extremes of the three main principal components of needle cross section shape shown by drawings and with full and empty grey circles depicting the extreme landmark positions. **b** Complete analysis of a needle cross section shape: shape variation corresponding to the first three principal components is visualized by changes in the landmark configuration caused by varying the values of principal components. The rows correspond to the principal components. The middle column shows the landmark configuration of the mean shape. The left (right) column shows the landmark configuration of the mean shape minus (plus) the first principal component multiplied by three times the standard deviation ($c=3$) along the principal component (respectively). Principal component 1 (PC1) corresponded to the flatness of the needle, PC2 to its lateral asymmetry, and PC3 to its abaxial/adaxial asymmetry. The units are μm

influence on needle cross-sectional area (Tables 1, 2). Sun needle cross-sectional areas were larger than shade needle cross-sectional areas. Upper needles had larger cross-sectional areas than did side needles, and side needles had larger cross-sectional areas than did lower needles. Sun needles had smaller cross-sectional areas in AC as compared to EC, while shade needles had mostly lower cross-sectional areas in EC as compared to AC (the exceptions being middle and tip cross sections of side needles). In both sun and shade needles, middle cross sections had larger areas than did tip cross sections. Sun needles had larger volumes than did shade needles in both CO_2 concentrations. The sun needle volume was significantly greater under elevated [CO_2] as compared to ambient [CO_2], but this difference was not observed in shade needles (Tables 1, 2). Mean needle length was significantly greater in sun needles as compared to shade needles. Upper needles were shorter. This explains why needle volume, in contrast to cross-sectional area, was not dependent on orientation. A smaller area was compensated by longer needle length (Tables 1, 2). Needle surface area was significantly larger in sun needles as compared to shade needles. Irradiance, CO_2 concentration, and their interaction significantly influenced needle surface area values (Tables 1, 2).

Discussion

Irradiance gradients: microscale within a shoot and macroscale within a crown

The strong irradiance microgradient within a shoot, observed as a consequence of needle spatial arrangement resulting in self-shading, was steeper in sun shoots. This circumstance was caused by sun shoot architecture and by the angle at which the needles were attached to the shoot. In addition, the sun shoots receive more direct light in comparison to shade shoots, as the ratio of direct to diffuse light decreases

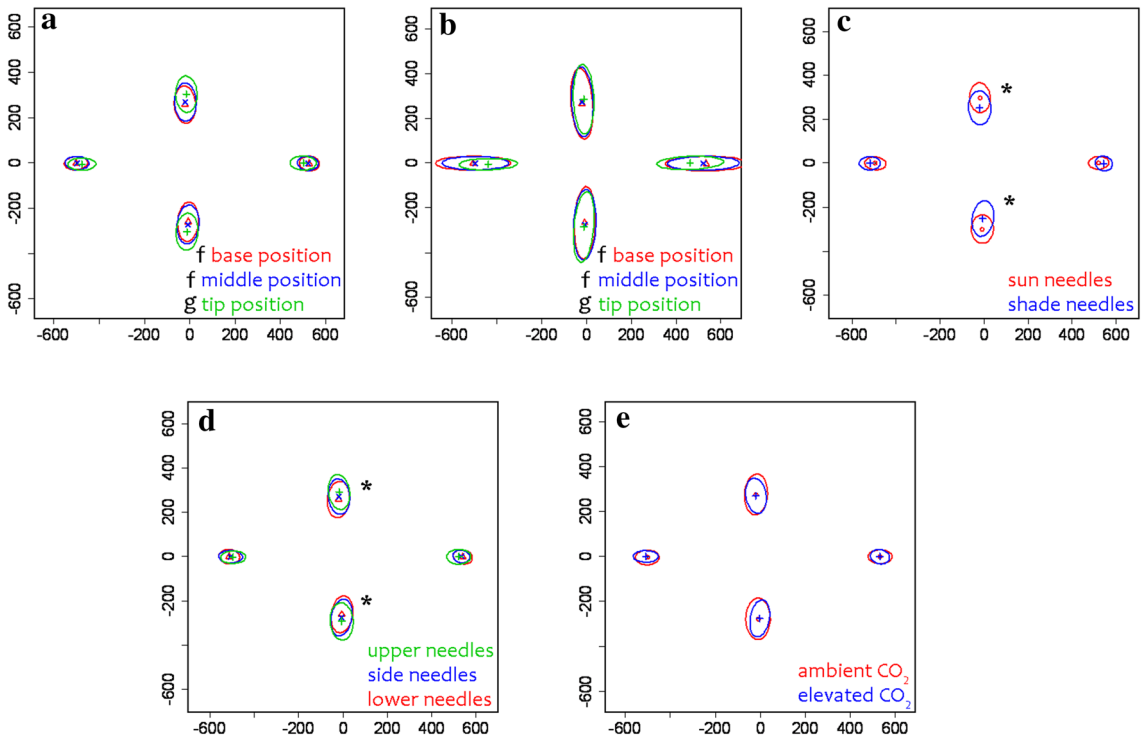

Fig. 5 The mean shape of needle cross sections affected by needle orientation on a shoot, irradiance, and CO_2 concentration. The character of the changes in the landmark configuration (and the leaf cross section as well) with the position in the data cloud along the principal directions is plotted in the graphs. For each tested group, mean landmark positions of all four landmarks with 95% confidence ellipses are shown. The units are µm. The differences were evaluated by Bonferroni-corrected two-group Hotelling's T^2 test and are indicated by the letters *f* and *g*. **a** Mean shape of needle cross sections from different positions: base, middle, and tip. The tip section shape differed from those of other sections (tip–middle: $p<0.001$, tip–base: $p<0.001$, base–middle: $p=0.048$). **b** Mean form (*shape* and size) of sections (generalized Procrustes analysis, not scaled) at different positions along the needle: base, middle, and tip (Fig. 1c). The tip section was obviously less wide and its form differed from that of other sections (tip–middle: $p<0.001$, tip–base: $p<0.001$, base–middle: $p=0.018$). **c** Mean shape of middle sections of sun and shade needles. The shapes were significantly different for PC1 (flatness) (sun–shade: $p<0.001$). **d** Mean shape of middle sections of upper, side, and lower needles. The shapes were significantly different for PC1: upper needles were less flat than side needles and side needles less flat than lower needles (upper–lower: $p<0.001$, side–lower: $p=0.56$, side–upper: $p=0.033$). **e** Mean shape of middle sections of needles in ambient and elevated [CO_2] (ambient–elevated: $p=0.032$). The shapes tended to differ in PC3 (adaxial/abaxial asymmetry)

down the forest canopy (Stenberg et al. 1998; Suzaki et al. 2003). The shade shoot morphology is thus adapted to utilize diffuse light incoming from various angles, while sun shoot morphology is adapted to avoid the negative effects of strong direct light and to enhance light diffusion into the canopy (Ishii et al. 2012). It should be mentioned, however, that our measurements were carried out under artificial, laboratory conditions, and thus the position of the shade shoot within a tree and its shading by other shoots was not simulated in this experiment.

Under natural conditions, the photosynthetic photon flux density usually reaches higher values in sun-exposed upper spruce canopy foliage (300–1000 µmol m^{-2} s^{-1}) than in shaded lower canopy foliage (0–100 µmol m^{-2} s^{-1}), as observed by Špunda et al. (1998) for a Norway spruce juvenile stand in Central Europe during a sunny day. Shade shoots are typically flat with fewer needles, and that explains why $STAR_{max}$ is generally higher in shade shoots as compared to sun shoots. We observed just that in trees grown under AC. Combining $STAR_{max}$ with photon recollision probability, needle spectral properties can be scaled up to shoot level (Rautiainen et al. 2012). Within-shoot heterogeneity in needle area density, and therefore, within-shoot light scattering is assumed to be the crucial parameters resulting in lower reflectance of coniferous canopies in comparison with that of broadleaved canopies in forest reflectance simulations (Rautiainen and Stenberg 2005). Provided that the total needle surface area did not differ among needles growing in different orientations on a shoot, we can assume that the needle surface is illuminated more evenly in shade shoots. This finding corresponds with the idea of there being a more even spatial distribution of photon–needle interactions in a shoot with a higher $STAR_{max}$ than in a shoot with a lower $STAR_{max}$ (Rautiainen et al. 2012). This result implies

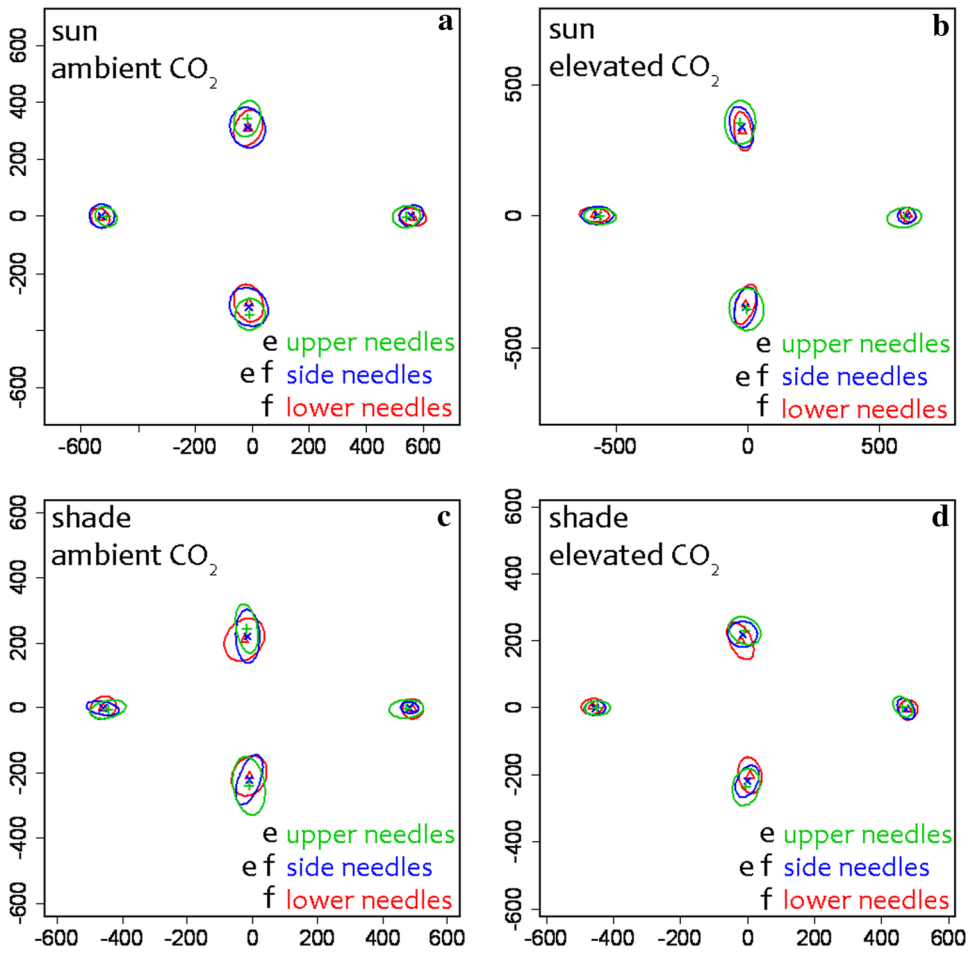

Fig. 6 Mean shape of middle needle cross sections sampled from different needle orientations on a shoot (upper, side, and lower). The character of the changes in the landmark configuration (and the leaf cross section as well) with the position in the data cloud along the principal directions are plotted in the graphs. Shown for each tested group are mean landmark positions of all four landmarks with 95% confidence ellipses. The units are µm. The differences were evaluated by the two-group Hotelling's T^2 test and are indicated by the letters *e* and *f*. **a** Sun needles, ambient [CO_2]. The difference between upper and lower needles was significant ($p = 0.002$). **b** Sun needles, elevated [CO_2]. The difference between upper and lower needles was significant ($p = 0.02$). **c** Shade needles, ambient [CO_2]. The difference between upper and lower needles was significant ($p = 0.023$). **d** Shade needles, elevated [CO_2]. The difference between upper and lower needles was significant ($p = 0.001$)

Table 1 Anatomical and morphological needle parameters for different positions along a needle and for needles from different orientations on a shoot (mean ± standard deviation)

CO2 concentration	Irradiance	Needle orientation	Mean area of sections (mm^2)			Needle parameter		
			Cross section position			Volume (mm^3)	Length (mm)	Surface area (mm^2)
			Base	Middle	Tip			
Ambient	Sun	Upper	0.812 ± 0.210	0.800 ± 0.198	0.722 ± 0.158	9.76 ± 3.59	12.16 ± 2.12	31.83 ± 8.19
		Side	0.713 ± 0.209	0.695 ± 0.205	0.625 ± 0.157	9.76 ± 3.66	14.00 ± 1.76	34.89 ± 7.92
		Lower	0.591 ± 0.158	0.595 ± 0.136	0.538 ± 0.101	8.34 ± 3.05	14.08 ± 2.20	32.93 ± 8.09
Ambient	Shade	Upper	0.462 ± 0.116	0.483 ± 0.119	0.451 ± 0.109	5.03 ± 1.96	10.56 ± 1.96	22.69 ± 5.74
		Side	0.393 ± 0.057	0.405 ± 0.095	0.370 ± 0.062	4.69 ± 1.08	12.08 ± 2.02	24.32 ± 4.50
		Lower	0.358 ± 0.044	0.365 ± 0.065	0.324 ± 0.051	4.51 ± 0.98	12.96 ± 2.34	25.27 ± 5.05
Elevated	Sun	Upper	0.905 ± 0.179	0.911 ± 0.155	0.869 ± 0.145	13.96 ± 4.07	15.28 ± 2.35	43.35 ± 8.61
		Side	0.807 ± 0.163	0.773 ± 0.117	0.707 ± 0.103	13.34 ± 4.43	17.12 ± 4.30	45.80 ± 13.07
		Lower	0.726 ± 0.124	0.703 ± 0.099	0.656 ± 0.082	12.86 ± 3.77	18.24 ± 4.05	47.15 ± 11.69
Elevated	Shade	Upper	0.434 ± 0.186	0.461 ± 0.190	0.431 ± 0.172	4.93 ± 3.40	10.24 ± 2.67	21.60 ± 9.61
		Side	0.388 ± 0.180	0.411 ± 0.176	0.374 ± 0.155	4.86 ± 3.41	11.28 ± 3.30	23.17 ± 11.38
		Lower	0.333 ± 0.159	0.342 ± 0.146	0.321 ± 0.121	4.35 ± 3.36	11.76 ± 3.74	23.17 ± 12.38

Table 2 Effects of environmental and spatial factors on geometric needle parameters of a cross section and needle size (analysis of variance table)

Analysis of variance table	Needle parameter							
	Cross section area		Volume		Length		Surface area	
	P value	*F* value	*P* value	*F* value	*P* value	*F* value	*P* value	*F* value
$[CO_2]$	$1.040e^{-06}$****	24.1998	$1.174e^{-07}$****	29.5292	$5.948e^{-05}$****	16.6084	$8.477e^{-07}$****	25.3416
Irradiance	$<2.2e^{-16}$****	1225.8381	$<2.2e^{-16}$****	310.6436	$<2.2e^{-16}$****	123.1260	$<2.2e^{-16}$****	222.1792
Position	$4.935e^{-05}$****	10.0312	na	na	na	na	na	na
Orientation	$<2.2e^{-16}$****	90.5685	0.1303	2.0528	$3.574e^{-07}$****	15.6364	0.1487	1.9186
$[CO_2]$:irradiance	$5.485e^{-10}$****	39.3903	$7.912e^{-08}$****	30.3745	$5.745e^{-10}$****	41.1603	6.823^{e-10}****	40.7763
$[CO_2]$:position	0.8605301	0.1502	na	na	na	na	na	na
Irradiance:position	0.0563199*	2.8863	na	na	na	na	na	na
$[CO_2]$:orientation	0.9354503	0.0667	0.9454	0.0562	0.9188	0.0847	0.8977	0.1079
Irradiance: orientation	0.0007872****	7.2065	0.7033	0.3524	0.7560	0.2800	0.9046	0.1003
Position:orientation	0.9565200	0.1641	na	na	na	na	na	na
$[CO_2]$:irradiance:position	0.9508716	0.0504	na	na	na	na	na	na
$[CO_2]$:irradiance:orientation	0.3864010	0.9519	0.7807	0.2478	0.4677	0.7620	0.6768	0.3909
$[CO_2]$:position:orientation	0.9781946	0.1124	na	na	na	na	na	na
Irradiance:position:orientation	0.9806475	0.1054	na	na	na	na	na	na
$[CO_2]$:irradiance:position:orientation	0.9612070	0.1540	na	na	na	na	na	na

na not applicable

Significance: * $p<0.1$; ** $p<0.05$; *** $p<0.01$; **** $p<0.001$

that for the upscaling of optical properties from needle to shoot levels, models presuming even distribution of photon–needle interactions (Rautiainen et al. 2012) would perform better for shade shoots.

The leaves in a tree canopy are able to adjust their structural and biochemical parameters to the specific light or temperature environment of a particular vertical crown layer (Bauerle et al. 2007), thereby maximizing their photosynthetic capacity (Niinemets 2007). In Norway spruce, the specific leaf area (SLA, leaf area per dry mass unit) and needle chlorophyll content decrease towards the crown top (e.g. Homolová et al. 2013). This vertical variation in SLA in conifers, which some authors explain by the decreasing gravitational component of water potential (Marshall and Monserud 2003), causes the vertical variation in area-based photosynthetic capacity to decline continuously from the upper to lower canopy (Ellsworth and Reich 1993; Niinemets2007; Urban et al. 2012b). On the canopy macroscale level, all morphological, biochemical (chlorophyll content), and physiological (CO_2 assimilation rate) parameters presented above confirmed the adaptations to incident irradiances leading to the formation of sun and shade photosynthetic apparatus. We deduce that the present variation in size and shape of needles on a microscale (within a shoot) was based on the needles' different exposure to irradiance, which probably caused differently functioning physiological processes such as light absorption and carbon assimilation in a manner similar to that seen on a macroscale (within a crown). Considering the findings discussed above, we accept our hypothesis H1 that within a shoot there is a microscale gradient in irradiance caused by needle self-shading.

Needle size and cross section shape on macroscale and microscale irradiance gradients

Our results obtained for geometrical parameters of sun and shade needles indicated that the differentiation in sun and shade ecotypes was in accordance with previous studies on conifers: mean needle length, volume, surface area, thickness, and cross-sectional area were significantly larger in sun needles as compared to shade needles. For example, Cescatti and Zorer (2003) reported that shade needles of *A. alba* were flatter as compared to the almost round sun needles. Similarly, Gebauer et al. (2011) found that shade needles of *P. abies* were shorter and thinner and had lower cross-sectional area than did sun needles. Furthermore, needles at the bottom position of the crown of black spruce *Picea mariana* Mill. (B.S.P.) were observed to have significantly smaller width than did needles at the top position of a crown (Major et al. 2013). In addition, Sprugel et al. (1996) reported that the most-exposed needles in *Abies amabilis* Dougl. ex Forbes were about 2.5 times thicker than the most-shaded ones.

Differences in needle cross section shape among upper, side, and lower needles detected within a shoot corresponded to the observed irradiance microgradient in both sun and shade shoots. The PCA revealed that the major component affecting needle cross section shape was needle flatness (PC1), which corresponds to observations made by other authors on sun and shade needles as presented above. In addition to needle flatness, the generalized Procrustes analysis enabled us also to evaluate the contribution of lateral and abaxial/adaxial asymmetries (PC2 and PC3, respectively) to cross section shape changes. Nevertheless, it was revealed that the latter two parameters made only minor contributions to needle cross section shape. This implies that needle flatness (PC1) is the major morphological parameter describing changes in cross section shape induced by the studied environmental factors.

We demonstrated that generalized Procrustes analysis is a powerful tool for detecting subtle intraspecific changes in needle morphology caused by various environmental factors. Needle shape is often assessed as the ratio of needle thickness to needle width as determined on the needle cross section (Sellin 2001; Apple et al. 2002; Palmroth et al. 2002; Gebauer et al. 2011, 2015; Homolová et al. 2013), or as the ratio of the perimeter and the major cross-sectional needle axis (Cescatti and Zorer 2003). Alternatively, it may be determined according to the width or thickness measured on fresh or scanned needles using a calliper tool (Sprugel et al. 1996; Major et al. 2013). Such approaches, however, reveal only some changes in needle shape or size. GPA, on the other hand, enables comparisons of shapes irrespective of the actual size of needle cross sections as well as comparisons of needle asymmetry. To our knowledge, this is the first study analysing needle cross section shapes by means of geometric morphometry using GPA. This approach enabled us to reveal even very subtle differences among shapes of cross sections in different positions along the needle. According to the argumentation presented above, we may accept our hypothesis H2 that needle size and cross section shape change similarly in sun and shade needle ecotypes according to their spatial orientation on a shoot.

Irradiance is a stronger morphogenic factor than is elevated CO_2 concentration

Our study was conducted on juvenile trees, which are generally presumed to be more CO_2-responsive in terms of needle anatomy and morphology than are mature trees. As expected, we detected significant CO_2-induced changes in cross-sectional area, needle volume, length, and surface area.

The sun needles under EC exhibited higher volume as compared to sun needles under AC. We thus conclude that sun needles under EC profited from both abundant light energy and high [CO_2]. To support this finding, we may discuss the study of Urban et al. (2012a) conducted on the same experimental trees in 2008. At that time, the light-saturated CO_2 assimilation rate per unit leaf area was 57% higher in current-year needles under EC as compared to AC (Urban et al. 2012a). Those trees, however, were up to 1 m tall and grew in an open canopy with no differentiation into sun and shade crown layers. The increase in light-saturated CO_2 assimilation rate under EC persisted until the canopy was closed and sun and shade shoots clearly differentiated. According to Terashima (2005), thicker needles are able to draw more CO_2 because CO_2 diffusion is easier due to there being more internal mesophyll area exposed to the intercellular spaces. When the internal leaf CO_2 concentration is high, the rate of photosynthesis is limited by the amount of regenerated ribulose-1,5-bisphosphate (RuBP) rather than by CO_2 availability. Consequently, RuBP regeneration is dependent on adenosine triphosphate synthesis via (1) availability of inorganic phosphate, and (2) the non-cyclic electron transport rate (Urban 2003). The rate of non-cyclic electron transport should be less limited by the amount of absorbed photosynthetic active radiation in sun needles than in shade needles.

In addition, the morphological needle parameters were significantly affected by the interaction between irradiance and [CO_2]. GPA revealed that irradiance on both macroscale and microscale had significant effect on needle cross section shape—and particularly on needle flatness (PC1)—that was in contrast to the effect of [CO_2]. Moreover, the shade shoots in our study exhibited reduced needle volume and thus adjusted to lower irradiance regardless of [CO_2]. Based on the lines of evidence presented above, we can accept our hypothesis H3 that irradiance is a stronger morphogenic factor than is elevated [CO_2].

Potential and limitations of the present study

The potential of the present study in terms of its linking to real forest conditions lies in the description of variability in various needle parameters of both sun and shade shoots due to an irradiance microgradient within a shoot. This gradient induced analogous needle variability in morphological and possibly physiological traits. It is important to consider this fact when sampling needles for anatomical and biochemical analyses, as the upper needles in both sun and shade shoots corresponded more to sun needle ecotype than did lower needles irrespective of [CO_2]. In future investigations, it would be beneficial to characterize physiological processes (light absorption, carbon assimilation) in needles oriented differently on the shoot to explain the described variation in needle structure parameters. However, determining photosynthetic parameters for single needles with different orientation on a shoot will be

a significant challenge. When using regular gas exchange equipment, a part of the whole shoot (i.e. with all needle orientations on it) is enclosed in the measurement chamber, thus preventing measurement of gas exchange for a single needle. Detaching the needles from a shoot for photosynthetic measurements is not feasible due to their small size and resulting rapid water loss. Another limitation of the present study is that the irradiance microgradient was measured on detached shoots under artificial laboratory conditions, without taking into account shading by other shoots in a real forest canopy. The purpose of the measurement, however, was to elucidate how shoot architecture influences light penetration within sun and shade shoots. We therefore focused only on the self-shading phenomenon within the shoot, not on the macroscale irradiance gradient within the tree crown. Moreover, similar controlled illumination of detached shoots has frequently been used to reveal the effects of the angle of incoming light on photosynthetic rate (Ishii et al. 2012) or optical shoot properties (Oker-Blom et al. 1988; Rautiainen et al. 2012).

Conclusions

In summary, all hypotheses were accepted. We confirmed that needle cross sections correspond to a more circular shape in sun needles and flatter shape in shade needles. The demonstration of a strong irradiance microgradient within a shoot as a consequence of needle self-shading may be regarded as a new and unique finding. The irradiance microgradient is steeper in sun shoots due to the needles' more homogeneous spatial distribution around a shoot axis as compared to shade shoots. Differences in needle cross section shape among upper, side, and lower needles detected within a single shoot corresponded to the observed irradiance microgradient in both sun and shade shoots. Upper needles exhibited more sun needle structural traits than did side and lower needles, particularly in terms of needle flatness. This implies that needle flatness is the major morphological parameter responding to the irradiance gradient on both microscale and macroscale. Furthermore, generalized Procrustes analysis proved that the irradiance, unlike CO_2 concentration, on both macroscale and microscale had a significant effect on needle cross section shape, and particularly on needle flatness. Based on the lines of evidence presented above, we conclude that irradiance was a stronger morphogenic factor than was elevated CO_2 concentration. Based on our study, we encourage the use of generalized Procrustes analysis in plant ecophysiological studies for evaluating environmentally induced changes in the shapes of plant organs and to do so not only on interspecific but also on intraspecific levels.

Author contribution statement ZK had the idea to evaluate Norway spruce needle shapes, participated in material collection, processed the needles, acquired the microscopic data, placed the landmarks, and contributed to writing the manuscript. JJ proposed the method of shape evaluation, performed the shape analysis and statistical tests in R, acquired the computed tomography data, and contributed to writing the manuscript. ZL assisted with study design, participated in material collection and results evaluation, and contributed to writing the manuscript. MŠ performed the gas exchange and chlorophyll measurements, evaluated photosynthetic traits at the shoot level, and contributed to manuscript revision. LK assisted with study design and results evaluation and contributed to writing the manuscript. JA assisted with study design and results evaluation and contributed substantially to the concept of the study and to writing the manuscript.

Acknowledgements This work was supported by the Czech Science Foundation [P501/10/0340], the Czech Academy of Sciences [RVO: 67985823], Charles University [SVV 260315], and the Ministry of Education, Youth and Sports of the Czech Republic [NPUI LO1417 and LO1415]. We also acknowledge the BioImaging Facility, Institute of Physiology, supported by the Czech-BioImaging large RI project funded by the Czech Ministry of Education, Youth and Sports [LM2015062], for support in obtaining scientific data presented in this paper. Our thanks also go to our colleagues from the research consortium of project P501/10/0340. We would like to thank, too, Miroslav Barták for technical help with shoot silhouette area measurement. We deeply appreciate the insightful comments of the reviewers, which led to the improvement of our article. The manuscript was edited by Gale A. Kirking, English Editorial Services.

Compliance with ethical standards

Conflict of interest The authors declare that they have no conflicts of interest.

References

Apple M, Tiekotter K, Snow M et al (2002) Needle anatomy changes with increasing tree age in Douglas-fir. Tree Physiol 22:129–136

Bauerle WL, Bowden JD, Wang GG (2007) The influence of temperature on within-canopy acclimation and variation in leaf photosynthesis: spatial acclimation to microclimate gradients among climatically divergent *Acer rubrum* L. genotypes. J Exp Bot 58:3285–3298. doi:10.1093/jxb/erm177

Carter GA, Smith WK (1985) Influence of shoot structure on light interception and photosynthesis in conifers. Plant Physiol 79:1038–1043

Cescatti A, Zorer R (2003) structural acclimation and radiation regime of Silver fir (*Abies alba* Mill.) Shoots along a light gradient. Plant Cell Environ 26:429–442

Dryden IL (2014) shapes Package. R Foundation for Statistical Computing, Vienna, Austria

Dryden IL, Mardia KV (1998) Statistical shape Analysis. John Wiley & Sons, Chichester

Eguchi N, Fukatsu E, Funada R et al (2004) Changes in morphology, anatomy, and photosynthetic capacity of needles of Japanese larch (*Larix kaempferi*) seedlings grown in high CO_2 concentrations. Photosynthetica 42:173–178

Ellsworth DS, Reich PB (1993) Canopy structure and vertical patterns of photosynthesis and related leaf traits in a deciduous forest. Oecologia 96:169–178. doi:10.1007/BF00317729

Fleck S, Niinemets U, Cescatti A, Tenhunen JD (2003) Three-dimensional lamina architecture alters light-harvesting efficiency in *Fagus*: a leaf-scale analysis. Tree Physiol Victoria 23:577–590

Gebauer R, Volarik D, Urban J et al (2011) Effect of thinning on anatomical adaptations of Norway spruce needles. Tree Physiol 31:1103–1113. doi:10.1093/treephys/tpr081

Gebauer R, Volařík D, Urban J et al (2015) Effects of prolonged drought on the anatomy of sun and shade needles in young Norway spruce trees. Ecol Evol 5:4989–4998

Hanba YT, Kogami H, Terashima I (2002) The effect of growth irradiance on leaf anatomy and photosynthesis in *Acer* species differing in light demand. Plant Cell Environ 25:1021–1030. doi:10.1046/j.1365-3040.2002.00881.x

Homolová L, Lukeš P, Malenovský Z et al (2013) Measurement methods and variability assessment of the Norway spruce total leaf area: Implications for remote sensing. Trees 27:111–121. doi:10.1007/s00468-012-0774-8

Ihaka R, Gentleman R (1996) R: A language for data analysis and graphics. J Comput Graph Stat 5:299–314. doi:10.1080/10618600.1996.10474713

Iio A, Fukasawa H, Nose Y et al (2009) Within-branch heterogeneity of the light environment and leaf temperature in a *Fagus crenata* crown and its significance for photosynthesis calculations. Trees 23:1053–1064. doi:10.1007/s00468-009-0347-7

Ishii H, Hamada Y, Utsugi H (2012) Variation in light-intercepting area and photosynthetic rate of sun and shade shoots of two *Picea* species in relation to the angle of incoming light. Tree Physiol 32:1227–1236. doi:10.1093/treephys/tps090

Kim G-T, Yano S, Kozuka T, Tsukaya H (2005) Photomorphogenesis of leaves: Shade-avoidance and differentiation of sun and shade leaves. Photoch Photobio Sci 4:770. doi:10.1039/b418440h

Klingenberg CP (2010) Evolution and development of shape: Integrating quantitative approaches. Nat Rev Genet 2010:623–635. doi:10.1038/nrg2829

Lhotáková Z, Urban O, Dubánková M et al (2012) The impact of long-term CO_2 enrichment on sun and shade needles of Norway spruce (*Picea abies*): Photosynthetic performance, needle anatomy and phenolics accumulation. Plant Sci 188–189:60–70. doi:10.1016/j.plantsci.2012.02.013

Lin J, Jach ME, Ceulemans R (2001) Stomatal density and needle anatomy of Scots pine (*Pinus sylvestris*) Are affected by elevated CO_2. New Phytol 150:665–674. doi:10.1046/j.1469-8137.2001.00124.x

Luomala E, Laitinen K, Sutinen S et al (2005) Stomatal density, anatomy and nutrient concentrations of Scots Pine needles are affected by elevated CO_2 and temperature. Plant Cell Environ 28:733–749

Major JE, Johnsen KH, Barsi DC, Campbell M (2013) Needle parameter variation of mature black spruce displaying genetic × soil moisture interaction in growth. Trees 27:1151–1166. doi:10.1007/s00468-013-0865-1

Marshall JD, Monserud RA (2003) Foliage height influences specific leaf area of three conifer species. Can J Forest Res 33:164–170. doi:10.1139/x02-158

Navrátil M, Špunda V, Marková I, Janouš D (2007) Spectral Composition of photosynthetically active radiation penetrating into a Norway spruce canopy: The opposite dynamics of the blue/red spectral ratio during clear and overcast days. Trees 21:311–320. doi:10.1007/s00468-007-0124-4

Neustupa J (2013) Patterns of symmetric and asymmetric morphological variation in unicellular green microalgae of the genus *Micrasterias* (Desmidiales, Viridiplantae). Fottea 13:53–63

Niinemets Ü (2007) Photosynthesis and resource distribution through plant canopies. Plant Cell Environ 30:1052–1071. doi:10.1111/j.1365-3040.2007.01683.x

Oker-Blom P, Smolander H (1988) The ratio of shoot silhouette area to total needle area in Scots pine. Forest Sci 34:894–906

Palmroth S, Stenberg P, Smolander S et al (2002) Fertilization has little effect on light-interception efficiency of *Picea abies* shoots. Tree Physiol 22:1185–1192. doi:10.1093/treephys/22.15-16.1185

Porra R, Thompson W, Kriedemann P (1989) Determination of accurate extinction coefficients and simultaneous equations for assaying chlorophylls a and b extracted with four different solvents: verification of the concentration of chlorophyll standards by atomic absorption spectroscopy. Biochim Biophys Acta 975:384–394

Rasband W (1997) ImageJ. US National Institutes of Health, Bethesda, Maryland, USA. https://imagej.nih.gov/ij/

Rautiainen M, Stenberg P (2005) Application of photon recollision probability in coniferous canopy reflectance simulations. Remote Sens Environ 96:98–107

Rautiainen M, Mõttus M, Yáñez-Rausell L et al (2012) A note on upscaling coniferous needle spectra to shoot spectral albedo. Remote Sens Environ 117:469–474. doi:10.1016/j.rse.2011.10.019

Reiter IM, Häberle K-H, Nunn AJ et al (2005) Competitive strategies in adult beech and spruce: space-related foliar carbon investment versus carbon gain. Oecologia 146:337–349. doi:10.1007/s00442-005-0146-9

Sanchez F, Orero A, Soriano A et al (2013) ALBIRA: a small animal PET/SPECT/CT imaging system. Med Phys 40:051906

Savriama Y, Klingenberg CP (2011) Beyond bilateral symmetry: geometric morphometric methods for any type of symmetry. BMC Evol Biol 11:1

Sellin A (2001) morphological and stomatal responses of Norway spruce foliage to irradiance within a canopy depending on shoot age. Environ Exp Bot 45:115–131

Sharp G, Kandasamy N, Singh H, Folkert M (2007) GPU-based streaming architectures for fast cone-beam CT image reconstruction and demons deformable registration. Phys Med Biol 52:5771

Sprugel DG, Brooks JR, Hinckley TM (1996) Effects of light on shoot geometry and needle morphology in *Abies amabilis*. Tree Physiol 16:91–98. doi:10.1093/treephys/16.1-2.91

Špunda V, Čajánek M, Kalina J et al (1998) Mechanistic differences in utilization of absorbed excitation energy within photosynthetic apparatus of Norway spruce induced by the vertical distribution of photosynthetically active radiation through the tree crown. Plant Sci 133:155–165

Stahl E (1883) Ueber den Einfluss des sonnigen oder schattigen Standortes auf die Ausbildung der Laubbläter. Gustav Fischer, Jena

Stenberg P (1996) Simulations of the effects of shoot structure and orientation on vertical gradients in intercepted light by conifer canopies. Tree Physiol 16:99–108. doi:10.1093/treephys/16.1-2.99

Stenberg P, Smolander H, Sprugel D, Smolander S (1998) Shoot structure, light interception, and distribution of nitrogen in an *Abies amabilis* canopy. Tree Physiol 18:759–767

Suzaki T, Kume A, Ino Y (2003) Evaluation of direct and diffuse radiation densities under forest canopies and validation of the light diffusion effect. J For Res-Jpn 8:283–290. doi:10.1007/s10310-003-0038-y

Terashima I (2005) Irradiance and phenotype: comparative eco-development of sun and shade leaves in relation to photosynthetic CO_2 diffusion. J Exp Bot 57:343–354. doi:10.1093/jxb/erj014

Thomas JF, Harvey CN (1983) Leaf anatomy of four species grown under continuous CO_2 enrichment. Bot Gaz 144:303–309

Urban O (2003) Physiological impacts of elevated CO_2 concentration ranging from molecular to whole plant responses. Photosynthetica 41:9–20

Urban O, Janouš D, Pokorný R et al (2001) Glass domes with adjustable windows: a novel technique for exposing juvenile forest stands to elevated CO_2 concentration. Photosynthetica 39:395–401. doi :10.1023/A:1015134427592

Urban O, Hrstka M, Zitová M et al (2012a) Effect of season, needle age and elevated CO_2 concentration on photosynthesis and Rubisco acclimation in *Picea abies*. Plant Physiol Bioch 58:135–141. doi:10.1016/j.plaphy.2012.06.023

Urban O, Klem K, Ač A et al (2012b) Impact of clear and cloudy sky conditions on the vertical distribution of photosynthetic CO_2 uptake within a spruce canopy. Funct Ecol 26:46–55. doi:10.1111/j.1365-2435.2011.01934.x

Viscosi V, Cardini A (2011) Leaf morphology, taxonomy and geometric morphometrics: A simplified protocol for beginners. PLoS One 6:e25630. doi:10.1371/journal.pone.0025630

Wellburn AR (1994) The spectral determination of chlorophylls *a* and *b*, as well as total carotenoids, using various solvents with spectrophotometers of different resolution. J Plant Physiol 144:307–313

Wylie R (1949) Differences in foliar organization among leaves from four locations in the crown of an isolated tree (*Acer platanoides*). Proc Iowa Acad Sci 189–198

Image Anal Stereol 2019;38:83-94 doi: 10.5566/ias.2005
Original Research Paper

UNBIASED ESTIMATION OF NORWAY SPRUCE (PICEA ABIES L. KARST.) CHLOROPLAST STRUCTURE: HETEROGENEITY WITHIN NEEDLE MESOPHYLL UNDER DIFFERENT IRRADIANCE AND [CO_2]

ZUZANA KUBÍNOVÁ[1], NATÁLIA GLANC[1], BARBORA RADOCHOVÁ[1,2], ZUZANA LHOTÁKOVÁ[1], JIŘÍ JANÁČEK[2], LUCIE KUBÍNOVÁ[2], JANA ALBRECHTOVÁ✉,[1]

[1]Department of Experimental Plant Biology, Faculty of Science, Charles University, Viničná 5, 128 44 Prague 2, Czech Republic; [2]Department of Biomathematics, Institute of Physiology of the Czech Academy of Sciences, Vídeňská 1083, 142 20 Prague 4, Czech Republic
e-mails: kubinova@natur.cuni.cz, glanc.nat@gmail.com, barbora.radochova@fgu.cas.cz, zuzana.lhotakova@natur.cuni.cz, jiri.janacek@fgu.cas.cz, lucie.kubinova@fgu.cas.cz, jana.albrechtova@natur.cuni.cz.
(Received August 29, 2018; revised January 25, 2019; accepted February 11, 2019)

ABSTRACT

The main objective of this study was to find out whether the selected chloroplast characteristics measured in the mesophyll layer nearest to the needle surface (*i.e.*, the first mesophyll layer) could be representative for the whole needle cross section. Two chloroplast sampling approaches were applied on Norway spruce needles during the investigation of the effects of different levels of air CO_2 concentration and irradiance: (i) sampling only from the first mesophyll layer, and (ii) systematic uniform random (SUR) sampling. The selected characteristics were: (i) chloroplast area, (ii) starch grain area, and (iii) starch areal density on median chloroplast cross sections, and (iv) chloroplast number per unit of needle volume. It was shown that the first mesophyll layer was not representative for estimating all evaluated characteristics except the chloroplast area. Sampling only there caused obtaining slightly biased results, while SUR sampling gave unbiased estimations at the cost of longer measuring time. The major effect of studied factors was in starch areal density and starch grain area, which were larger in sun needles in elevated CO_2 concentration in comparison with sun needles in ambient CO_2 concentration. In conclusion, it was demonstrated that the first layer of mesophyll is not always representative for the needle cross section. If technically feasible, SUR is recommended for analysis of chloroplast ultrastructure. The simplified sampling design can be applied, *e.g.,* for comparisons of many different treatments. However, it should be combined with other approaches to characterize the chloroplast function and the results carefully considered and interpreted.

Keywords: chloroplast number, chloroplast ultrastructure, elevated CO_2, needle anatomy, stereology.

INTRODUCTION

Chloroplasts are the photosynthetic organelles of plant cells. They absorb solar energy to run carbon fixation, during which the carbon from CO_2 is built into organic compounds. The atmospheric concentration of CO_2 is ever increasing (ESRL, 2018); therefore, the global carbon cycling process is affected. Forest trees significantly participate in carbon cycling representing an important carbon sink (rev. Calfapietra *et al*., 2010). One such important species is the Norway spruce (*Picea abies* L. Karst.), currently the most abundant conifer in Central European forests. Due to its importance and abundance, appropriate approaches to study its responses to environmental factors, including changes of chloroplast structural characteristics, are of great importance.

Trees are known to accommodate their growth based on sink prioritization in response to environmental factors (Polák *et al*., 2006). Under elevated CO_2 concentration (EC), plants may invest the extra carbon to their growth or to the production of secondary metabolites (Gebauer *et al*., 1997; Räisänen *et al*., 2008). Moreover, as a result of EC, leaf anatomy (Lin *et al*., 2001; Eguchi *et al*., 2004) and chloroplast ultrastructure (Pritchard *et al*., 1997; Sallas *et al*., 2003; Günthardt-Goerg and Vollenweider, 2015) may change. Nevertheless, the effect of CO_2 on mesophyll structural characteristics and phenolics accumulation can be ambiguous, as Lhotáková *et al*. (2012) found no change, even though enhanced light-saturated CO_2 assimilation rates and reduced dark respiration in the current-year needles were observed. Irradiance is apparently a stronger morphogenetic factor than EC,

principally affecting needle differentiation and phenolics content (Lhotáková *et al*., 2012), and needle shape even within an irradiance gradient on a shoot (Kubínová *et al*., 2018).

Thus, to study the chloroplast ultrastructure and its quantitative characteristics, careful consideration should be taken concerning the methods applied, including relevant chloroplast sampling for measure-ments, so as to yield unbiased estimations of the observed characteristics.

Chloroplasts can be easily detected using light microscopy; however, its resolution is insufficient for observation of their ultrastructure. Chloroplast ultrastructure, including starch grain cross-section area and the arrangement of the thylakoid membrane system is usually studied on images acquired by transmission electron microscopy (TEM). Because it is difficult to obtain series of ultrathin sections, the studies are usually done on single TEM sections (*e.g.,* Albertsson and Andreasson, 2004; Kubínová and Kutík, 2007; Demmig-Adams *et al*., 2015). The comparability of 3D characteristics estimated on 2D cross sections between samples is usually ensured by analysing only those chloroplasts that are sectioned in the middle perpendicularly to the prevailing plane of thylakoid membranes, *i.e.*, in their median cross section (FIG 1C, D; Sharkova and Bubolo, 1996; Kutík *et al*., 2004).

For chloroplast ultrastructural studies in broad leaves, the first or upper layers of leaf photosynthetic tissue, mesophyll, (Fig. 1A) are often analysed (Günthardt-Goerg *et al*., 2000; Wheeler and Fagerberg 2000; Valkama *et al*., 2003; Velikova *et al*., 2009; Sun *et al*., 2011; Mašková *et al*., 2017). The first layer of mesophyll receives more incident irradiance than its deeper layers and thus, it can be regarded as the most important layer for photosynthesis. This is also true for conifer needles, where the chloroplast ultrastructure in the outermost mesophyll layer was found to be the most affected by the environmental factors (Anttonen, 1992; Kivimäenpää *et al*., 2005). Many studies of conifer needle ultrastructure do not specify in detail the part of the needle or the place on needle cross section used for measurements (Palomäki *et al*., 1996; Pritchard *et al*., 1997; Kainulainen *et al*., 2000; Lepeduš *et al*., 2001; Demmig-Adams *et al*., 2015). Depending on the type of study, chloroplasts are sampled only from one part of a needle (Utriainen *et al*., 2000; Jönsson *et al*., 2001; Sallas *et al*., 2003; Siefermann-Harms *et al*., 2004) or from the sun-exposed side of a needle and the mesophyll layer closest to the centre of a needle (Soikkeli, 1978; Wulff *et al*., 1996; Kivimäenpää 2003; Kivimäenpää *et al*., 2014).

In order to quantify leaf structure, it is necessary to be aware of possible heterogeneity within the leaf and existing leaf anatomic gradients. A gradient in both irradiance and carbon dioxide concentration is known to exist inside the broad leaves (Parkhust *et al*., 1988; Smith *et al*., 1997) and irradiance gradient was also recorded within the needle (DeLucia *et al*., 1992). In our previous study, we observed a gradient in Norway spruce needle section shape based on the irradiance microgradient within a shoot due to self-shading of needles (Kubínová *et al*., 2018). It is probable that irradiance microgradient within a needle affects the chloroplast ultrastructure. However, information about the heterogeneity of chloroplast characteristics within needles is still scarce. For example, it was shown that chloroplast alterations caused by ozone are more pronounced in the outer mesophyll cell layers and in the upper side of the needle compared to the inner mesophyll layers and lower side of the needle (Kivimaënpää *et al*., 2005). This information is essential for proper sampling design for quantitative studies where the absolute values for the whole leaf are needed. As far as we know, no study has yet systematically tested different parts of Norway spruce mesophyll in the sense of representativeness for the whole needle cross section.

In the present study, we focused on methodical and ecophysiological aims. The methodical aim was to test the assumption of the first mesophyll layer representativeness for the whole needle cross section regarding four selected chloroplast characteristics: chloroplast density in mesophyll, chloroplast size, starch grain area and starch areal density. We have compared characteristics of chloroplasts selected within the cells in the first mesophyll layer and cells from systematically uniform randomly selected positions within the mesophyll. The ecophysiological aim was to test whether the selected chloroplast characteristics are influenced by CO_2 concentration and irradiance, and to what extent.

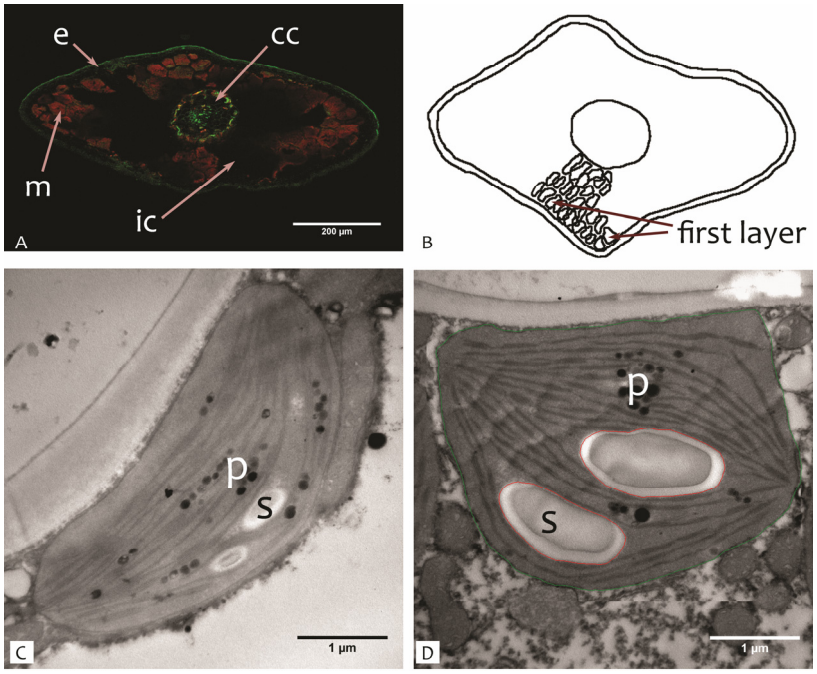

Fig. 1. *Needle cross section and chloroplasts. A – Confocal image of needle cross section, bar 200 µm; m – mesophyll with chloroplasts fluorescent in red, cc – central cylinder, ic – intercellular space, e – epidermis and hypodermis fluorescent in green. B – Scheme showing location of the first mesophyll layer in the needle cross section. C – TEM image of SUR sampled chloroplast from a deeper mesophyll layer, bar 1 µm. D – TEM image of chloroplast (encircled by a green line) from the first mesophyll layer, bar 1 µm; s - starch grains (encircled by a red line); p – plastoglobuli.*

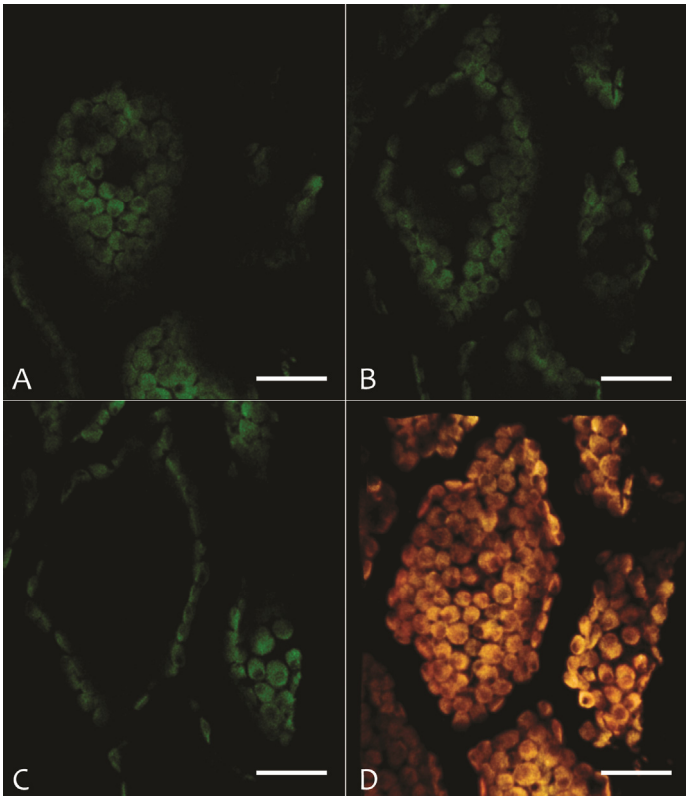

Fig. 2. *Confocal images of Norway spruce mesophyll cells. A, B, C – single optical cross sections 1.95 µm apart with visible, autofluorescent chloroplasts (in green) showing that chloroplasts are located in the narrow cytoplasm layer below the cell membrane; D – volume rendering showing chloroplasts within 21 µm thick layer. Bar 20 µm.*

MATERIAL AND METHODS

EXPERIMENTAL SITE AND SAMPLE COLLECTION

Norway spruce needles were collected from the experimental site of CzechGlobe AS CR in Moravskoslezské Beskydy (Beskid Mountains, Czech Republic), where the glass domes had controlled levels of CO_2 concentration; with ambient atmospheric CO_2 concentration (AC) and elevated CO_2 concentration (EC = 700 ppm) (Urban *et al*., 2001). The comparison was done separately in four combinations of CO_2 concentration and irradiance: sun needles in ambient CO_2 (AC sun), shade needles in ambient CO_2 (AC shade), sun needles in elevated CO_2 (EC sun) and shade needles in elevated CO_2 (EC shade). Current-year sun (3^{rd} whorl) and shade (6^{th} whorl) needles from both CO_2 concentrations were collected in October 2011 from south- and south-west-facing branches of 11-year-old trees grown under these experimental conditions from the year 2005. The tree crowns were differentiated into sun and shade crown parts. For chloroplast counting, whole needles were frozen for confocal microscopy (Lhotáková *et al*., 2008). For ultrastructural analysis, segments (about 1 mm long) from the middle part of the needle were immediately fixed in 5% glutaraldehyde (v/v) and transported to the laboratory.

TRANSMISSION ELECTRON MICROSCOPY

In the laboratory, the fixed samples were transferred into an automated microwave tissue processor Leica EM AMW (Leica Microsystems, Vienna, Austria). All steps of sample preparation were carried out automatically following the protocol according to Zechmann and Zellnig (2009). Samples were then manually transferred into the polymerization forms containing fresh Spurr's epoxy resin (Spurr, 1969) and polymerised at 70 °C for 48 h.

Ultrathin sections (70 nm) were cut by an ultramicrotome (Leica EM UC7, Leica Microsystems, Vienna, Austria) and mounted on 1 × 2 mm formvar coated slot grids. Images of needle cross sections and of individual chloroplasts were captured using transmission electron microscope JEOL JEM 1011 (JEOL, Tokyo, Japan).

For the analysis of chloroplast size and starch grain area and areal density, two different approaches were chosen. Firstly, chloroplasts from the first layer of mesophyll cells below the hypodermis (Fig. 1A) were chosen systematically, one from each third, fourth or fifth cell depending on the number of cells on a needle cross section, so that at least 7 chloroplasts per needle cross section were sampled. Secondly, chloroplasts from the whole needle cross sections (images captured at low magnification, 100×) were chosen using stereological systematic uniform random (SUR) sampling (Gundersen and Jensen, 1987). At least 5 sampling fields were selected using our custom-made plug-in 'Rectangles' (Ellipse software, Vidito, Košice, Slovakia) (Fig. 3), and the first nearly median section of chloroplast from the middle of the sampling field was then captured for measurements (at 25,000 × magnification).

LASER SCANNING CONFOCAL MICROSCOPY

For laser scanning confocal microscopy, a cross section was made in the middle of the needle using a hand microtome. Series of optical sections were captured by Leica SP2 AOBS confocal laser scanning microscope (Ar laser excitation 488 nm and autofluorescence detection in green and red channels: 494-577 nm and 625-710 nm). For chloroplast number estimation in the whole needle cross section, the procedure described in Kubínová *et al*. (2014) was applied: sampling fields were selected using systematic uniform random sampling (SUR, Fig. 3 A) in the image captured by 10× objective (Fig. 1A). Detailed series were acquired by 63× objective. For chloroplast number estimation in the first mesophyll layer, 5 sampling fields around the needle in the image by 10× objective were selected using systematic sampling in the newly developed 'Object sampling' plug-in (Ellipse software, Vidito, Košice, Slovakia) (Fig. 3B). Detailed series were acquired by 63× objective (water immersion, NA 1.2, Fig. 2).

STEREOLOGICAL MEASUREMENTS

We compared chloroplast parameters acquired from the first mesophyll layer with those acquired from different positions on needle cross sections selected by SUR. In total, 215 chloroplasts from the first mesophyll layer and 183 chloroplasts selected by SUR were analysed to estimate the starch grain area, chloroplast area and starch areal density. For chloroplast number estimation, 100 and 104 series of confocal microscope images from the first mesophyll layer and selected by SUR, respectively, were analysed.

Starch grain cross-section size and starch areal density were determined on chloroplast median cross sections in TEM images using the method of interactive segmentation, based on drawing a line along the borders of the object under study using the software Ellipse (ViDiTo, Košice, SR).

Chloroplast number was estimated by the optical disector method (Kubínová *et al.*, 2014) from the series of optical sections acquired by the confocal microscope using 63× objective. For each needle, the number of chloroplasts per unit of needle volume was estimated by the formula (Sterio, 1984; Gundersen, 1986) (each term defined below):

$$estN_{Vneedle}(chl) = \frac{\sum_{i=1}^{n} Q_i(chl)}{\sum_{i=1}^{n} P_i} \cdot \frac{p}{a \cdot h}, \qquad (1)$$

$estN_{Vneedle}$ *(chl)* – estimated number of chloroplasts per unit of needle volume;
$Q_i(chl)$ – sum of all sampled chloroplasts in all disector probes within a needle;
$\sum P_i$ – sum of all points falling within a needle in all 3D probes (for calculation needle volume in each probe) used for chloroplast counting;
p – number of test points in a grid in a sampling frame used for chloroplast counting;
a – area of disector sampling frame (base of the 3D probe) used for chloroplast counting;
h – height of the disector probe used for chloroplast counting.

STATISTICAL ANALYSES

Two sample unequal variance t-tests were used for testing the hypothesis whether the first mesophyll layer is representative for the whole needle cross section. Chloroplast number in mesophyll, chloroplast cross-section area, starch grain cross-section size and starch grain areal density were compared for each combination of CO_2 concentration and irradiance separately. The second step to test representativeness of first mesophyll layer one–way analysis of variance (ANOVA) and Tukey-Kramer Multiple-Comparison test was employed on two different datasets of chloroplast characteristics acquired from 1) the first mesophyll layer and 2) from SUR. These results of one–way ANOVA were compared to evaluate the representativeness of the first mesophyll layer.

To evaluate the effects of CO_2 and irradiance on chloroplast characteristics, two-way nested ANOVA was then employed using NCSS 9.0 software (NCSS, LCC Kaysville, Utah, USA). This type of ANOVA takes into account that sun and shade needles from one tree are not independent observations. The individual tree replicates were evaluated as a nested factor (subject variable), while CO_2 treatment, and irradiance were used as fixed between factor variables. Differences were always considered as significant if $p < 0.05$.

RESULTS

The time needed for chloroplast sampling by SUR was approximately six times longer than for selecting suitable chloroplasts from the first mesophyll layer.

In all four cases studied, the chloroplast number and chloroplast area estimated by evaluation of the first mesophyll layer were not significantly different from the chloroplast number and area measured in the whole needle cross section (Fig. 4 A, B). Thus, at this stage, we could not reject the hypothesis that chloroplast number and chloroplast area measurements in the first mesophyll cell layer were representative for the whole needle cross section. In three of four cases (AC shade, EC sun, EC shade) there was also no significant difference between both starch area and starch areal density assessed from the first mesophyll layer and the whole needle cross section (Fig. 4 C, D). However, both characteristics behaved differently in sun needles under ambient CO_2: starch area and starch areal density were significantly higher when assessed from the whole needle cross section in comparison with the first mesophyll layer (indicated by asterisks in Fig. 4 C, D). Regarding both the starch grain area and starch areal density, we thus cannot claim the first mesophyll layer as representative for the whole needle cross section. If we assume that the first mesophyll layer is representative for the whole needle regarding studied chloroplast characteristics, we should obtain identical results of

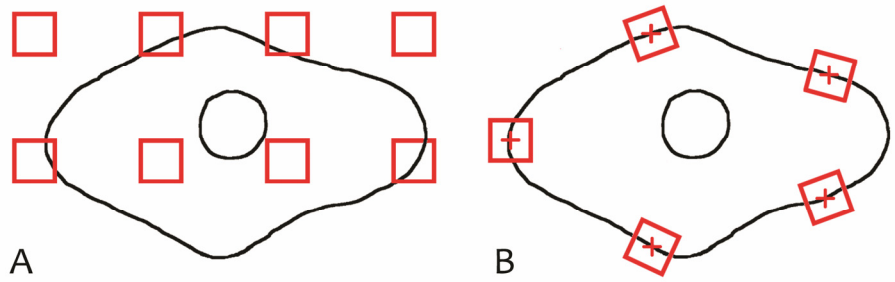

Fig. 3. *Scheme of sampling of series of images by confocal microscopy on needle cross section. A – Systematic uniform random sampling using Ellipse plug-in 'Rectangles'. B – sampling in the first mesophyll layer using polygonal selection and Ellipse plug-in 'Object Sampling' to determine equidistant midpoints (crosses) of images captured using field rotation in the microscope.*

ANOVA from both datasets. However, this was not the case for all the characteristics studied (Table 1). The chloroplast number appeared to be significantly affected by CO_2 concentration if tested on SUR sampled dataset. On the contrary, no effect of either CO_2 concentration or irradiance was revealed if the dataset from the first mesophyll layer was used for analysis. In case of starch areal density, significant effect of both CO_2 concentration and irradiance was detected for both datasets. However, the interaction of the environmental factors was significant only if the dataset from the first mesophyll layer was analysed. Therefore, we express an uncertainty regarding the representativeness of the first mesophyll layer for chloroplast number and starch areal density. On the other hand, both chloroplast area and starch grain area showed consistent ANOVA results for both datasets, with only the p-values slightly differing between the samplings (see p-values for CO_2 concentration and interaction for starch grain area in Table 1).

Based on the comparisons presented above, we put in doubt the representativeness of the first mesophyll cell layer regarding three of four studied chloroplast characteristics: chloroplast number, starch grain area and starch areal density. The only characteristic, for which we did not clearly reject the first layer representativeness hypothesis, was the chloroplast area.

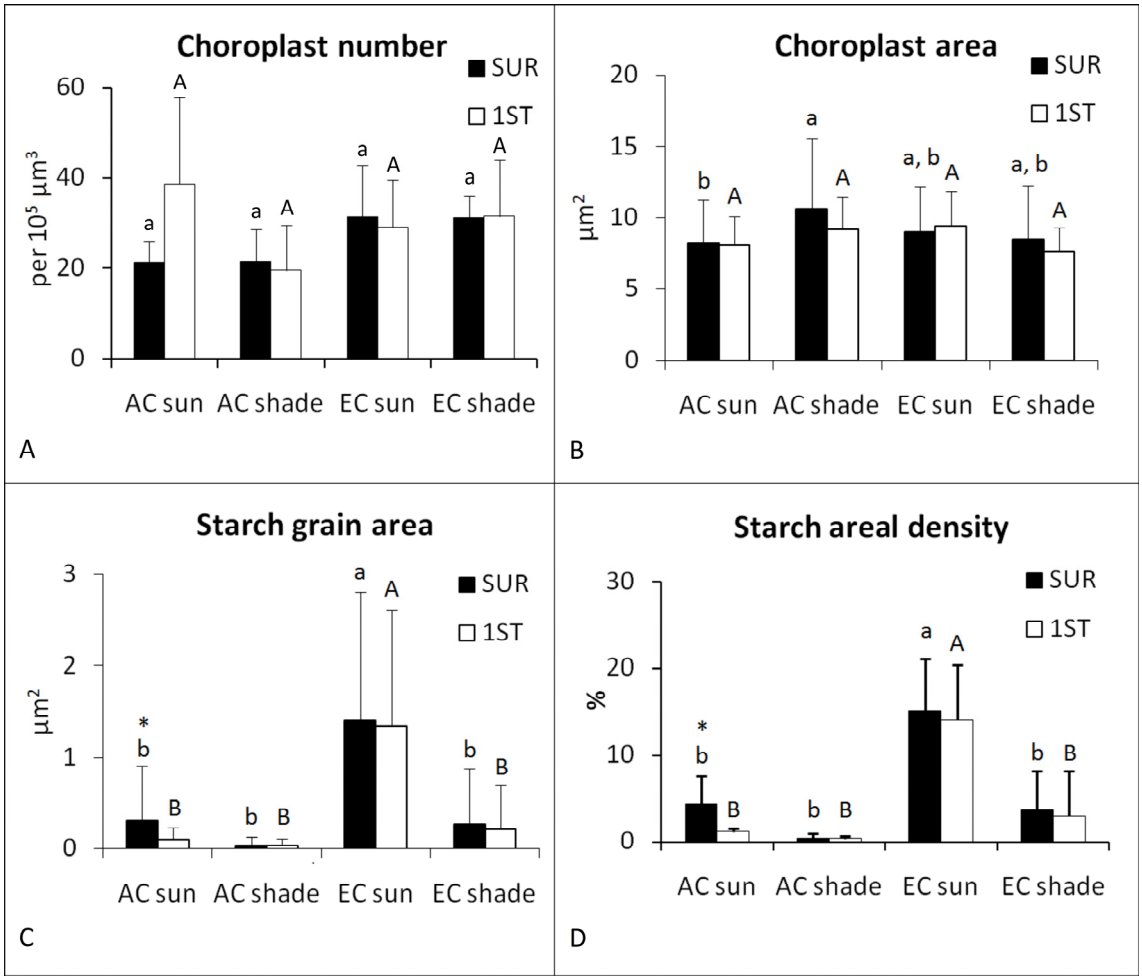

Fig. 4. *Comparison of chloroplast characteristics sampled from the first mesophyll layer (1ST) and systematic uniform random sampling (SUR). A – Chloroplast number per mesophyll volume. B – Chloroplast cross-section area. C – Starch grain cross-section area. D – Starch areal density on chloroplast cross section. AC – ambient CO_2 concentration, EC – elevated CO_2 concentration, black – SUR – systematically uniformly randomly sampled from the whole needle cross-section area, white – 1ST – sampled from the first layer of mesophyll. Bars – standard deviation.* – significant difference between SUR and the first layer within the same growth conditions at $p < 0.05$ by two-sample t-test. Lower case letters above the bars – Tukey-Kramer Multiple-Comparison Test among SUR values, upper case letters above the bars – Tukey-Kramer Multiple-Comparison Test among 1ST values; bars having the same letter are not significantly different according to the test.*

Table 1. *Effects of CO_2 concentration, irradiance and interaction of both factors on chloroplast number per mesophyll volume and selected ultrastructural characteristics on median chloroplast cross section analysed by Two-way nested Analysis of Variance (p-value). SUR – sampled systematically uniformly randomly from the whole needle cross-section area. First layer – sampled from the first layer of mesophyll. AC – ambient CO_2 concentration, EC – elevated CO_2 concentration. Significance: * = p<0.05; ** = p<0.01; n.s. = not significant.*

Structural characteristic	Factor	SUR		First layer	
		p value	Significance	p value	Significance
Chloroplast number	Irradiance	0.979370	n.s.	0.166354	n.s.
	CO_2	0.022420	*	0.861250	n.s.
	Interaction	0.960103	n.s.	0.083487	n.s.
Chloroplast area	Irradiance	0.051896	n.s.	0.540956	n.s.
	CO_2	0.394268	n.s.	0.843852	n.s.
	Interaction	0.010480	*	0.040781	*
Starch grain area	Irradiance	0.004692	**	0.004037	**
	CO_2	0.004592	**	0.015830	*
	Interaction	0.044399	*	0.007329	**
Starch areal density	Irradiance	0.003792	**	0.001111	**
	CO_2	0.005008	**	0.013513	*
	Interaction	0.093614	n.s.	0.002512	**

Assuming that we cannot consider the first mesophyll layer to be fully representative for all studied chloroplast characteristics, emphasis was put on evaluation of the EC and irradiance effects based on the characteristics acquired by systematic uniform random sampling. A nested analysis of variance, which considered that sun and shade needles were col-lected from one tree, revealed significant effects of CO_2 concentration on chloroplast number, starch grain area and starch areal density (Table 1). Chloroplasts were more abundant in needles from trees grown under EC in comparison with those grown under AC (Fig. 4 A), however, according to the multiple comparison test, the differences were not significant. The chloroplast area was not affected by CO_2 concentration (Fig. 4 B), but in the chloroplasts from sun needles in EC, the starch grain area and starch areal density were larger (Fig. 4 C, D). The irradiance was found to have no effect on either chloroplast number or chloroplast area (Table 1). However, there was a significant interaction between CO_2 and irradiance. This corresponds with the result of the multiple comparison Tukey-Kramer test, which showed a significant difference in chloroplast area between sun and shade needles grown under ambient CO_2 concentration but not in EC. Furthermore, the characteristics describing starch accumulation were strongly sensitive to irradiance. In EC, chloroplasts from the shade needles had lower starch grain area and starch areal density. According to the multiple comparison Tukey-Kramer test, both starch characteristics were significantly higher in sun needles from EC in comparison with the rest three CO_2 and irradiance combinations (Fig. 4 C, D).

The same statistical analysis applied on the chloroplast characteristics assessed from the first mesophyll layer showed slightly different results than on SUR. The effect of EC on chloroplast number was not detected, probably due to high variance and higher values of this characteristic in sun needles grown in ambient CO_2 concentration (Fig. 4A; Table 1). The effect of EC on starch grain area and starch areal density was significant, however slightly weaker in the first layer (see p-values for the first layer in Table 1). Lastly, the significance of the interaction between irradiance and CO_2 concentration was more pronounced for starch grain area and starch areal density (see p-values for the first layer in Table 1). Thus, for the majority of the studied structural characteristics, irradiance proved to be a stronger morphogenetic factor than EC.

DISCUSSION

Despite the clear importance of proper sampling in measurements of plant structure, this issue is often inadequately addressed in plant studies as pointed out recently by Kubínová *et al*. (2017). If the study aims for estimation of unbiased quantitative parameters for the whole plant organ, then SUR and stereological methods are recommended (West, 2012).

In this study, selected chloroplast characteristics measured on the same needle cross section sampled in the first mesophyll layer and sampled by SUR were

in some cases significantly different. Thus, the first mesophyll layer was not always representative for every structural characteristic and every treatment. This is in agreement with the findings of Kivimäenpää and Sutinen (2007) who reported that mesophyll cells near the epidermis of four year old needles of *Pinus sylvestris* had smaller chloroplasts with lower area of starch grains than cells in the inner part of the needle. Furthermore, Senser *et al*. (1975) noticed in *Picea abies* that the chloroplasts in cells near to the epidermis had higher amounts of starch than cells near the central cylinder, according to the gradient in light intensity. Both studies confirm the variability of measured structural characteristics within the needle cross section.

Taking into account that measurements of chloroplast ultrastructure are extremely time consuming, we restricted our study to cross sections cut in the middle of the needle and not in a higher number of positions along the needle corresponding to a SUR sampling principle (for needle see *e.g.*, Lhotáková *et al*., 2008). Even this restricted examination clearly reveals that sometimes chloroplast structural characteristics measurements give different results when evaluated from all layers of mesophyll cells in the needle than just in the first mesophyll layer. Unlike the evaluation of chloroplast ultrastructure where TEM is necessary, the measurement of plant anatomical characteristics is feasible by confocal microscopy (Albrechtová *et al*., 2007). This approach is much less time consuming than procedures necessary for ultrastructure measurements using TEM, and thus SUR sampling of needle sections can be recommended for proper chloroplast counting. This was shown by Kubínová *et al*. (2014) where the practical issues connected with the evaluation of thick needle sections by using confocal microscopy are discussed in detail.

In studies of chloroplast characteristics, description of sampling procedure on TEM images is often restricted to mere stating of how many cells were counted in a cross section, while further details of sampling within the section are omitted (Back and Huttunen, 1992; Oksanen *et al*., 2001; Bondada and Syvertsen, 2003). The SUR sampling is theoretically the best choice for unbiased measurement. However, it should be noted that using SUR on TEM images of conifer needles requires good fixation that can be challenging because of the thick, nearly impermeable cuticle, the extremely differentiated cell walls, with deposition of phenolics or even lignin (Soukupová *et al*., 2000), and a system of intercellular spaces (Meyberg, 1988; Ebel *et al*., 1990). Moreover, the size of whole cross sections of conifer needles (dimensions of approx. 2 × 1 mm) is rather large for ultrathin sectioning, which adversely affects the quality of the sections (Hayat, 1970). Kivimäenpää *et al*. (2001, 2003) halved the needle longitudinally to cut the ultrathin sections from either adaxial or abaxial side of the needle, thus it was easier to get undistorted ultrathin sections. Preservation of chloroplast ultrastructure in conifers may also be improved by changing the buffers or embedding media (Ebel *et al*., 1990), by changing the molarity of buffers according to season (Soikkeli, 1980) or by using microwaves during sample processing (Zechman and Zellnig, 2009). Furthermore, even when SUR is used on TEM images, one should be aware, that the TEM image has a large depth of field, so that the single image may be in fact an overprojection. Therefore the use of electron tomography is recommended for more precise measurements (Vanhecke *et al*., 2007).

Another complication that makes SUR sampling more challenging in transmission electron microscopy is poststaining of the sections on slot grids. The slot grids are suitable for SUR sampling as they enable us to view whole large cross sections of the needle without interference of grid bars. Poststaining, if it is done manually on a drop of stain solutions (uranyl acetate followed by lead citrate), is technically challenging as the formvar coating on the slots is prone to ruptures. It is always possible to view sections without poststaining, as in this study, but it significantly decreases the observed contrast and resolution (Hayat, 1970; Ellis, 2007). Due to lower contrast in the deeper layers of mesophyll (Fig. 1C), we were able to quantify only the starch grain area but not the parameters of thylakoid membranes. A fully automated system for contrasting ultrathin sections (Yang *et al*., 2017) might solve this problem.

Lastly, SUR sampling can be much more time consuming depending on the equipment accessible for the study. In our case, SUR sampling was about six times more time consuming because of the need to pick the chloroplasts manually from the low contrast sections that were not poststained. However, the availability of the cutting edge equipment should certainly reduce or even diminish this difference (automated poststaining, automated acquisition).

Our study shows that chloroplast characteristics estimations acquired from the first mesophyll layers and SUR cannot always substitute each other. Based on our results, measurement of chloroplast characteristics from the first mesophyll layer slightly underestimates the effect of CO_2 concentration. In the case of starch grain characteristics, this bias could mask CO_2 concentration impact if only TEM analysis is used. If the possibility of using SUR for chloroplast

evaluation is impeded by the extreme laboriousness or technical constraints, we recommend to combine TEM analysis with other physiological approaches, *e.g.*, starch biochemical assessment (Mašková *et al.*, 2017) or determination of photosystem activities and fluorescence parameters.

As discussed above, there are several objective constraints and challenges of using SUR in extensive studies based on TEM. In our case, we faced the difficulty in acquisition of high-quality and high-contrast ultrathin sections of the whole needle for SUR sampling and chloroplast selection. Considering the extreme laboriousness of sample preparation, the difficulties associated with technical processing and financial costs of TEM working hours, some simplifications of sampling principles are acceptable if the aim is for comparison of ultrastructural characteristics between different treatments.

The following discussion is based on results from SUR sampling. A trend to higher chloroplast number observed in the mesophyll of needles from trees grown under EC in comparison with those grown under AC agrees with studies on herbaceous plants and broad-leaved trees (Oksanen *et al.*, 2001; Wang *et al.*, 2004; Oksanen *et al.*, 2005; Teng *et al.*, 2006). The effect of irradiance on chloroplast number is not always unambiguous, as it was in our case. In some previous studies, more chloroplasts were observed in sun than in shade leaves (Cui *et al.*, 1991), and in high light compared with low light grown plants (Zhang *et al.*, 2015). On the contrary, increased chloroplast number in shade conditions was also reported (Shao *et al.*, 2014). Thus, the influence of irradiance on chloroplast number in conifers remains unclear.

Higher starch areal density and starch grain area in sun EC needles in comparison with sun AC needles is in agreement with previous findings in both leaves and needles in EC (Pritchard *et al.*, 1997; Griffin *et al.*, 2001; Oksanen *et al.*, 2001; Eguchi *et al.*, 2004; Liu *et al.*, 2004; Sholtis *et al.*, 2004; Liu *et al.*, 2005; Teng *et al.*, 2006; Onoda *et al.*, 2007; Cabálková *et al.*, 2008), and both starch characteristics were significantly higher in sun needles from EC in comparison with the other three CO_2 and irradiance combinations. The difference may be explained by enhanced photosynthetic rate in EC (rev. Leakey *et al.*, 2009), which may be more pronounced in sun needles leading to higher production of starch. Another explanation may be that the winter hardening process in the EC needles, sampled in October, was delayed as has been previously reported (Utriainen *et al.*, 2000; Palomäki *et al.*, 1996). In summary, the main influence of CO_2 concentration, irradiance and their interaction was on the starch grain area and areal density, which were found to be largest in sun needles in EC.

CONCLUSION

Based on the results of our study, we conclude that the first mesophyll layer cannot be always considered as representative for chloroplast characteristics in the mesophyll on the whole cross section of Norway spruce needles. Therefore, if technically possible, we recommend the use of systematic uniform random sampling for the selection of examined cells and chloroplasts in conifers, which yields unbiased estimations of chloroplast ultrastructure, though depending on the equipment accessible it can be more time-consuming. However, in the case of limited time, technical equipment and resources in combination with large sample numbers in ecophysiological studies, we do not completely reject measuring the chloroplast ultrastructural characteristics from the first mesophyll layer if the aim is for comparison between different treatments. If such simplified sampling instead of SUR sampling is applied, it is advisable to combine the TEM analyses with different approaches to characterize the chloroplast function and to carefully consider and interpret the results.

ACKNOWLEDGEMENTS

We would like to thank the Global Change Research Centre of the Czech Academy of Sciences for providing us with the opportunity for plant cultivation and particularly to Dr. Otmar Urban and Dr. Miroslava Šprtová for their support and care for cultures We also thank to Mrs. Ivana Nováková for her excellent technical assistance with TEM sample preparation and to our colleague Mgr. Drahomíra Bartáková for a technical help. We gratefully acknowledge our colleague Dr. Kevin Jia-Jin Loo for language correction of the text. This study was supported by: Czech Science Foundation [P501/10/0340; 18-23702S]; Czech Academy of Sciences [RVO:67985823]; Charles University in Prague [SVV]; Ministry of Education, Youth and Sports of the Czech Republic [NPUI LO1417]; BioImaging Facility, Institute of Physiology - Czech-BioImaging large RI project [LM2015062 funded by MEYS CR]; MEYS (CZ.02.1.01/0.0/0.0/16_013/0001775 Modernization and support of research activities of the national infrastructure for biological and medical imaging Czech-BioImaging funded by OP RDE), Project ERDF, OPPK BrainView CZ.2.16/3.1.00/21544, CESNET storage facilities provided under the programme "Projects of Large Research, Development, and Innovations Infrastructures" (CESNET LM2015042).

REFERENCES

Albertsson PA, Andreasson E (2004). The constant proportion of grana and stroma lamellae in plant chloroplasts. Physiol Plantarum 121:334–42

Albrechtová J, Janáček J, Lhotáková Z, Radochová B, Kubínová L (2007). Novel efficient methods for measuring mesophyll anatomical characteristics from fresh thick sections using stereology and confocal microscopy: application on acid rain-treated Norway spruce needles. J Exp Bot 58:1451–61.

Anttonen S (1992). Changes in lipids of *Pinus sylvestris* needles exposed to industrial air pollution. Ann Bot Fenn:89–99.

Bäck J, Huttunen S (1992). Structural responses of needles of conifer seedlings to acid rain treatment. New Phytol 120:77–88.

Bondada BR, Syvertsen JP (2003). Leaf chlorophyll, net gas exchange and chloroplast ultrastructure in citrus leaves of different nitrogen status. Tree Physiol 23: 553–9.

Cabálková J, Přibyl J, Skládal P, Kulich P, Chmelík J (2008). Size, shape and surface morphology of starch granules from Norway spruce needles revealed by transmission electron microscopy and atomic force microscopy: effects of elevated CO_2 concentration. Tree Physiol 28:1593–9.

Calfapietra C, Ainsworth EA, Beier C, De Angelis P, Ellsworth, DS, Godbold DL, *et al*. (2010). Challenges in elevated CO_2 experiments on forests. Trends Plant Sci 15:5–10.

Cui M, Vogelmann T, Smith W (1991). Chlorophyll and light gradients in sun and shade leaves of *Spinacia oleracea*. Plant Cell Environ 14:493–500.

DeLucia EH, Day TA, Vogelman TC (1992). Ultraviolet-B and visible light penetration into needles of two species of subalpine conifers during foliar development. Plant Cell Environ 15: 921–9.

Demmig-Adams B, Muller O, Stewart JJ, Cohu CM, Adams WW (2015). Chloroplast thylakoid structure in evergreen leaves employing strong thermal energy dissipation. Journal of Photochemistry and Photobiology B: Biology 152:357–66.

Ebel B, Hamelmann U, Nieß C (1990). A rapid preparation method for ultrastructural investigations of conifer needles. J Microsc-Oxford 160:67–74.

Eguchi N, Fukatsu E, Funada R, Tobita H, Kitao M, Maruyama Y, *et al*. (2004). Changes in morphology, anatomy, and photosynthetic capacity of needles of Japanese larch (*Larix kaempferi*) seedlings grown in high CO_2 concentrations. Photosynthetica 42:173–8.

Ellis EA (2007). Poststaining Grids for Transmission Electron Microscopy. In: Kuo J ed. Electron Microscopy. Ch. 6. Totowa: Humana Press, 97–106.

ESRL Global Monitoring Division, NOAA, U.S. Department of Commerce Trends in Atmospheric Carbon Dioxide - Recent Monthly Average Mauna Loa CO_2. http://www.esrl.noaa.gov/gmd/ccgg/trends/index.html. Accessed 29 Jan 2018

Gebauer RL, Strain BR, Reynolds JF (1997). The effect of elevated CO_2 and N availability on tissue concentrations and whole plant pools of carbon-based secondary compounds in loblolly pine (*Pinus taeda*). Oecologia 113:29–36.

Griffin KL, Anderson OR, Gastrich MD, Lewis JD, Lin G, Schuster W, *et al*. (2001). Plant growth in elevated CO_2 alters mitochondrial number and chloroplast fine structure. P Natl Acad Sci-Biol 98:2473–8.

Gundersen H, Jensen E (1987). The efficiency of systematic sampling in stereology and its prediction. J Microsc-Oxford 147:229–63.

Gundersen H-JG (1986). Stereology of arbitrary particles. J Microsc-Oxford 143:3–45.

Günthardt-Goerg MS, McQuattie CJ, Maurer S, Frey B (2000). Visible and microscopic injury in leaves of five deciduous tree species related to cur, rent critical ozone levels. Environ Pollut 109:489–500.

Günthardt-Goerg MS, Vollenweider P (2015). Responses of beech and spruce foliage to elevated carbon dioxide, increased nitrogen deposition and soil type. AoB Plants 7:plv067.

Hayat MA (1970). Principles and Techniques of Electron Microscopy. New York: Van Nostrand Reinhold Company.

Jönsson AM, Kivimäenpää M, Stjernquist I, Sutinen S (2001). Frost hardiness in bark and needles of Norway spruce in southern Sweden. Trees 15:171–6.

Kainulainen P, Utriainen J, Holopainen JK, Oksanen J, Holopainen T (2000). Influence of elevated ozone and limited nitrogen availability on conifer seedlings in an open-air fumigation system: effects on growth, nutrient content, mycorrhiza, needle ultrastructure, starch and secondary compounds. Glob Change Biol 6:345–55.

Kivimäenpää M (2003). Cell Structural Changes in the Needles of Norway Spruce Exposed to Long-term Ozone and Drought. Ann Bot-London 92:779–93.

Kivimäenpää M, Selldén G, Sutinen S (2005). Ozone-induced changes in the chloroplast structure of conifer needles, and their use in ozone diagnostics. Environ Pollut 137:466–75.

Kivimäenpää M, Sutinen S (2007). Microscopic structure of Scots pine (*Pinus sylvestris* (L.)) needles during ageing and autumnal senescence. Trees 21:645–59.

Kivimäenpää M, Riikonen J, Sutinen S, Holopainen T (2014). Cell structural changes in the mesophyll of Norway spruce needles by elevated ozone and elevated temperature in open-field exposure during cold acclimation. Tree Physiol 34:389–403.

Kivimäenpää M, Sutinen S, Medin E-L, Karlsson PE, Selldén G (2001). Diurnal changes in microscopic structures of mesophyll cells of Norway spruce, *Picea abies* (L.) Karst., and the effects of ozone and drought. Ann Bot-London88:119–30.

Kubínová L, Kutík J (2007). Surface density and volume density measurements of chloroplast thylakoids in maize (*Zea mays* L.) under chilling conditions. Photosynthetica 45:481–8.

Kubínová L, Radochová B, Lhotáková Z, Kubínová Z, Albrechtová J (2017). Stereology, an unbiased methodological approach to study plant anatomy and cytology: past, present and future. Image Anal Stereol 35: 187–205.

Kubínová Z, Janáček J, Lhotáková Z, Kubínová L, Albrechtová J (2014). Unbiased estimation of chloroplast number in mesophyll cells: advantage of a genuine three-dimensional approach. J Exp Bot 65:609–20.

Kubínová Z, Janáček J, Lhotáková Z, Šprtová M, Kubínová L, Albrechtová J (2018). Norway spruce needle size and cross section shape variability induced by irradiance on a macro-and microscale and CO_2 concentration. Trees 32:231–44.

Kutík J, Holá D, Kočová M, Rothová O, Haisel D, Wilhelmová N, *et al*. (2004). Ultrastructure and dimensions of chloroplasts in leaves of three maize (*Zea mays* L.) inbred lines and their F1 hybrids grown under moderate chilling stress. Photosynthetica 42: 447–55.

Leakey ADB, Ainsworth EA, Bernacchi CJ, Rogers A, Long SP, Ort DR (2009). Elevated CO_2 effects on plant carbon, nitrogen, and water relations: six important lessons from FACE. J Exp Bot 60:2859–76.

Lepeduš H, Cesar V, Ljubešić N (2001). Chloroplast ultrastructure and chlorophyll levels in vegetative buds and needles of Norway spruce (*Picea abies* L. Karst.). Periodicum biol (Zagreb) 103:61–5.

Lhotáková Z, Albrechtová J, Janáček J, Kubínová L (2008). Advantages and pitfalls of using free-hand sections of frozen needles for three-dimensional analysis of mesophyll by stereology and confocal microscopy. J Microsc-Oxford 232:56–63.

Lhotáková Z, Urban O, Dubánková M, Cvikrová M, Tomášková I, Kubínová L, *et al*. (2012). The impact of long-term CO_2 enrichment on sun and shade needles of Norway spruce (Picea abies): Photosynthetic performance, needle anatomy and phenolics accumulation. Plant Sci 188:60–70.

Lin JX, Jach ME, Ceulemans R (2001). Stomatal density and needle anatomy of Scots pine (*Pinus sylvestris*) are affected by elevated CO_2. New Phytol 150:665–74.

Liu X, Kozovits AR, Grams TE, Blaschke H, Rennenberg H, Matyssek R (2004). Competition modifies effects of enhanced ozone/carbon dioxide concentrations on carbohydrate and biomass accumulation in juvenile Norway spruce and European beech. Tree Physiol 24: 1045–55.

Liu X-P, Grams TEE, Matyssek R, Rennenberg H (2005). Effects of elevated pCO_2 and/or pO_3 on C-, N-, and S-metabolites in the leaves of juvenile beech and spruce differ between trees grown in monoculture and mixed culture. Plant Physiol Bioch 43:147–54.

Mašková P, Radochová B, Lhotáková Z, Michálek J, Lipavská H (2017). Nonstructural carbohydrate-balance response to long-term elevated CO_2 exposure in European beech and Norway spruce mixed cultures: biochemical and ultrastructural responses. Can J Forest Res 47:1488–94.

Meyberg M (1988). Selective staining of fungal hyphae in parasitic and symbiotic plant-fungus associations. Histochemistry 88:197–9.

Oksanen E, Riikonen J, Kaakinen S, Holopainen T, Vapaavuori E (2005). Structural characteristics and chemical composition of birch (*Betula pendula*) leaves are modified by increasing CO_2 and ozone. Glob Change Biol 11:732–48.

Oksanen E, Sober J, Karnosky DF (2001). Impacts of elevated CO_2 and/or O_3 on leaf ultrastructure of aspen (*Populus tremuloides*) and birch (*Betula papyrifera*) in the Aspen FACE experiment. Environ Pollut 115:437–46.

Onoda Y, Hirose T, Hikosaka K (2007). Effect of elevated CO_2 levels on leaf starch, nitrogen and photosynthesis of plants growing at three natural CO_2 springs in Japan. Ecol Res 22:475–84.

Palomäki V, Laitinen K, Holopainen T, Kellomäki S (1996). First-year results on the effects of elevated atmospheric CO_2 and O_3 concentrations on needle ultrastructure and gas exchange responses of Scots pine saplings. Silva Fenn 30:123–34.

Parkhurst DF, Wong S-C, Farquhar GD, Cowan IR (1988). Gradients of intercellular CO_2 levels across the leaf mesophyll. Plant Physiol 86:1032–37.

Polák T, Rock BN, Campbell PE, Soukupová J, Solcová B, Zvára K, *et al*. (2006). Shoot growth processes, assessed by bud development types, reflect Norway spruce vitality and sink prioritization. Forest Ecol Manag 225:337–48.

Pritchard SG, Peterson CM, Prior SA, Rogers HH (1997). Elevated atmospheric CO_2 differentially affects needle chloroplast ultrastructure and phloem anatomy in *Pinus palustris*: Interactions with soil resource availability. Plant Cell Environ 20:461–71.

Räisänen T, Ryyppö A, Julkunen-Tiitto R, Kellomäki S (2008). Effects of elevated CO_2 and temperature on secondary compounds in the needles of Scots pine (*Pinus sylvestris* L.). Trees 22:121–35.

Sallas L, Luomala E-M, Utriainen J, Kainulainen P, Holopainen JK (2003). Contrasting effects of elevated carbon dioxide concentration and temperature on Rubisco activity, chlorophyll fluorescence, needle ultrastructure and secondary metabolites in conifer seedlings. Tree Physiol 23:97–108.

Senser M, Schötz F, Beck E (1975). Seasonal changes in structure and function of spruce chloroplasts. Planta 126:1–10.

Shao Q, Wang H, Guo H, Zhou A, Huang Y, Sun Y, *et al*. (2014). Effects of Shade Treatments on Photosynthetic Characteristics, Chloroplast Ultrastructure, and Physiology of *Anoectochilus roxburghii*. PLoS ONE 9: e85996.

Sharkova VE, Bubolo LS (1996). Effect of heat stress on the arrangement of thylakoid membranes in the chloroplasts of mature wheat leaves. Russ J Plant Physl+ 43: 358–65.

Sholtis JD, Gunderson CA, Norby RJ, Tissue DT (2004). Persistent stimulation of photosynthesis by elevated CO_2 in a sweetgum (*Liquidambar styraciflua*) forest stand. New Phytol 162:343–54.

Siefermann-Harms D, Boxler-Baldoma C, von Wilpert K, Heumann H-G (2004). The rapid yellowing of spruce at a mountain site in the Central Black Forest (Germany). Combined effects of Mg deficiency and ozone on biochemical, physiological and structural properties of the chloroplasts. J Plant Physiol 161:423–37.

Smith WK, Vogelmann TC, DeLucia EH, Bell DT, Shepherd KA (1997). Leaf form and photosynthesis. Bioscience 47:785–93.

Soikkeli S (1978). Seasonal changes in mesophyll ultrastructure of needles of Norway spruce (*Picea abies*). Can J Botany 56:1932–40.

Soikkeli S (1980). Ultrastructure of the mesophyll in Scots pine and Norway spruce: seasonal variation and molarity of the fixative buffer. Protoplasma 103:241–52.

Soukupová J, Cvikrová M, Albrechtová J, Rock BN, Eder J (2000). Histochemical and biochemical approaches to the study of phenolic compounds and peroxidases in needles of Norway spruce (*Picea abies*). New Phytol 146:403–14.

Spurr AR (1969). A low-viscosity epoxy resin embedding medium for electron microscopy. J Ultra Struct R 26: 31–43.

Sterio D (1984). The unbiased estimation of number and sizes of arbitrary particles using the disector. J Microsc-Oxford 134:127–36.

Sun ZP, Li TL, Liu YL (2011). Effects of elevated CO_2 applied to potato roots on the anatomy and ultrastructure of leaves. Biol plant 55: 675.

Teng N, Wang J, Chen T, Wu X, Wang Y, Lin J (2006). Elevated CO_2 induces physiological, biochemical and structural changes in leaves of Arabidopsis thaliana. New Phytol 172:92–103.

Urban O, Janouš D, Pokorný R, Markova I, Pavelka M, Fojtík Z, *et al*. (2001). Glass Domes with Adjustable Windows: A Novel Technique for Exposing Juvenile Forest Stands to Elevated CO_2 Concentration. Photosynthetica 39:395–401.

Utriainen J, Janhunen S, Helmisaari H-S, Holopainen T (2000). Biomass allocation, needle structural characteristics and nutrient composition in Scots pine seedlings exposed to elevated CO_2 and O_3 concentrations. Trees 14:475–84.

Valkama E, Kivimäenpää M, Hartikainen H, Wulff A (2003). The combined effects of enhanced UV-B radiation and selenium on growth, chlorophyll fluorescence and ultrastructure in strawberry (*Fragaria* × *ananassa*) and barley (*Hordeum vulgare*) treated in the field. Agr Forest Meteorol 120:267–78.

Vanhecke D, Studer D, Ochs M (2007). Stereology meets electron tomography: Towards quantitative 3D electron microscopy. J Struct Biol 159:443–50.

Velikova V, Tsonev T, Barta C, Centritto M, Koleva D, Stefanova M, *et al.* (2009). BVOC emissions, photosynthetic characteristics and changes in chloroplast ultrastructure of *Platanus orientalis* L. exposed to elevated CO_2 and high temperature. Environ Pollut 157:2629–37.

Wang X, Anderson OR, Griffin KL (2004). Chloroplast numbers, mitochondrion numbers and carbon assimilation physiology of *Nicotiana sylvestris* as affected by CO_2 concentration. Environ Exp Bot 51:21–31.

West MJ (2012). Only total quantities will do: Beware the reference trap. In: Basic stereology for biologists and neuroscientists. Ch. 1.7. New York, Cold Spring Harbor Laboratory Press, 8–9.

Wheeler WS, Fagerberg WR (2000). Exposure to low levels of photosynthetically active radiation induces rapid increases in palisade cell chloroplast volume and thylakoid surface area in sunflower (*Helianthus annuus* L.). Protoplasma 212:38–45.

Wulff A, Ahonen J, Kärenlampi L (1996). Cell ultrastructural evidence of accelerated ageing of Norway spruce needles in industrial areas. New Phytol 133:553–61.

Yang R, Wang S, Wang J, Luo X, Zhao W, Zhang Q, *et al*. (2017). Comparison of manual and automatic processing of biological samples for electron microscopy. Microsc Res Techniq 80:570–77.

Zechmann B, Zellnig G (2009). Microwave-assisted rapid plant sample preparation for transmission electron microscopy. J Microsc-Oxford 233:258–68.

Zhang LX, Guo QS, Chang QS, Zhu ZB, Liu L, Chen YH (2015). Chloroplast ultrastructure, photosynthesis and accumulation of secondary metabolites in *Glechoma longituba* in response to irradiance. Photosynthetica 53:144–53.

Image Anal Stereol 2017;35:187-205 doi: 10.5566/ias.1848
Review Paper

STEREOLOGY, AN UNBIASED METHODOLOGICAL APPROACH TO STUDY PLANT ANATOMY AND CYTOLOGY: PAST, PRESENT AND FUTURE

LUCIE KUBÍNOVÁ✉,[1], BARBORA RADOCHOVÁ[1,2], ZUZANA LHOTÁKOVÁ[2], ZUZANA KUBÍNOVÁ[2], JANA ALBRECHTOVÁ[2]

[1]Department of Biomathematics, Institute of Physiology of the Czech Academy of Sciences, Vídeňská 1083, Prague 4, CZ-14220, Czech Republic; [2]Department of Experimental Plant Biology, Faculty of Science, Charles University, Viničná 5, Prague 2, Czech Republic
e-mail: lucie.kubinova@fgu.cas.cz, barbora.radochova@fgu.cas.cz, zuza.lhotak@seznam.cz, kubinova@natur.cuni.cz, jana.albrechtova@natur.cuni.cz
(Received October 11, 2017; revised November 22, 2017; accepted November 26, 2017)

ABSTRACT

This review presents an historical overview of stereological methods used for the quantitative evaluation of plant anatomical and cytological structures. It includes the origins of these methods up to the most recent developments such as the application of stereology based on 3D images. We focus especially on leaf, as the vast majority of studies of plant microscopic structure examine this organ. An overview of plant cell ultrastructure measurements as well as plant anatomical characteristics (*e.g.*, plant tissue volume density, internal leaf surface area, number and mean size of mesophyll cells and chloroplast number), which were estimated by stereological methods most frequently, is presented. We emphasize the importance of proper sampling needed for unbiased measurements. Furthermore, we mention other methods used for plant morphometric studies and briefly discuss their relevance, precision, unbiasedness and efficiency in comparison with unbiased stereology. Finally, we discuss reasons for the sparse use of stereology in plant anatomy and consider the future of stereology in plant research.

Keywords: chloroplast, confocal microscopy, leaf anatomy, mesophyll, stereological methods, systematic uniform random sampling

INTRODUCTION

Plant anatomical and cytological structure has been studied since the introduction of the first magnifying devices in the 16th century. By the end of the 19th century, a number of basic developmental and functional concepts in plant anatomy were well understood (Eames and MacDaniels, 1925). For example, Julius von Sachs (1834-1897) proposed the first physiological classification of plant tissues based on their origin from uniform meristem. While some quantitative methods for studying physiological processes in plant organisms were being established, these early findings were largely based on descriptive analyses of plant anatomical structure. There was a clear need for quantitative evaluation of plant anatomy for studying relations between the function and structure of the plant body. Thus, plant scientists began to quantitatively assess anatomical characteristics, initially by morphometric, intuitive methods, and later by more rigorous approaches made possible by stereological methods.

This review presents the history of stereology applied in plant studies and discusses other methods for measuring plant structural parameters. Particular focus is given to the evaluation of leaf structure as the leaf is the most frequently studied plant organ. This is due to the fact that the specific leaf tissues, cells, and organelles (Figs. 1, 2, 8) are involved in the transfer of carbon dioxide during the process of light capture and photosynthesis, which has crucial importance for the function of the plant organism. Quantitative analysis of changes in the leaves can be very helpful in many applications studying the effect of environmental factors on plants, such as analysis of the effect of air pollution (Albrechtová *et al.*, 2007), elevated CO_2 concentration (Lhotáková *et al.*, 2012) or temperature (Juurola *et al.*, 2005). Moreover, leaf geometrical characteristics may be useful for interpreting physiological measurements, three-dimensional (3D) modelling during photosynthesis (Juurola *et al.*, 2005) and for phenotyping (Flood *et al.*, 2016).

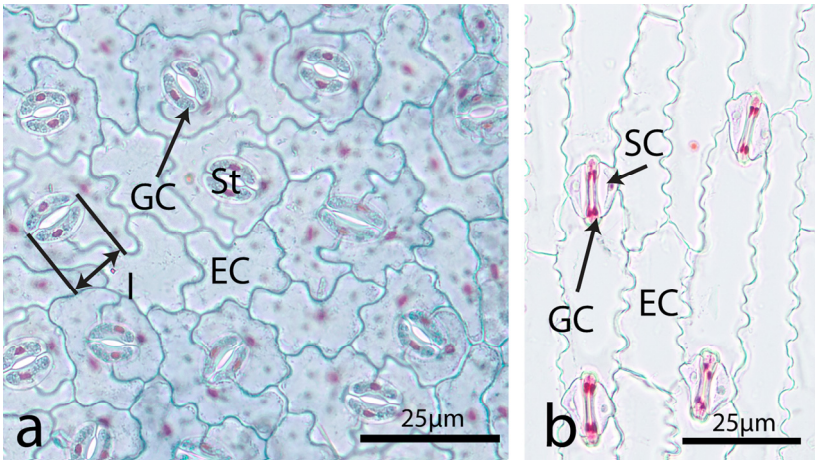

Fig. 1. *Leaf epidermis. (a) Oregano (Origanum spp.) - dicotyledonous plant. St – stoma composed of two guard cells (GC), EC – epidermal cell, l – stoma length. (b) Maize (Zea mays L.) - monocotyledonous plant. Stomatal apparatus: two dumble-shaped guard cells (GC) and two subsidiary cells (SC), EC – epidermal cell.*

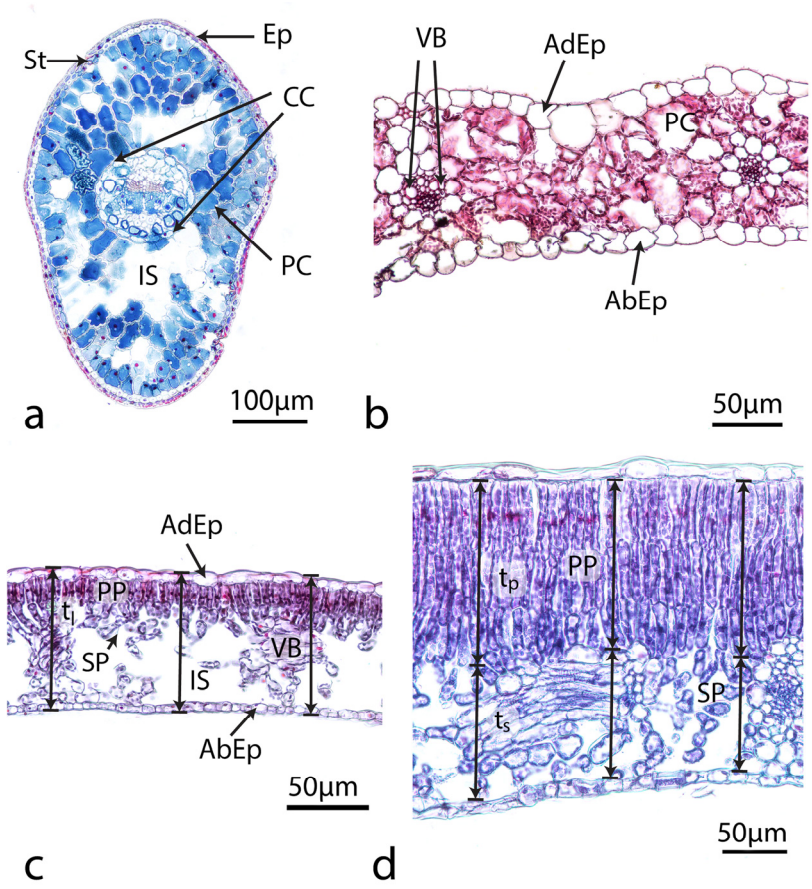

Fig. 2. *Leaf internal structure in cross sections. (a) Norway spruce needle (Picea abies L. Karst): Ep – epidermis, St – stoma, CC – central cylinder with vascular tissues (round structure between arrows), mesophyll composed of parenchyma cells (PC) and intercellular spaces (IS). (b) Monocotyledonous leaf (barley, Hordeum vulgare L.): AdEp – adaxial epidermis, AbEp – abaxial epidermis, VB – vascular bundle, PC – mesophyll parenchyma cell. (c, d) Dorsiventral leaf (apple tree, Malus spp.): AdEp – adaxial epidermis, AbEp – abaxial epidermis, VB – vascular bundle, mesophyll composed of palisade parenchyma (PP), spongy parenchyma (SP), and intercellular spaces (IS). Shade leaf (c) with one layer of palisade parenchyma and sun leaf (d) with three layers of palisade parenchyma. t_l – leaf thickness, t_p – palisade parenchyma thickness, t_s – spongy parenchyma thickness.*

SHORT HISTORY OF QUANTIFICATION OF PLANT ANATOMICAL STRUCTURE

The earliest quantitative data characterizing plant anatomy were published by Friedrich Wilhelm Heinrich Alexander von Humboldt already in 1786 who presented data on stomatal density (*i.e.*, number of stomata per unit leaf area, see Fig. 1; Pazourek, 1988). Since then, many plant anatomists have used quantitative methods in their research, quite often in connection with physiological (particularly ecophysiological) and taxonomic studies, as summarized in reviews by Nátr (1988) and Pazourek (1988).

In the history of the development of quantitative approaches to investigating plant anatomy, the work of Salisbury (1928) is of particular note. Salisbury introduced the application of statistical methods in the analysis of quantitative data. He focused on determining stomatal distribution on the leaf surface and tried to prove the relations between various stomatal characteristics. He introduced the concept of stomatal index - the percentage of the number of stomata per unit leaf area with respect to the number of epidermal cells including stomata in the same unit area. A key finding of this study was determining stomatal index as less variable than stomatal density (*i.e.*, number of stomata per unit leaf area) within a particular plant species.

In general, stomatal density and stoma length in the leaves were found to be the most frequently studied plant anatomical parameters. Stoma length is usually evaluated from epidermal peels or imprints, *i.e.* from practically two-dimensional (2D) structures (Fig. 1). Leaf thickness or thickness of its tissue layers is another frequently reported parameter. It is usually measured in 2D leaf cross-sections (Fig. 2c). The thickness of tissue layers was often measured in dorsiventral leaves (Turell, 1936; Wylie, 1949). This parameter can be useful when studying important physiological phenomena associated with irradiance-affected leaf morphogenesis, *e.g.*, differentiation of dorsiventral leaves into thicker and denser sun leaves with more layers of palisade mesophyll parenchyma in comparison with shade leaf ecotypes (Fig. 2 c, d). In other plant organs, the most frequently measured parameter was the length of the root system. The root length in 2D was usually measured by the line-intercept method (Newmann, 1966), the principle of which had already been proposed by Buffon in 1777.

In the studies of internal leaf structure (Fig. 2), the physiologically important characteristics most often measured were the number and dimensions of mesophyll cells, internal leaf surface area (*i.e.*, the surface area of mesophyll cell walls adjoining the intercellular spaces), and the proportion of intercellular spaces. In one of the first comprehensive studies of leaf mesophyll, Meyer (1923) measured the dimensions of mesophyll palisade cells - the ratio of their length to the width, variations in the length of palisade cells within a blade, the number of palisade cell layers, the angle of orientation of palisade cells to the leaf surface, and the arm palisade cells surface area. The following methods for measurement of mesophyll parameters were most frequently used: Mesophyll cell dimensions were usually measured by applying a model-based approach, *i.e.*, assuming that the cells could be modelled by simple geometrical bodies (Maksymowych, 1963; Chonan, 1966; 1970). The number of mesophyll cells was most frequently obtained by counting isolated cells after maceration (Maksymowych, 1959). Regarding internal leaf surface area, Turrell (1934) also applied a model-based approach. He emphasized the importance of this parameter for photosynthetic performance, since the gas exchange is via exposed mesophyll cell walls. Furthermore, Nius (1931) examined the physiological importance of the relative volume of intercellular spaces using the infiltration method according to Unger (1854).

Following the development of electron microscopy, the first quantitative measurements of chloroplast ultrastructure emerged in the 1960s. Parameters such as the number of grana per chloroplast or thylakoids per granum were measured and 3D models of chloroplasts were introduced (Wehrmeyer and Röbbelen, 1965; Paolillo and Falk, 1966). Stereological methods were increasingly applied in the following decades, including estimating area and/or volume densities of different chloroplast compartments (Gamalei and Kulikov, 1978; Fagerberg, 1983; Kutík *et al.*, 1984).

After the establishment of stereology as a new scientific discipline in the 1960s and 70s (Weibel, 1979; Howard and Reed, 1998), design-based stereological methods emerged and began to be used also in quantitative studies of plant structures. The first applications of stereology in plant anatomy were published by Pazourek (1975; 1977), Chabot and Chabot (1977), Parkhurst (1982), Morris and Thain (1983), and Hajibagheri *et al.* (1984). Later, a number of design-based stereological methods for the estimation of various leaf characteristics were introduced by Kubínová (1987; 1989b; 1991; 1993; 1994). Characteristics highlighted included mesophyll volume, proportion of intercellular spaces in mesophyll, internal leaf surface area, mesophyll cell number and mean mesophyll cell volume, based on measurements in 2D leaf sections. Further-

more, a specific approach to root length estimation using the stereological method of total vertical projections (Cruz-Orive and Howard, 1991) was presented by Albrechtová *et al.* (1998).

Although stereological methods proposed for the estimation of leaf characteristics from 2D sections were known to be reliable, they have rarely been applied. This is mainly due to their laborious nature. Therefore, there was a clear need for less demanding, efficient and unbiased methods for measuring physiologically important mesophyll anatomical characteristics, such as internal leaf surface area, mean mesophyll cell volume and cell number in the leaf. Stereological methods based on 3D images acquired by confocal microscopy, electron tomography and other modalities, are suitable for this purpose since they are efficient and unbiased. Moreover, confocal microscopy can be applied to thick fresh plant tissue sections, thus minimizing the time spent on tissue specimen preparation and avoiding deformation of tissues due to fixation and embedding procedures.

Stereology based on 3D confocal images, called confocal stereology (for reviews see Peterson, 1999; Kubínová *et al.*, 2002; 2004, 2005; Kubínová and Janáček, 2015) is a contemporary approach that evaluates structures using a combination of stereological methods and confocal microscopy (Pawley, 1995; 2006) enabling the obtainment of perfectly registered stacks of thin serial optical sections (approx. 350 nm thick) within thick specimens. Digital images of such stacks represent 3D image data suitable for quantitative measurements. Howard *et al.* (1985) presented the first application of confocal microscopy to stereological measurements in their concept of an unbiased sampling brick. Confocal microscopy proved to be useful especially in the application of stereological methods based on spatial estimators evaluating small 3D samples of structures (Howard *et al.*, 1985; Howard and Sandau, 1992; Kubínová and Janáček, 1998; Kubínová *et al.*, 1999; Kubínová *et al.*, 2002). A 3D sample of examined tissue can be analysed if a rectangle within the microscope's field of view is focused through. Using specialized software, different virtual test probes with an arbitrary pre-defined (*e.g.*, random) position and orientation can be generated within the stack of sections and can be applied directly to this 3D image data. Albrechtová *et al.* (2007) presented the confocal stereological methods used to evaluate the mesophyll structure of narrow leaves, such as conifer needles. Kubínová *et al.* (2014) showed the application of confocal microscopy for counting chloroplasts in a mesophyll cell using optical disector principle (see below).

OVERVIEW OF STEREOLOGICAL METHODS APPLIED IN PLANT ANATOMY

Many of the stereological methods developed over the past fifty years can be applied (directly or after suitable modification) in studies of plant anatomical structures. In this review, we present the most frequently measured plant anatomical characteristics estimated by stereological methods.

Firstly, let us mention specific features of plant anatomical structures and relevant consequences: Plant organs and cells exhibit highly variable morphology with significant differences in dimension and shape. Anisotropy (arrangement with preferential orientation) is often observed in plant tissues as well as inhomogeneity, *e.g.*, gradient in stomatal frequency in different parts of leaves, as shown by Slavík (1963) and Pazourek (1966; 1969). Gradients in tissue proportions within a leaf (Pazourek, 1977) and in mesophyll cell size along the leaf (Kubínová, 1989a) were also observed. Therefore, design-based stereological methods, yielding unbiased results without placing any assumptions on shape and arrangement of structures, are especially useful in quantitative plant anatomy.

The correct application of design-based stereological methods is critically dependent on proper sampling of tissue blocks, sections, test frames, point grids, etc. In stereology, geometrical properties of the object (in this case, the leaf) are derived from the information collected from relatively small parts of the object (*i.e.*, leaf sections). Therefore, when evaluating a specific parameter of the object (*e.g.*, the proportion of mesophyll in the leaf), just its specific parts (*e.g.*, leaf sections) are measured to estimate the parameter. In order to obtain reasonable results, these parts should be sampled in a way ensuring the estimate is close enough to the true parameter value and yielding no systematic bias. This can be achieved by proper sampling, examples of which are presented below.

SAMPLING

Systematic uniform random sampling (SURS)

SURS ensures an efficient and convenient way of unbiased sampling. It has been used in the application of many stereological methods in plant research, such as the Cavalieri principle, point-counting, vertical sections, or disector methods. In leaf investigations, it can be applied for sampling leaf segments, 2D sections (Fig. 3, 4) and (3D) thick slices used in confocal stereology (Fig. 5).

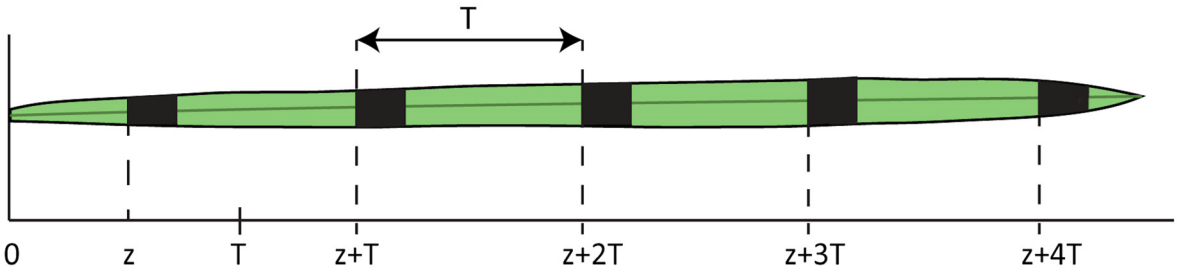

Fig. 3. *Systematic uniform random sampling of segments and sections in a grass leaf. Firstly, the distance (T) (mm) between two consecutive sections is chosen. For the position (z), a random number is then selected from the set {0,1,...,T-1}. The transverse sections are made in the positions z, z+ T, z + 2T, ... For example, if T= 40 mm, z = 20 mm, and the leaf length is 200 mm, then the transverse sections would be cut at distances of 20 mm, 60 mm, 100 mm, 140 mm and 180 mm from the leaf base. (After Kubínová, 1993.)*

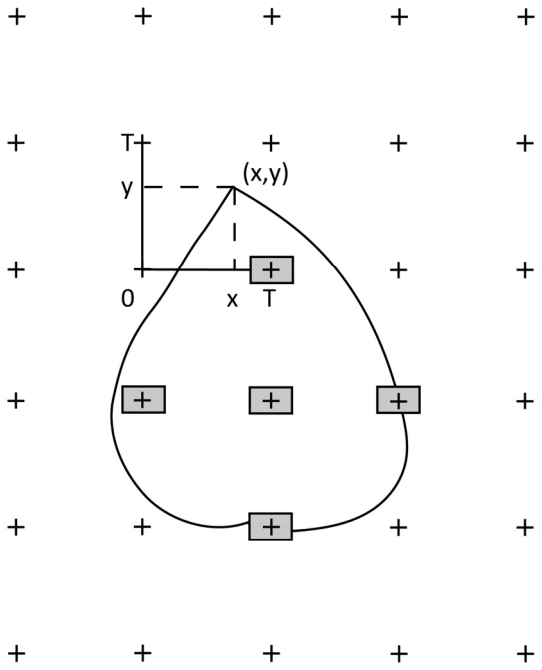

Fig. 4. *Systematic uniform random sampling of segments and sections in a flat bifacial leaf. The distance (T) (mm) between the central points of the leaf segments is chosen first. For the position (x,y), two numbers are then (independently) selected at random from the set {0,1,...,T-1}. By placing the leaf tip in the position (x, y), the uniform random position of the grid of central points is ensured. The leaf segments are then cut as indicated in the figure and cross-sections are cut in the middle of the segments. (After Kubínová, 1993.)*

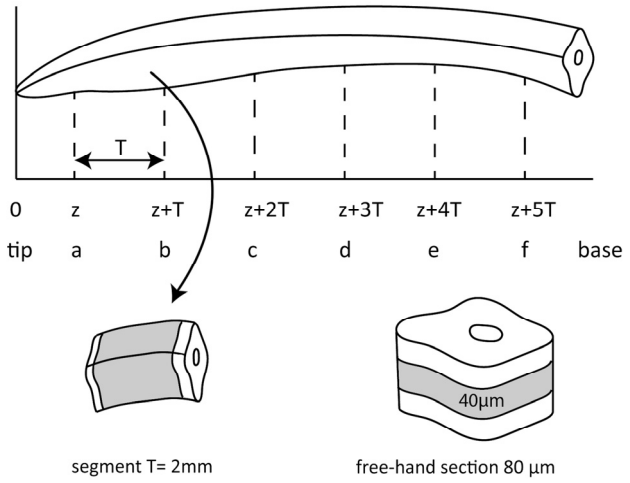

Fig. 5. *Sampling design of needle specimen preparation. Upper: Systematic uniform random sampling of transverse free-hand sections: z = random position of the first section within (0; T]. The distance T between free-hand sections is chosen first. In this specific case, T = 2 mm. Positions of transverse sections along the needle longitudinal axis are denoted by a, b, c, d, e, f. Lower: Left: 2-mm-thick needle segment. Right: 80-µm-thick free-hand section from which the 40µm thick stack of optical sections is acquired by confocal microscopy. (After Lhotáková et al., 2008.)*

Vertical uniform random sampling (VURS)

VURS is applied in the vertical sections method (Baddeley *et al.*, 1986). It enables the estimation of internal leaf surface area, which is one of the physiologically most important plant anatomical parameters. The practical application of VURS for narrow leaves is shown in Fig. 6.

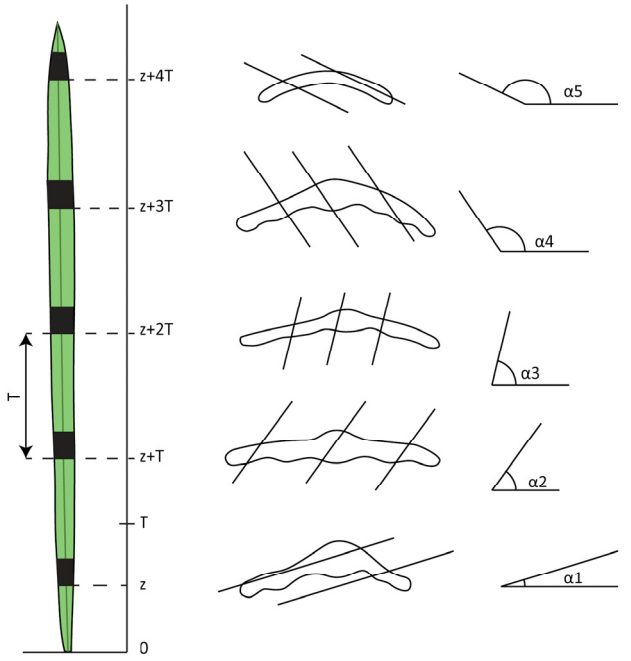

Fig. 6. *Construction of vertical sections of the grass leaf. Firstly, the systematic uniform random sampling of leaf segments is done as shown on the left (see also Fig. 3). The direction of the vertical axis is chosen to be parallel to the main axis of the leaf, i.e. the vertical sections are cut in parallel with the leaf axis. At the same time they are cut around the leaf axis by an angle generated in the horizontal plane (which is perpendicular to the vertical plane) as illustrated in the figure: In the horizontal plane of the first segment (i.e. the nearest one to the leaf base; the face of the segment is shown as the lowest one in the figure), angle* α_1 *(0°<* α_1 *< 180°) is selected uniformly at random (e.g.,* α_1 *is a random number from the set {0°, 10°, 20°,..., 170°}). The vertical sections of the first segment are cut in this direction. With m segments in the leaf, the direction of the vertical section in the j-th segment is given by the angle* $\alpha_j = \alpha_1 + (j-l) * (180°/m)$ *(j=l,...,m). (For example, if m = 5 and* $\alpha_1 = 10°$*, then* $\alpha_2 = 10°+1 * (180°/5) = 46°$*,* $\alpha_3 = 82°$*,* $\alpha_4 = 118°$*, and* $\alpha_5 = 154°$*.) Within the segment, the series of equidistant parallel sections (illustrated by lines intersecting the faces of sampled segments seen from above) are cut in a way analogous to the one described in Fig. 3. (After Kubínová, 1993.)*

Unbiased sampling of particles by disector principle

The unbiased counting or sampling of three-dimensional particles can be achieved by using the stereological method called disector principle (Sterio, 1984; Gundersen, 1986). The disector is a 3D probe which samples particles with a uniform probability in 3D space, irrespective of their size and shape, as shown in Fig 7.

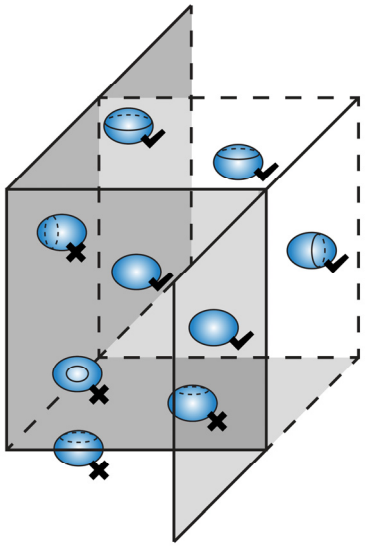

Fig. 7. *Disector. Particles that are inside the 3D disector probe are counted and particles intersecting its planes are also counted except those intersecting the exclusion planes (in grey). In this example, 5 particles are counted (ticked) and 4 particles are not counted (crossed). After Kubínová et al. (2014).*

PLANT ANATOMICAL CHARACTERISTICS ESTIMATED BY STEREOLOGICAL METHODS

Plant tissue volume density

The volume density of a specific tissue in the leaf is usually estimated by the ratio of the area of the tissue section to the area of the leaf section. The corresponding areas were measured by a point-counting method, based on counting points of the test grid falling in the tissue under study (Chabot and Chabot, 1977; Pazourek, 1977; Pazourek and Nátr, 1981; Parkhurst, 1982; Hajibagheri *et al.*, 1984; Gowland *et al.*, 1987; Pazourek *et al.*, 1987; Kubínová, 1991; Albrechtová, 1994), by a planimeter (Turrell, 1936), by cutting out the enlarged drawings of the sections and weighing them (El-Sharkawy and Hesketh, 1965; Charles-Edwards *et al.*, 1972; Dengler and MacKay, 1975), by a semiautomatic image analyser (Parker and Ford, 1982) or by a stereological method based on length measurements (linear integration method, Weibel, 1979; Thain, 1983). A number of studies (*e.g.*, Gundersen and Jensen, 1987) showed that, in general, the point-counting method using a regular grid of points (which is positioned uniformly at random on the section) is the most effective one. Its efficiency is low only if the structure is periodic with

the same periodicity as the point grid. This can be avoided simply by changing the distances between the grid points.

The application of a point counting method for the estimation of the proportion of intercellular spaces in barley leaf was presented by Kubínová (1989b, 1991). Using this approach, the volume density of individual tissues in a leaf was measured by Edwards *et al.* (1999), Klich (2000), Luković *et al.* (2001), Bray and Reid (2002), Luković (2006), Marin *et al.* (2006), Zorić *et al.* (2011; 2014), Moura and Alves (2014), Bernardo *et al.* (2017), and Bertel *et al.* (2017). The proportion of intercellular spaces in mesophyll was also investigated by Albrechtová and Kubínová (1991), Kukkola *et al.* (2005), Albrechtová *et al.* (2007), Lhotáková *et al.* (2008), Yiotis and Psaras (2011), and Zorić *et al.* (2011; 2014). The proportion of intercellular spaces in the palisade parenchyma was measured by Konoplyova et al. (2008) from micrographs of paradermal sections of the leaves. Furthermore, volume density of needle tissues (Albrechtová *et al.*, 2007; Lhotáková *et al.*, 2012), trichomes in the leaf (Marin *et al.*, 2008), and petiole tissues (Luković *et al.*, 2016) were estimated.

The Cavalieri principle, which is based on multiplying the sum of areas of SURS sections by the distance between the subsequent sections (Gundersen and Jensen, 1987), was used for estimating volume of leaf and/or leaf components by Kubínová (1989b, 1991, 1993), Albrechtová and Kubínová (1991), Edwards *et al.* (1999), Klich (2000), Marin *et al.* (2008), and Albrechtová *et al.* (2007). Detailed instructions on how to apply this method are given in the overview of stereological methods for the measurement of leaf characteristics (Kubínová, 1993).

Surface area of mesophyll cells and internal leaf surface area

An unbiased stereological method of vertical sections (Baddeley *et al.*, 1986) was applied for the estimation of internal leaf surface area (*i.e.*, the surface area of mesophyll cell walls adjoining the intercellular spaces) and surface area of mesophyll cells (*i.e.*, the surface area of entire mesophyll cell walls) by Kubínová (1991). The method is based on counting the intersections of a special cycloidal test system with the measured surface on 2D sections generated by using VURS (Fig. 6). For more details and practical application in both narrow and broad leaves see Kubínová (1993).

Another approach was presented by Kubínová and Janáček (1998) showing application of their fakir method for the estimation of the internal surface area of a barley leaf, and later by Albrechtová *et al.* (2007) and Lhotáková *et al.* (2008) for measuring the internal surface area of a conifer needle using confocal microscopy. Unlike the vertical sections method, which is applied to 2D physical sections, the fakir method does not require randomizing section orientation; hence the physical thick sections can be cut in any arbitrary direction. Therefore, the slices were cut perpendicular to the main axis of the needle, which is most suitable from a technical point of view (Fig. 6). The fakir method was used also by Lhotáková *et al.* (2012).

Number of mesophyll cells and chloroplasts

Unbiased counting or sampling of three-dimensional particles can be achieved by using the stereological method of disector (Sterio, 1984; Gundersen, 1986); for its principle see Fig. 7. Application of the disector method for estimation of mesophyll cell density and total number of mesophyll cells in a leaf was introduced by Kubínová (1989a,b; 1991). Detailed instructions on how to apply this method using SURS are given in her overview of stereological methods for estimating the number and sizes of stomata and mesophyll cells (Kubínová, 1994). The disector method for counting mesophyll cells was also used by Albrechtová and Kubínová (1991) and in combination with confocal microscopy by Kubínová and Janáček (2001), Kubínová *et al.* (2002; 2005) and Albrechtová *et al.* (2007). Kubínová *et al.* (2014) also used confocal stereology introducing the application of the disector method for estimation of chloroplast number per mesophyll cell in Norway spruce needles and comparing this approach with other methods for chloroplast counting.

Mean volume and surface area of mesophyll cells

Mean volume and/or surface area of mesophyll cells is estimated simply by the ratio of the mesophyll cell volume, resp. surface area, and the mesophyll cell number (for the measurement of these characteristics see above). Unbiased stereological methods were used for estimation of these characteristics by Kubínová (1989a,b; 1991; 1994; 1998), Albrechtová and Kubínová (1991) and Albrechtová *et al.* (2007).

PLANT CELL ULTRASTRUCTURE MEASUREMENTS

Plant cell ultrastructure is often studied by transmission electron microscopy (TEM). Qualitative asses-

sment of changes in chloroplasts (Fig. 8) or other cell components is common. Most studies focused on the accumulation of starch and/or plastoglobuli, formation of lipid bodies, fragmentation of vacuoles, condensation of cytoplasm, thylakoid swelling or electron density of stroma. In some studies, a system of classes is used to describe the severity of cellular injury (Wulff *et al.*, 1996; Kivimäenpää *et al.*, 2003).

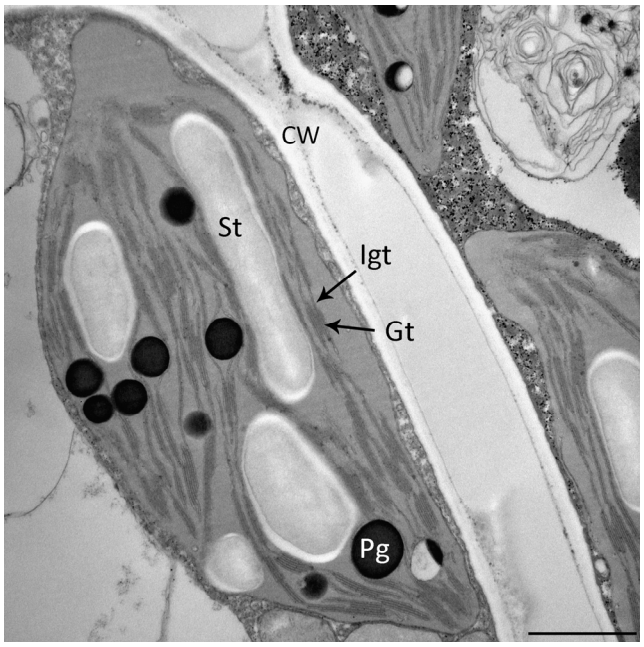

Fig. 8. *Chloroplast ultrastructure. Transmission electron micrograph of chloroplast cross-section from leaf of European beech; Gt – granal thylakoids, Igt – intergranal thylakoids, St – starch, Pg – plastoglobulus, CW – cell wall. Bar = 1 μm.*

It should be stated that although leaf ultrastructure was sometimes evaluated by stereological methods, the application of these methods was usually done without SURS at the leaf blade level. Due to the costs and time-consuming work associated with sample preparation for transmission electron microscopy, samples for analysis were taken from the middle part or the middle third of the leaf blade or needle (in the case of conifers). Random sampling within the leaf was sometimes applied but in many studies the description of sampling design was not given in detail. In conifers, samples were taken from the middle part of the needle cross-section or from the first layer of mesophyll. Furthermore, differences in ultrastructure between the outer and inner parts of mesophyll were evaluated, mainly in studies describing the effect of stress treatment (Kivimäenpää *et al.*, 2003; Kivimäenpää *et al.*, 2014). In bifacial leaves, the ultrastructure of palisade parenchyma cells is of greater interest than spongy parenchyma cells.

For stereological analysis, the volume density of a specific part of the cell (*e.g.*, chloroplast, mitochondria, peroxisome) was estimated by the ratio of the area of the cell part to the area of the whole cell. Volume densities of thylakoids, starch, plastoglobuli and stroma inside chloroplasts were estimated by measuring the corresponding areas using the point-counting method (Kutík *et al.*, 1995; Miroslavov *et al.*, 1996; Fagerberg and Bornman, 1997; Razem and Davis, 1999; Vassilyev, 2000; Wheeler and Fagerberg, 2000; Griffin *et al.*, 2001; Gabarayeva and Grigorjeva, 2002; Pechová *et al.*, 2003; Vičánková and Kutík, 2005; Gregoriou *et al.*, 2007; Kubínová and Kutík, 2007; Holá *et al.*, 2008, Mašková *et al.* 2017).

Volume densities were usually measured on randomly sampled images of cells or organelles. Their volumes were determined only in some of the studies: Fagerberg and Bornman (1997) and Wheeler and Fagerberg (2000) used the standard leaf volume for calculation of organelle volume; Vassilyev (2000) assumed ellipsoid form of different organelles (plastids, mitochondria, peroxisomes, and dictyosomes) and calculated their volumes from their lengths and widths.

For measurements of surface densities or surface area of chloroplasts, a Merz curvilinear grid with semi-circles in a square grid was used by Fagerberg and Bornman (1997). The method of „local vertical windows“ suggested by Baddeley *et al.* (1986) was applied by Kubínová and Kutík (2007) for estimation of surface densities of thylakoid membranes. Albertsson and Andreasson (2004) estimated surface area of thylakoid membranes by drawing parallel lines across the chloroplast micrograph (perpendicular to the long axis of the chloroplast) and counting the number of membrane transections using the fact that the membrane length in randomly cut chloroplast sections is statistically proportional to the surface area of the membrane. A similar approach was also chosen by Gao *et al.* (2006).

DISCUSSION

OTHER MORPHOMETRIC METHODS IN PLANT ANATOMY IN COMPARISON WITH STEREOLOGICAL METHODS

In order to obtain a complex, full overview of the quantification of plant structures, it should be pointed out that many approaches other than stereological methods have been used in the past and are still being used today. However, compared to stereological methods, most methods as listed below provide biased results, most often due to improper sampling

and model-based design application. Those methods regarding their relevance, precision, unbiasedness and efficiency will be discussed below.

Plant tissue volume density

Many authors did not measure the volume density of plant tissues in the entire leaf, but rather their tissue proportions in individual 2D sections located in non-randomized specific positions of the leaf, *e.g.*, only in the middle of the leaf (Soper and Mitchell, 1956; Sant, 1969; Charles-Edwards *et al.*, 1972; 1974; Parker and Ford, 1982). Some used specialised image analysis software for this measurement (Niinemets, 2007; Lukjanova *et al.*, 2013). However, this approach does not involve proper representative sampling, and thus it does not yield unbiased information about the proportion of tissues in the entire 3D organ.

The volume of intercellular spaces is often measured by the infiltration method (Unger, 1854; Nius, 1931; Czerski, 1968; Morrod, 1974; Byott, 1976; Smith and Heurer, 1981; Eleftheriou, 1987). Its drawbacks were discussed by Smith and Heurer (1981) and by Morris and Thain (1983). In short, the volume of intercellular spaces can be overestimated if the substance used for the infiltration enters the cells in addition to filling the intercellular spaces (Smith and Heurer, 1981), or it can be underestimated if tissue infiltration is incomplete (Morris and Thain, 1983). On the other hand, the estimation of the volume of intercellular spaces in the leaf by methods based on the evaluation of leaf section preparations can be affected by the microtechnical processing or by the section thickness effect.

Surface area of mesophyll cells and internal leaf surface area

Many different methods have been developed for the measurement of the internal leaf surface area (sometimes also called „exposed surface area of mesophyll“). A particularly laborious procedure based on the evaluation of several transverse and paradermal sections of the leaf was proposed by Turrell (1936). The palisade and spongy mesophyll were treated separately and a kind of model shape of cells was assumed in both cases. The formula for the palisade mesophyll holds, for example, if the surface of all palisade cells exposed to the intercellular spaces are represented by the surface of cylinders (without their bases) having the same height and axes exactly perpendicular to the leaf surface. Any inclination, swelling or wrinkling of cell walls causes underestimation of the surface area of palisade cells. Similarly, the procedure described for the spongy parenchyma can lead to the underestimation or in some cases even to the overestimation of its surface area.

A less laborious, but similarly biased method was used by Dornhoff and Shibles (1976) for different tissue layers of a soybean leaf (*Glycine max* L.). The exposed surface area of different mesophyll layers was estimated by the product of the thickness of the tissue layer and the total length of the trace of exposed cell walls, obtained from paradermal sections. This procedure resulted in the underestimation of the exposed surface area, because it again assumes that the orientation of cell walls is exactly perpendicular to the leaf surface and that the walls are not curved.

This method for the measurement of the surface area of mesophyll cells, also used by Dengler and MacKay (1975) and later by other authors (Parker and Ford, 1982; Barbour and Farquhar, 2004), was criticized and modified by Thain (1983), who proposed several curvature correction factors eliminating the error caused by the curvature of cell surfaces, assuming different model shapes of mesophyll cells. Some of these mesophyll cell model shapes were more realistic than cylinders with hemispheres on each end (assumed by Nobel *et al.*, 1975) or spheres (Bunce *et al.*, 1977).

Thain's method (1983) was used also by Longstreth *et al.* (1985), Miyazawa and Terashima (2001) and Oguchi *et al.* (2003). Sasahara considered the palisade mesophyll cells of *Brassiceae* leaves as special solids of 'intermediate shapes between spheroids and columns' (Sasahara, 1971) and the mesophyll cells of *Triticum* as systems of interconnected cylinders with hemispheres on each end (Sasahara, 1982). A similar model of the *Triticum* mesophyll cell was used by Chonan (1965). It should be stressed here that it is always necessary to verify the appropriateness of the model for each type of structure under study, which may be difficult and laborious.

The stereological method, based on counting intersection points between the studied surface and line probes, has also been used for the estimation of the internal leaf surface area per unit leaf volume or the surface area of mesophyll cells per unit leaf volume. However, certain model assumptions were always considered. Morris and Thain (1983) claim that they achieved isotropic orientation of cell walls (*i.e.*, with no preferred orientation) by preparing a suspension of the isolated mesophyll cells, which were then embedded and cut. The isotropic structure of the spongy mesophyll of tobacco (*Nicotiana tabacum* L.) leaf was assumed (and verified) by Gowland *et al.* (1987) who considered the palisade

mesophyll as a partially orientated linear system of surfaces.

The stereological method based on counting intersections was also used by Parkhurst (1982) for the estimation of internal leaf surface area. Special models of mesophyll cells (cylindrical type, isotropic type, and a rather controversial intermediate type of structure) were assumed. Some of the pitfalls of Parkhurst's approach (disregarding the end surface of cylinder-like cells, subjective estimation of the degree of 'cylindricity' of the tissue) were discussed by Thain (1983). James *et al.* (1999) also used a model-based approach to the measurement of the mesophyll surface area per leaf area from oblique-paradermal sections – the latter exploited Image-Pro Plus software. Slaton and Smith (2002), Khramtsova *et al.* (2003), and Rhizoupoulou and Psaras (2003) also measured this parameter by model-based methods.

In summary, all the above mentioned methods for the estimation of surface area of mesophyll cells and internal leaf surface area were based on the choice of a specific, more or less realistic model of mesophyll cells. This model-based approach, when applied to real biological objects, such as mesophyll cells, brings about a bias which is challenging to quantify. Moreover, this approach cannot be reasonably used for the measurement of structures which cannot be approximated by simple geometrical models. This is the case for the mesophyll of grass leaves and coniferous needles where the cells have an irregularly lobed shape and possess a certain degree of anisotropy. Recently, Theroux-Rancourt *et al.* (2017) have tested several model-based methods for mesophyll surface area estimation. They found that the model-based methods often led to underestimation of this parameter (up to 30%) in comparison with 3D method based on the evaluation of 3D image data acquired by microCT using specialized ImageJ plugins. However, they have not tested stereological methods, since "these methods have been less adopted in recent years".

Unbiased stereological methods can indeed avoid the above mentioned problems. They are using the design-based approach, where uniform random position and random orientation of line probes must be ensured, as is the case for the methods of vertical sections (Kubínová, 1993) and fakir method (Kubínová and Janáček, 1998) described above. This approach is precise and more efficient (especially the fakir method in combination with confocal microscopy as shown by Albrechtová *et al.*, 2007) than model-based methods. Its advantages have been acknowledged by other authors (El-Sharkawy, 2009).

Number of mesophyll cells and chloroplasts

The number of mesophyll cells was usually determined by counting isolated cells after their maceration (Maksymowych, 1959; 1963; Smith, 1970; Morrod, 1974; Jellings and Leech, 1984; Sasahara, 1982; Lieckfeldt, 1989). This method may lead to the loss of cells during manipulation of the cell suspension or by damage to certain cells and, accordingly, to the underestimation of the cell number. Wilson and Cooper (1967) and Adachi *et al.* (2013) applied a 2D approach where they counted cell profiles while making assumptions about cell shapes, potentially leading to biased results. Using the stereological method of optical disector gives a theoretically unbiased result. However, in practice it is necessary to fulfil the so called General Requirement, *i.e.*, each cell has to be unambiguously identifiable from its profiles in studied stacks of optical sections (*i.e.*, 3D image data containing a disector probe, typically acquired by widefield or confocal microscope).

One of the most frequently used methods for the estimation of chloroplast number per mesophyll cell in herbaceous plants in 2D is counting chloroplasts in separated mesophyll cells obtained by maceration procedures as it was described by Possingham and Saurer (1969). This technique was used by many authors (Possingham and Smith, 1972; Boffey *et al.*, 1979; Lamppa *et al.*, 1980; Molin *et al.*, 1982; Tymms *et al.*, 1983; Sung and Chen, 1989; Pyke and Leech, 1991; Yamasaki *et al.*, 1996; Marrison *et al.*, 1999; Ivanova and P'yankov, 2002; Meyer *et al.*, 2006; Stettler *et al.*, 2009). This estimation is unbiased since counting is done in the whole cell, provided the chloroplasts in the specimen are not overlapping and the cells used for chloroplast counting are selected in an unbiased way. However, in some plant species it is impossible to macerate separate cells, especially in coniferous needles and leaves with mesophyll cells with lignified cell walls. In this case the disector method (Fig. 7) can be efficiently used for unbiased estimation of chloroplast number per mesophyll cell using confocal microscopy (Kubínová *et al.*, 2014).

Practical and theoretical tests presented by Kubínová *et al.* (2014) demonstrated that the frequently used method for chloroplast number estimation by counting profiles of particles from 2D sections yielded biased estimates (e. g. Boffey *et al.*, 1979; Miyazawa and Terashima, 2001; Sam *et al.*, 2003; Zechmann *et al.*, 2003; Wang *et al.*, 2004; Hayashida *et al.*, 2005; Oguchi *et al.*, 2005; Teng *et al.*, 2006;

Gopi *et al.*, 2008; Maslova *et al.*, 2009; Jin *et al.*, 2011; Simon *et al.*, 2013) and that the results may be one order of magnitude different from the real chloroplast numbers. Another possible method is to count the chloroplasts in cells directly during focusing through the specimen using conventional light microscopy (Ellis and Leech, 1985; Bockers *et al.*, 1997) which can be applied if entire cells can be focused through and the chloroplasts are sparsely distributed in cells. However, chloroplasts usually tend to be densely packed along the cytoplasmic membrane. The chloroplast number per cell was also determined in 3D reconstructions made from a series of confocal microscope images (Mozafari *et al.*, 1997; Dinkins *et al.*, 2001; Coate *et al.*, 2012; Xu *et al.*, 2012). Such a method can yield an unbiased estimate if SUR sampling is applied and a sufficient number of cells is analysed. However, this is a much more time-consuming approach than direct application of the disector method in combination with confocal microscopy. In conclusion, the disector method can be applied universally and provide unbiased estimation of the number of particles.

Mean volume and surface area of mesophyll cells

The volume of a mesophyll cell is usually estimated by the volume of a simple geometrical body by which the cell is approximated. Palisade cells were modelled by ellipsoids (Wild and Wolf, 1980) and cylinders (Maksymowych, 1963; Morrod, 1974; Gowland *et al.*, 1987) or by cylinders with hemispherical ends (Sasahara, 1971; Barbour and Farquhar 2004; Burundukova *et al.*, 2003; Khramtsova *et al.*, 2003). Spongy cells were approximated by spheres (Morrod, 1974; Charles-Edwards *et al.*, 1974) or ellipsoids (Wild and Wolf, 1980). Chonan (1965) and Sasahara (1982) modelled lobed mesophyll cells of wheat (*Triticum* sp.) by systems of parallel cylinders with hemispherical ends (standing side-by-side).

In most cases a model-based approach was chosen. Taking into account that it is often difficult to judge the appropriateness of the model used, this approach brings about a bias which is difficult to quantify. Moreover, this approach cannot reasonably be used for the measurement of cells which cannot be approximated by simple geometrical bodies.

As in the cell volume measurements, the model-based approach to the measurement of the surface area of mesophyll cells prevailed (Chonan, 1965; Morrod, 1974; Sasahara, 1971; 1982; Bunce *et al.*, 1977; Tichá and Čatský, 1977; Ivanova and P´yankov, 2002). It should be emphasized that, in comparison with the cell volume measurement, the estimation of the cell surface area by the surface area of a simple geometrical body can lead to even more pronounced bias since neither the inclinations, swellings nor wrinklings of the cell wall are taken into account. This can cause severe underestimation of the cell surface area.

In summary, unbiased stereological methods avoid the problems of model-based approach discussed above and can be recommended for mesophyll cell volume and surface area measurement. For this purpose, combination with confocal microscopy is especially useful (Albrechtová *et al*., 2007).

OTHER METHODS FOR THE MEASUREMENT OF PLANT CELL ULTRASTRUCTURE

Plant cell ultrastructure is recently most often quantified by image analysis on digitized images of plant cells or chloroplasts acquired by transmission electron microscopy (TEM). Typical parameters measured are thickness of the cell wall, size of organelles (length, width, profile area) – mostly of chloroplasts and mitochondria, proportions (in %) and numbers of the organelles (Liu and Dengler, 1994; Lepeduš *et al.*, 2001; Oksanen *et al.*, 2001; Yu *et al.*, 2017). Inside the chloroplasts, the size, number and profile area of starch grains, plastoglobuli and granal thylakoids are measured (Wulff *et al.*, 1996; Pritchard *et al.*, 1997; Schmitt *et al.*, 1999; Bondada and Syvertsen, 2003; Riikonen *et al.*, 2003). Thylakoids are also quite frequently counted and presented as numbers of thylakoids per granum (Demmig-Adams *et al.*, 2015; Ren *et al.*, 2017). It is a well-known fact that the number of thylakoids per granum is different for plants grown in sun or shade conditions (Boardman, 1977). Unfortunately, most studies do not describe sampling design in detail and counting of particles on 2D sections of chloroplasts or cells is probably biased in a similar way as in the case of chloroplast number estimation.

Some authors realize that counting particles in 2D may not be reliable. For example, Kivimäenpää *et al.* (2014) did not count the number of mitochondria on 2D sections, because they realized that the individual mitochondrial cross-sections can be from the same, long, branched and folded organelle.

3D methods for the determination of plant cell ultrastructure are used rather sparsely. In some studies (Perktold *et al.*, 1998; Zellnig *et al*., 2004) the method of ultrathin serial sections was used as a way to build up a 3D image of the organelles, where the volumes of the organelles and their parts could be estimated

(using Cavalieris principle). Crumpton-Taylor *et al.* (2012) used a FIB-SEM method for measurements of chloroplast and starch granule volume as well as granule numbers in *Arabidop*sis. In comparison with the serial sectioning and TEM, this method has advantages of speed and accuracy as there is no distortion of the image surface and alignment of the images is rather simple. Unfortunately, this method requires very expensive equipment. Using 3D methods, all starch granules inside the chloroplasts can be counted; any possible bias is thus limited to the possibility of incorrect sampling of small tissue samples or differential shrinkage of cell compartments during the sample preparations.

SPARSE USE OF STEREOLOGY IN PLANT ANATOMY

Although stereology provides a number of valuable tools for unbiased and precise measurement of plant structural characteristics, it has been used in this field sparsely until now. This is illustrated by the graph in Fig. 9 showing that the gap between the number of publications on stereology in plant science and their number in animal/human biosciences has been increasing since the 1990s. (The graph is just indicative as it is clear that it does not show all publications using stereological methods.)

What can be the reason for the sparse use of stereology in plant anatomy? It may be that many plant biologists are not acquainted with stereological methods and/or find them to be too complicated and laborious. In the community of plant biologists, broader publicity should be made through educational materials such as courses, tutorials, reviews, Wiki, etc. We envisage that this can be made possible on a broader scale by collaborative efforts such as the International Society for Stereology and Image Analysis (http://www.issia.net/). It should be made clear to the plant biological community that stereological methods are not so difficult to apply and yield unbiased results unlike many other methods, which can lead to erroneous results and, moreover, are often also quite tedious and time consuming. More studies bringing supporting arguments and comparisons of stereological and other methods should be made. This has been done, for example, for the estimation of volume and surface area of tobacco cell chains (Kubínová *et al.*, 1999) where different stereological and image analysis methods were compared. In this case, it was concluded that the fakir method and the Cavalieri principle enable interactive, unbiased and efficient estimation of the cell surface area and volume.

It should also be noted that the application of automatic image analysis methods for measurements of plant structures is often limited by difficulties with proper automatic detection (segmentation) of these structures in microscopic images.

The popularity of stereological methods could also be increased by decreasing their laboriousness. This is possible by using specially dedicated software, either directly connected with image acquisition equipment, or stand-alone software modules. A combination with semi-automatic image analysis, while keeping proper sampling schemes, can also make measurements more efficient in some cases. Special attention should be paid also to the selection of suitable methods for each specific type of measurement and to the most efficient sampling design, as well as to all practical aspects of the measurement procedure.

Based on the above facts, we believe that stereology will find its way to the community of plant biologists and become one of the most powerful tools for investigation of plant anatomical and cytological structures.

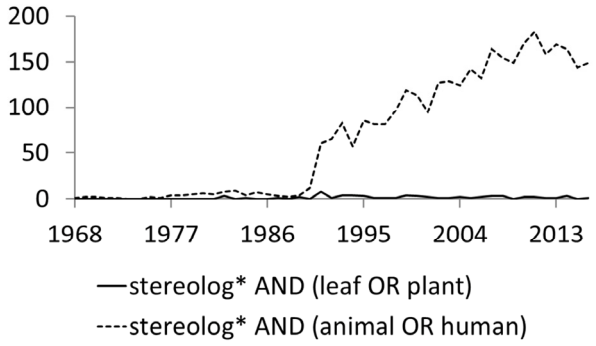

Fig. 9. *Number of publications on stereology in plant and animal/human biosciences in the past 48 years, i.e., since the first publication including the key world stereolog* has appeared. Based on the result of search in Web of Science with key words (stereolog* AND (leaf OR plant)) or (stereolog* AND (animal OR human)), respectively.*

ACKNOWLEDGEMENTS

This study was supported by the Ministry of Education, Youth and Sports of the Czech Republic (LM2015062 Czech-BioImaging project; NPUI LO1417 project; CZ.02.1.01/0.0/0.0/16_013/0001775 Modernization and support of research activities of the national infrastructure for biological and medical imaging Czech-BioImaging funded by OP RDE), project ERDF, OPPK BrainView CZ.2.16/3.1.00/21544, and by the project SVV of the Charles University. We

thank Drahomíra Bartáková for technical help with anatomical preparations and Miroslav Barták (both from the Faculty of Science, Charles University) for his help with photographing and figure processing.

REFERENCES

Adachi S, Nakae T, Uchida M, Soda K, Takai T, Oi T, Yamamoto T, Ookawa T, Miyake H, Yano M (2013). The mesophyll anatomy enhancing CO_2 diffusion is a key trait for improving rice photosynthesis. J Exp Bot 64:1061–72.

Albertsson P, Andreasson E (2004). The constant proportion of grana and stroma lamellae in plant chloroplasts. Physiol Plantarum 121:334–42.

Albrechtová J (1994). Quantitative analysis of leaves of sun and shade ecotypes of *Solanum dulcamara* L. Acta Stereol 13:467-72.

Albrechtová J, Janáček J, Lhotáková Z, Radochová B, Kubínová L (2007). Novel efficient methods for measuring mesophyll anatomical characteristics from fresh thick sections using stereology and confocal microscopy: application on acid rain-treated Norway spruce needles. J Exp Bot 58:1451–61.

Albrechtová J, Kubínová L (1991). Quantitative analysis of the structure of etiolated barley leaf using stereological methods. J Exp Bot 42:1311–14.

Albrechtová J, Kubínová L, Votrubová O, Eliášová K (1998). Non-destructive stereological method for estimating the length of rigid root systems. Biol Plantarum 40: 311–6.

Baddeley A, Gundersen H-JG, Cruz-Orive LM (1986). Estimation of surface area from vertical sections. J Microsc-Oxford 142:259–76.

Barbour M, Farquhar G (2004). Do pathways of water movement and leaf anatomical dimensions allow development of gradients in $H_2{}^{18}O$ between veins and the sites of evaporation within leaves? Plant Cell Environ 27:107–21.

Bernardo S, Dinisa L-T, Luzio A, Pinto G, Meijón M, Valledor L, Conde A, Gerós H, Correia CM, Moutinho-Pereira J (2017). Kaolin particle film application lowers oxidative damage and DNA methylation on grapevine (*Vitis vinifera* L.). Env Exp Bot 139:39–47.

Bertel C, Schönswetter P, Frajman B, Holzinger A, Neuner G (2017). Leaf anatomy of two reciprocally non-monophyletic mountain plants (*Heliosperma* spp.): does heritable adaptation to divergent growing sites accompany the onset of speciation? Protoplasma 254:1411–20.

Boardman N (1977). Comparative photosynthesis of sun and shade plants. Ann Rev Plant Physio 28:355–77.

Bockers M, Čapková V, Tichá I, Schäfer C (1997). Growth at high CO_2 affects the chloroplast number but not the photosynthetic efficiency of photoautotrophic *Marchantia polymorpha* culture cells. Plant Cell Tiss Org 48:103–10.

Boffey SA, Ellis JR, Selldén G, Leech RM (1979). Chloroplast division and DNA synthesis in light-grown wheat leaves. Plant Physiol 64:502–5.

Bondada BR, Syvertsen JP (2003). Leaf chlorophyll, net gas exchange and chloroplast ultrastructure in citrus leaves of different nitrogen status. Tree Physiol 23:553–9.

Bray S, Reid DM (2002). The effect of salinity and CO_2 enrichment on the growth and anatomy of the second trifoliate leaf of *Phaseolus vulgaris*. Can J Botany 80:349–59.

Buffon GLL (1777). Essai d´arithmétique morale. In: Histoire naturelle, générale et particulière: servant de suite à la théorie de la terre, & d'introduction à l'histoire des minéraux. De l'imprimerie royale, Paris, pp 46–148.

Bunce JA, Patterson DT, Peet MM, Alberte RS (1977). Light acclimation during and after leaf expansion in soybean. Plant Physiol 60:255–8.

Burundukova O, Zhuravlev YN, Solopov N, P'yankov V (2003). A method for calculating the volume and surface area in rice mesophyll cells. Russian Journal of Plant Physiol 50:133–9.

Byott G (1976). Leaf air space systems in C3 and C4 species. New Phytol 76:295–9.

Chabot BF, Chabot JF (1977). Effects of light and temperature on leaf anatomy and photosynthesis in *Fragaria vesca*. Oecologia 26:363–77.

Charles-Edwards DA, Charles-Edwards J, Sant F (1972). Models for mesophyll cell arrangement in leaves of ryegrass (*Lolium perenne* L.). Planta 104:297–305.

Charles-Edwards DA, Charles-Edwards J, Sant F (1974). Leaf photosynthetic activity in six temperate grass varieties grown in contrasting light and temperature environments. J Exp Bot 25:715–24.

Chonan N (1965). Studies on the photosynthetic tissues in the leaves of cereal crops. I. The mesophyll structure of wheat leaves inserted at different levels of the shoot. Proc Crop Sci Soc Jpn 33:388–93.

Chonan N (1966). Studies on the photosynthetic tissues in the leaves of cereal crops. II. Effect of shading on the mesophyll structure of the wheat leaves. Proc Crop Sci Soc Jpn 35:78–82.

Chonan N (1970). Studies on the photosynthetic tissues in the leaves of cereal crops. V. Comparison of the mesophyll structure among seedling leaves of cereal crops. Proc Crop Sci Soc Jpn 39:418–25.

Coate JE, Luciano AK, Seralathan V, Minchew KJ, Owens TG, Doyle JJ (2012). Anatomical, biochemical, and photosynthetic responses to recent allopolyploidy in *Glycine dolichocarpa* (*Fabaceae*). Am J Bot 99:55–67.

Crumpton-Taylor M, Grandison S, Png KM, Bushby AJ, Smith AM (2012). Control of starch granule numbers in *Arabidopsis* chloroplasts. Plant Physiol 158:905–16.

Cruz-Orive LM, Howard CV (1991). Estimating the length of a bounded curve in three dimensions using total vertical projections. J Microsc-Oxford 163:101–13.

Czerski J (1968). Gasometric method of water deficit measurement in leaves. Biol Plantarum 10:275–83.

Demmig-Adams B, Muller O, Stewart JJ, Cohu CM, Adams WW (2015). Chloroplast thylakoid structure in evergreen leaves employing strong thermal energy dissipation. J Photoch Photobio B 152:357–66.

Dengler NG, MacKay LB (1975). The leaf anatomy of beech, *Fagus grandifolia*. Can J Botany 53:2202–11.

Dinkins R, Reddy SM, Leng M, Collins GB (2001). Overexpression of the *Arabidopsis* thaliana MinD1 gene alters chloroplast size and number in transgenic tobacco plants. Planta 214:180–8.

Dornhoff GM, Shibles R (1976). Leaf morphology and anatomy in relation to CO_2-exchange rate of soybean leaves. Crop Sci 16:377–81.

Eames AJ, MacDaniels LH (1925). An Introduction to Plant Anatomy. McGraw-Hill Book Co. Inc., New York, pp. 321–42.

Edwards SJ, Isaac S, Collin HA, Clipson NJ (1999). Stereological analysis of celery leaves infected by *Septoria apiicola*. Mycol Res 103:750–6.

Eleftheriou E (1987). A comparative study of the leaf anatomy of olive trees growing in the city and the country. Environ Exp Bot 27:105–17.

Ellis J, Leech R (1985). Cell size and chloroplast size in relation to chloroplast replication in light-grown wheat leaves. Planta 165:120–5.

El-Sharkawy MA, Hesketh J (1965). Photosynthesis among species in relation to characteristics of leaf anatomy and CO_2 diffusion resistances. Crop Sci 5: 517–21.

El-Sharkawy MA (2009). Pioneering research on C_4 leaf anatomical, physiological, and agronomic characteristics of tropical monocot and dicot plant species: Implications for crop water relations and productivity in comparison to C_3 cropping systems. Photosynthetica 47:163-83.

Fagerberg W (1983). A quantitative study of daily variation in the cellular ultrastructure of palisade chlorenchyma from sunflower leaves. Ann Bot-London 52:117–26.

Fagerberg WR, Bornman JF (1997). Ultraviolet-B radiation causes shade-type ultrastructural changes in *Brassica napus*. Physiol Plantarum 101:833–44.

Flood PJ, Kruijer W, Schnabel SK, van der Schoor R, Jalink H, Snel JFH, Harbinson J, Aarts MGM (2016). Phenomics for photosynthesis, growth and reflectance in Arabidopsis thaliana reveals circadian and long-term fluctuations in heritability. Plant Methods 12:14.

Gabarayeva NI, Grigorjeva VV (2002). Exine development in *Stangeria eriopus* (*Stangeriaceae*): ultrastructure and substructure, sporopollenin accumulation, the equivocal character of the aperture, and stereology of microspore organelles. Rev Palaeobot Palyno 122: 185–218.

Gamalei YuV, Kulikov GV (1978). Razvitie khlorenkhimy lista. [Development of leaf chlorenchyma.]. Nauka, Leningrad.

Gao H, Sage TL, Osteryoung KW (2006). FZL, an FZO-like protein in plants, is a determinant of thylakoid and chloroplast morphology. P Natl Acad Sci-Biol 103: 6759–64.

Gopi R, Jaleel CA, Panneerselvam R (2008). Leaf anatomical responses of *Amorphophallus campanulatus* to triazoles fungicides. Eurasia J Biosci 2, 46-52.

Gowland A, Briarty LG, Davey MR (1987). Tobacco leaf structure-an analytical problem. Acta Stereol 6:497–502.

Gregoriou K, Pontikis K, Vemmos S (2007). Effects of reduced irradiance on leaf morphology, photosynthetic capacity, and fruit yield in olive (*Olea europaea* L.). Photosynthetica 45:172–81.

Griffin KL, Anderson OR, Gastrich MD, Lewis JD, Lin G, Schuster W, Seemann JR, Tissue DT, Turnbull MH, Whitehead D (2001). Plant growth in elevated CO_2 alters mitochondrial number and chloroplast fine structure. P Natl Acad Sci-Biol 98:2473–8.

Gundersen HJG, Jensen E (1987). The efficiency of systematic sampling in stereology and its prediction. J Microsc-Oxford 147:229–63.

Gundersen HJG (1986). Stereology of arbitrary particles - a review of unbiased number and size estimators and the presentation of some new ones, in memory of Thompson,William, R. J Microsc-Oxford 143:3–45.

Hajibagheri M, Hall J, Flowers T (1984). Stereological analysis of leaf cells of the halophyte *Suaeda maritima* (L.) Dum. J Exp Bot 35:1547–57.

Hayashida A, Takechi K, Sugiyama M, Kubo M, Itoh R, Takio S, Fujita T, Hiwatashi Y, Hasebe M, Takano H (2005). Isolation of mutant lines with decreased numbers of chloroplasts per cell from a tagged mutant library of the moss *Physcomitrella patens*. Plant Biol 7:300–6.

Holá D, Kutík J, Kočová M, Rothová O (2008). Low-temperature induced changes in the ultrastructure of maize mesophyll chloroplasts strongly depend on the chilling pattern/intensity and considerably differ among inbred and hybrid genotypes. Photosynthetica 46:329–38.

Howard CV, Reed MG (1998). Unbiased stereology: three-dimensional measurement in microscopy. Springer, New York.

Howard CV, Sandau K (1992) Measuring the surface area of a cell by the method of the spatial grid with a CSLM – a demonstration. J Microsc 165: 183-88.

Howard V, Reid S, Baddeley A, Boyde A (1985). Unbiased estimation of particle density in the tandem scanning reflected light microscope. J Microsc-Oxford 138:203–12.

Ivanova L, P'yankov V (2002). Structural adaptation of the leaf mesophyll to shading. Russian Journal of Plant Physiol 49:419–31.

James SA, Smith WK, Vogelmann TC (1999). Ontogenetic differences in mesophyll structure and chlorophyll distribution in *Eucalyptus globulus* ssp. *globulus* (*Myrtaceae*). Am J Bot 86:198–207.

Jellings AJ, Leech RM (1984). Anatomical variation in first leaves of nine *Triticum* genotypes, and its relationship to photosynthetic capacity. New Phytol 96:371–82.

Jin B, Wang L, Wang J, Jiang K-Z, Wang Y, Jiang X-X, Ni C-Y, Wang Y-L, Teng N-J (2011). The effect of experimental warming on leaf functional traits, leaf structure and leaf biochemistry in *Arabidopsis thaliana*. BMC Plant Biol 11:35.

Juurola E, Aalto T, Thum T, Vesala T, Hari P (2005). Temperature dependence of leaf-level CO_2 fixation: revising biochemical coefficients through analysis of leaf three-dimensional structure. New Phytol 166: 205-15.

Khramtsova E, Kiseleva I, Lyubomudrova E, Malkova N (2003). Optimization of the leaf mesophyll structure in alloploid and diploid wheat species. Russian journal of Plant Physiol 50:19–27.

Kivimäenpää M, Sutinen S, Karlsson PE, Selldén G (2003). Cell structural changes in the needles of Norway spruce exposed to long-term ozone and drought. Ann Bot-London 92:779-93.

Kivimäenpää M, Riikonen J, Sutinen S, Holopainen T (2014). Cell structural changes in the mesophyll of Norway spruce needles by elevated ozone and elevated temperature in open-field exposure during cold acclimation. Tree Physiol 34:389–403.

Klich MG (2000). Leaf variations in *Elaeagnus angustifolia* related to environmental heterogeneity. Environ Exp Bot 44:171–83.

Konoplyova A, Petropoulou Y, Yiotis C, Psaras GK, Manetas Y (2008). The fine structure and photosynthetic cost of structural leaf variegation. Flora-Morphology, Distribution, Functional Ecology of Plants 203:653–62.

Kubínová L (1987). Application of stereological methods to the anatomy of the leaf blade of barley. Acta Stereol 6:99–104.

Kubínová L (1989a). Stereological analysis of the leaf of barley. Acta Stereol 8:19–26.

Kubínová L (1989b). Effect of light intensity on anatomical structure of the leaf blade of barley: Stereological analysis. Acta Stereol 8:389–94.

Kubínová L (1991). Stomata and mesophyll characteristics of barley leaf as affected by light: stereological analysis. J Exp Bot 42:995–1001.

Kubínová L (1993). Recent stereological methods for the measurement of leaf anatomical characteristics: estimation of volume density, volume and surface area. J Exp Bot 44:165–73.

Kubínová L (1994). Recent stereological methods for measuring leaf anatomical characteristics: estimation of the number and sizes of stomata and mesophyll cells. J Exp Bot 45:119–27.

Kubínová L (1998). Stereology in plant anatomy: application of recent stereological principles to evalution of plant cells. Fol Anat 26 (Suppl.1).:1–7.

Kubínová L, Janáček J (1998). Estimating surface area by the isotropic fakir method from thick slices cut in an arbitrary direction. J Microsc-Oxford 191:201–11.

Kubínová L, Janáček J (2001). Confocal microscopy and stereology: Estimating volume, number, surface area and length by virtual test probes applied to three-dimensional images. Microsc Res Techniq 53:425–35.

Kubínová L, Janáček J (2015). Confocal stereology: an efficient tool for measurement of microscopic structures. Cell Tissue Res 360:13–28.

Kubínová L, Janáček J, Albrechtová J, Karen P (2005). Stereological and digital methods for estimating geometrical characteristics of biological structures using confocal microscopy. In: Evangelista V, Barsanti L, Passarelli V, Gualtieri P (eds). From Cells to Proteins: Imaging Nature across Dimensions. Springer, pp 271–321.

Kubínová L, Janáček J, Guilak F, Opatrný Z (1999). Comparison of several digital and stereological methods for estimating surface area and volume of cells studied by confocal microscopy. Cytometry 36:85–95.

Kubínová L, Janáček J, Karen P, Radochová B, Difato F, Krekule I (2004). Confocal stereology and image analysis: methods for estimating geometrical characteristics of cells and tissues from three-dimensional confocal images. Physiol Res 53:S47-56.

Kubínová L, Janáček J, Krekule I (2002). Stereological methods for estimating geometrical parameters of microscopical structure studied by three-dimensional microscopical techniques. In: Diaspro A (ed). Confocal and Two-photon Microscopy. Wiley-Liss, New York, pp 299–332.

Kubínová L, Kutík J (2007). Surface density and volume density measurements of chloroplast thylakoids in maize (*Zea mays* L.) under chilling conditions. Photosynthetica 45:481–8.

Kubínová Z, Janáček J, Lhotáková Z, Kubínová L, Albrechtová J (2014). Unbiased estimation of chloroplast number in mesophyll cells: advantage of a genuine three-dimensional approach. J Exp Bot 65:609–20.

Kukkola E, Rautio P, Huttunen S (2005). Long-term symptoms due to metal and acid precipitation treatments in Scots pine (*Pinus sylvestris*). needles in the subarctic. Arct Antarct Alp Res 37:68–74.

Kutík J, Nátr L, Demmers-Derks H, Lawlor DW (1995). Chloroplast ultrastructure of sugar beet (*Beta vulgaris* L.) cultivated in normal and elevated CO_2 concentrations with two contrasted nitrogen supplies. J Exp Bot 46:1797–802.

Kutík J, Šesták Z, Volfová A (1984) Ontogenetic changes in the internal limitations to bean-leaf photosynthesis. VIII: Primary leaf blade characteristics and chloroplast number, size and ultrastructure. Photosynthetica 18:1–8.

Lamppa GK, Elliot LV, Bendich AJ (1980). Changes in chloroplast number during pea leaf development. Planta 148:437–43.

Lepeduš H, Cesar V, Ljubesic N (2001). Chloroplast ultrastructure and chlorophyll levels in vegetative buds and needles of Norway spruce (*Picea abies* L. Karst.). Period Biol 103(1): 61-5.

Lhotáková Z, Albrechtová J, Janáček J, Kubínová L (2008). Advantages and pitfalls of using free-hand sections of frozen needles for three-dimensional analysis of mesophyll by stereology and confocal microscopy. J Microsc-Oxford 232:56–63.

Lhotáková Z, Urban O, Dubánková M, Cvikrová M, Tomášková I, Kubínová L, Zvára K, Marek MV, Albrechtová J (2012). The impact of long-term CO_2 enrichment on sun and shade needles of Norway spruce (*Picea abies*).: Photosynthetic performance, needle anatomy and phenolics accumulation. Plant Sci 188:60–70.

Lieckfeldt E (1989). Importance of leaf anatomy for characterization of primary leaf photosynthetic efficiency in different genotypes of wheat (*Triticum*). Photosynthetica 23:63–70.

Liu Y, Dengler NG (1994). Bundle sheath and mesophyll cell differentiation in the C_4 dicotyledon *Atriplex rosea*: quantitative ultrastructure. Can J Botany 72:644–57.

Longstreth DJ, Bolaños JA, Goddard RH (1985). Photosynthetic rate and mesophyll surface area in expanding leaves of *Alternanthera philoxeroides* grown at two light levels. Am J Bot 72:14–9.

Lukjanova A, Mandre M, Saarman G (2013). Impact of alkalisation of the soil on the anatomy of Norway spruce (*Picea abies*) needles. Water Air Soil Poll 224:1620.

Luković J (2006). Stereological analysis of the flag leaf of some *Triticum* L. species. Cereal Res Commun 34: 1005–12.

Luković J, Zorić L, Piperac J, Nagl N, Karanović D, Kekić SM, Milić D (2016). The analysis of petiole histological traits through an evaluation of water deficit tolerance of sugar beet genotypes. Sugar Tech 18:160–7.

Luković J, Kraljević-Balalić M, Vujičić D (2001). Characteristics of the flag leaf vascular tissue in two *Triticum* species. Cereal Res Commun 29: 151–8.

Maksymowych R (1959). Quantitative analysis of leaf development in *Xanthium pensylvanicum*. Am J Bot 46:635–44.

Maksymowych R (1963). Cell division and cell elongation in leaf development of *Xanthium pensylvanicum*. Am J Bot 50:891–901.

Marin M, Koko V, Duletić-Laušević S, Marin PD (2008). Micromorphology of trichomes of Thymus malyi (Lamiaceae). J Microsc-Oxford 232:406–9.

Marin M, Koko V, Duletić-Laušević S, Marin PD, Rančić D, Dajić-Stevanović Z (2006). Glandular trichomes on the leaves of Rosmarinus officinalis: Morphology, stereology and histochemistry. S Afr J Bot 72:378–82.

Marrison JL, Rutherford SM, Robertson EJ, Lister C, Dean C, Leech RM (1999). The distinctive roles of five different ARC genes in the chloroplast division process in *Arabidopsis*. Plant J 18:651–62.

Mašková P, Radochová B, Lhotáková Z, Michálek J, Lipavská H (2017). Nonstructural carbohydrate-balance response to long-term elevated CO_2 exposure in European beech and Norway spruce mixed cultures: biochemical and ultrastructural view. Can J Forest Res 47:1488-94.

Maslova T, Mamushina N, Sherstneva O, Bubolo L, Zubkova E (2009). Seasonal structural and functional changes in the photosynthetic apparatus of evergreen conifers. Russ J Plant Phys 56:607–15.

Meyer FJ (1923). Das trophische Parenchym. A. Assimilationsgewebe. In: Handbuch der Pflanzenanatomie. Allgemeiner Teil: Histologie (Linsbauer K, ed.), 2nd edn. Berlin, Bd. 5, 1. Hälfte: pp 1–87.

Meyer R, Yuan J, Afzal J, Iqbal M, Zhu M, Garvey G, Lightfoot DA (2006). Identification of Gsr1 in *Arabidopsis thaliana*: a locus inferred to regulate gene expression in response to exogenous glutamine. Euphytica 151:291–302.

Miroslavov EA, Voznesenskaya EV, Bubolo LS (1996). Chloroplast structure in northern plants in relation to chloroplast adaptation to arctic conditions. Russian Journal of Plant Physiol 43:325–30.

Miyazawa S, Terashima I (2001). Slow development of leaf photosynthesis in an evergreen broad-leaved tree, *Castanopsis sieboldii*: relationships between leaf anatomical characteristics and photosynthetic rate. Plant Cell Environ 24:279–91.

Molin WT, Meyers SP, Baer GR, Schrader LE (1982). Ploidy effects in isogenic populations of *Alfalfa* II. Photosynthesis, chloroplast number, ribulose-1,5-bisphosphate carboxylase, chlorophyll, and DNA in protoplasts. Plant Physiol 70:1710-4.

Morris P, Thain J (1983). Improved methods for the measurement of total cell surface area in leaf mesophyll tissue. J Exp Bot 34:95–8.

Morrod R (1974). A new method for measuring the permeability of plant cell membranes using epidermis-free leaf discs. J Exp Bot 25:521–33.

Moura BB, Alves ES (2014) Climatic factors influence leaf structure and thereby affect the ozone sensitivity of *Ipomoea nil* 'Scarlet O'Hara.' Environ Pollut 194:11–6.

Mozafari J, Wolyn D, Ali-Khan S (1997). Chromosome doubling via tuber disc culture in dihaploid potato as determined by confocal microscopy. Plant Cell Rep 16:329–33.

Nátr L (1988). Quantitative anatomy of plants. Acta U Carol Biol 31:5–13.

Newman E (1966). A method of estimating the total length of root in a sample. J Appl Ecol 139–45.

Niinemets U (2007). Photosynthesis and resource distribution through plant canopies. Plant Cell Environ 30:1052–71.

Nius E (1931). Untersuchungen über den Einfluß des Interzellularvolumens und der Öffnungsweite der Stomata auf die Luftwegigkeit der Laubblätter. Jb Wiss Bot 74:33–126.

Nobel PS, Zaragoza LJ, Smith WK (1975). Relation between mesophyll surface area, photosynthetic rate, and illumination level during development for leaves of *Plectranthus parviflorus* Henckel. Plant Physiol 55:1067–70.

Oguchi R, Hikosaka K, Hirose T (2003). Does the photosynthetic light-acclimation need change in leaf anatomy? Plant Cell Environ 26:505–12.

Oguchi R, Hikosaka K, Hirose T (2005). Leaf anatomy as a constraint for photosynthetic acclimation: differential responses in leaf anatomy to increasing growth irradiance among three deciduous trees. Plant Cell Environ 28: 916–27.

Oksanen E, Sober J, Karnosky D (2001). Impacts of elevated CO_2 and/or O_3 on leaf ultrastructure of aspen (*Populus tremuloides*). and birch (*Betula papyrifera*). in the Aspen FACE experiment. Environ Pollut 115: 437–46.

Paolillo Jr DJ, Falk RH (1966). The ultrastructure of grana in mesophyll plastids of Zea mays. Am J Bot 173–80.

Parker M, Ford M (1982). The structure of the mesophyll of flag leaves in three *Triticum* species. Ann Bot-London 49:165–76.

Parkhurst DF (1982). Stereological methods for measuring internal leaf structure variables. Am J Bot 69:31–9.

Pawley JB (1995). Handbook of biological confocal microscopy, 2nd edn. Plenum Press, New York.

Pawley JB (2006). Handbook of Biological Confocal Microscopy, 3rd edn. Springer US, Boston, MA.

Pazourek J (1966). Anatomical gradients. Acta U Carol Biol Suppl. 1/2:19–25.

Pazourek J (1969). Anatomical gradients of stomatal apparatus in leaves of *Hordeum distichon* L. Adv Front Pl Sci 23:9–18.

Pazourek J (1975). Transversale anatomische Gradienten in der Kartoffelknolle. Biol Plantarum 17:263–7.

Pazourek J (1977). The volumes of anatomical components in leaves of *Typha angustifolia* L. and *Typha latifolia* L. Biol Plantarum 19:129–35.

Pazourek J (1988). The evolution of quantitative plant anatomy. Acta Univ Carol, Biol 31:15–25.

Pazourek J, Nátr L (1981). Changes in the anatomical structure of the first two leaves of barley caused by the absence of nitrogen or phosphorus in the nutrient medium. Biol Plantarum 23:296–301.

Pazourek J, Nátr L, Marková L (1987). Genotype differences in the proportion of different tissues in the leaves of spring barley. Biol Plantarum 29:54–62.

Pechová R, Kutík J, Holá D, Kočová M, Haisel D, Vičánková A (2003). The ultrastructure of chloroplasts, content of photosynthetic pigments, and photochemical activity of maize (*Zea mays* L.) as influenced by different concentrations of the herbicide amitrole. Photosynthetica 41:127–36.

Perktold A, Zellnig G, Guttenberger H, Gailhofer M (1998). 3D reconstruction of chloroplasts and their ultrastructure using ultra-thin-serial-sections. Phyton-Horn- 38: 159–66.

Peterson DA (1999). Quantitative histology using confocal microscopy: implementation of unbiased stereology procedures. Methods 18:493–507.

Possingham JV, Saurer W (1969). Changes in chloroplast number per cell during leaf development in spinach. Planta 86:186–94.

Possingham JV, Smith JW (1972). Factors affecting chloroplast replication in spinach. J Exp Bot 23:1050–9.

Pritchard S, Peterson C, Prior S, Rogers H (1997). Elevated atmospheric CO_2 differentially affects needle chloroplast ultrastructure and phloem anatomy in *Pinus palustris*: interactions with soil resource availa-bility. Plant Cell Environ 20:461–71.

Pyke KA, Leech RM (1991). Rapid image analysis screening procedure for identifying chloroplast number mutants in mesophyll cells of *Arabidopsis thaliana* (L.) Heynh. Plant Physiol 96:1193–5.

Razem FA, Davis AR (1999). Anatomical and ultrastructural changes of the floral nectary of *Pisum sativum* L. during flower development. Protoplasma 206:57–72.

Ren B, Liu W, Zhang J, Dong S, Liu P, Zhao B (2017). Effects of plant density on the photosynthetic and chloroplast characteristics of maize under high-yielding conditions. Sci. Nat. 104:12.

Rhizopoulou S, Psaras GK (2003). Development and structure of drought-tolerant leaves of the mediterranean shrub *Capparis spinosa* L. Ann Bot-London 92:377–83.

Riikonen J, Oksanen E, Peltonen P, Holopainen T, Vapaavuori E (2003). Seasonal variation in physiological characteristics of two silver birch clones in the field. Can J Forest Res 33:2164–76.

Salisbury E (1928). On the causes and ecological significance of stomatal frequency, with special reference to the woodland flora. Philos T R Soc Lon B 216:1–65.

Sam O, Ramírez C, Coronado M, Testillano P, Risueño M del C (2003). Changes in tomato leaves induced by NaCl stress: leaf organization and cell ultrastructure. Biol Plantarum 47:361–6.

Sant F (1969). A comparison of the morphology and anatomy of seedling leaves of *Lolium multiflorum* Lam. and *L. perenne* L. Ann Bot-London 33:303–13.

Sasahara T (1971). Genetic Variations in Cell and Tissue Forms in Relation to Plant Growth.: II. Total Cell Surface Area in the Palisade Parenchyma and Total Cell Surface Area: Total Nitrogen Content Ratio in Relation to Photosynthetic Activity in Brassica. Jpn J Breed 21:61–8.

Sasahara T (1982). Influence of genome on leaf anatomy of *Triticum* and *Aegilops*. Ann Bot-London 50:491–7.

Sawidis TH, Eleftheriou EP, Tsekos I (1989). The floral nectaries of *Hibiscus rosa-sinensis* in. A morphometric and ultrastructural approach. Nord J Bot 9:63–71.

Schmitt V, Kußmaul A, Wild A (1999). Interaction of elevated CO_2 and ozone concentrations and irrigation regimes on leaf anatomy and carbohydrate status of young oak (*Quercus petraea*) trees. Z Naturforsch C 54:812–23.

Simon UK, Polanschütz LM, Koffler BE, Zechmann B (2013). High resolution imaging of temporal and spatial changes of subcellular ascorbate, glutathione and H_2O_2 distribution during *Botrytis cinerea* infection in *Arabidopsis*. PLoS One 8:e65811.

Slaton MR, Smith WK (2002). Mesophyll architecture and cell exposure to intercellular air space in alpine, desert, and forest species. Int J Plant Sci 163:937–48.

Slavík B (1963). The distribution pattern of transpiration rate, water saturation deficit, stomata number and size, photosynthetic and respiration rate in the area of the tobacco leaf blade. Biol Plantarum 5:143–53.

Smith H (1970). Changes in plastid ribosomal-RNA and enzymes during the growth of barley leaves in darkness. Phytochemistry 9:965–75.

Smith JAC, Heuer S (1981). Determination of the volume of intercellular spaces in leaves and some values for CAM plants. Ann Bot-London 48:915–7.

Soper K, Mitchell K (1956). The developmental anatomy of perennial ryegrass (*Lolium perenne* L.) New Zeal J Sci 37:484–504.

Steer MW (1981). Understanding cell structure. Cambridge University Press, Cambridge.

Sterio D (1984). The unbiased estimation of number and sizes of arbitrary particles using the disector. J Microsc-Oxford 134:127–36.

Stettler M, Eicke S, Mettler T, Messerli G, Hörtensteiner S, Zeeman SC (2009). Blocking the metabolism of starch breakdown products in *Arabidopsis* leaves triggers chloroplast degradation. Mol Plant 2:1233–46.

Sung F, Chen J (1989). Changes in photosynthesis and other chloroplast traits in lanceolate leaflet isoline of soybean. Plant Physiol 90:773–7.

Teng N, Wang J, Chen T, Wu X, Wang Y, Lin J (2006). Elevated CO_2 induces physiological, biochemical and structural changes in leaves of *Arabidopsis thaliana*. New Phytol 172:92–103.

Thain J (1983). Curvature Correction Factors in the Measurement of Cell Surface Areas in Plant Tissues 1. J Exp Bot 34:87–94.

Théroux-Rancourt G, Earles JM, Gilbert ME, Zwieniecki MA, Boyce CK, McElrone AJ, Brodersen CR (2017). The bias of a two-dimensional view: comparing two-dimensional and three-dimensional mesophyll surface area estimates using noninvasive imaging. New Phytol 215:1609–22.

Tichá I, Čatský J (1977). Ontogenetic changes in the internal limitations to bean leaf photosynthesis, 3: Leaf mesophyll structure and intracellular conductance for carbon dioxide transfer. Photosynthetica 11:361-6.

Turrell FM (1934). Leaf surface of a twenty-one-year old catalpa tree. Proc Iowa Acad Sci 41:79–84.

Turrell FM (1936). The area of the internal exposed surface of dicotyledon leaves. Am J Bot 23:255–64.

Tymms MJ, Scott NS, Possingham JV (1983). DNA content of *Beta vulgaris* chloroplasts during leaf cell expansion. Plant Physiol 71:785–8.

Unger F (1854). Beiträge zur Physiologie der Pflanzen. Sitzber d Wien Akad d Wiss 12:367.

Vassilyev AE (2000). Quantitative ultrastructural data of secretory duct epithelial cells in *Rhus toxicodendron*. Int J Plant Sci 161:615–30.

Vičánková A, Kutík J (2005). Chloroplast ultrastructural development in vascular bundle sheath cells of two different maize (*Zea mays* L.) genotypes. Plant Soil Environ 51:491–5.

Wang X, Anderson OR, Griffin KL (2004). Chloroplast numbers, mitochondrion numbers and carbon assimilation physiology of *Nicotiana sylvestris* as affected by CO_2 concentration. Environ Exp Bot 51:21–31.

Wehrmeyer W, Röbbelen G (1965). Räumliche Aspekte zur Membranschichtung in den Chloroplasten einer *Arabidopsis*-Mutante unter Auswertung von Serienschnitten. Planta 64:312–29.

Weibel ER (1979). Stereological methods, Vol 1. Practical methods for biological morphometry. Academic Press, London.

Wheeler W, Fagerberg W (2000). Exposure to low levels of photosynthetically active radiation induces rapid increases in palisade cell chloroplast volume and thylakoid surface area in sunflower (*Helianthus annuus* L.) Protoplasma 212:38–45.

Wild A, Wolf G (1980). The effect of different light intensities on the frequency and size of stomata, the size of cells, the number, size and chlorophyll content of chloroplasts in the mesophyll and the guard cells during the ontogeny of primary leaves of *Sinapis alba*. Z Pflanzenphysiol 97:325–42.

Wilson D, Cooper J (1967). Assimilation of *Lolium* in relation to leaf mesophyll. Nature 214:989–92.

Wulff A, Ahonen J, Kärenlampi L (1996). Cell ultrastructural evidence of accelerated ageing of Norway spruce needles in industrial areas. New Phytol 133:553–61.

Wylie RB (1949). Differences in foliar organization among leaves from four stations in the crown of an isolated tree (*Acer platanoides*). Proc Iowa Acad Sci 56:189–98.

Xu C-Y, Salih A, Ghannoum O, Tissue DT (2012). Leaf structural characteristics are less important than leaf chemical properties in determining the response of leaf mass per area and photosynthesis of *Eucalyptus saligna* to industrial-age changes in [CO_2] and temperature. J Exp Bot 63:5829–41.

Yamasaki T, Kudoh T, Kamimura Y, Katoh S (1996). A vertical gradient of the chloroplast abundance among leaves of *Chenopodium album*. Plant Cell Physiol 37: 43–8.

Yiotis C, Psaras GK (2011). *Dianthus caryophyllus* stems and *Zantedeschia aethiopica* petioles/pedicels show anatomical features indicating efficient photosynthesis. Flora-Morphology, Distribution, Functional Ecology of Plants 206:360–4.

Yu W, Liu Y, Song L, Jacobs DF, Du X, Ying Y, Shao Q, Wu J (2017). Effect of differential light quality on morphology, photosynthesis, and antioxidant enzyme activity in *Camptotheca acuminata* seedlings. J Plant Growth Regul 36:148–160.

Zechmann B, Müller M, Zellnig G (2003). Cytological modifications in zucchini yellow mosaic virus (ZYMV)-infected Styrian pumpkin plants. Arch Virol 148:1119–33.

Zellnig G, Zechmann B, Perktold A (2004). Morphological and quantitative data of plastids and mitochondria within drought-stressed spinach leaves. Protoplasma 223:221–7.

Zorić L, Luković J, Matić-Kekić S, Merkulov L (2011). Modified stereological method for analysis of compound leaves and an example of its application. J Biol Syst 19:617–27.

Zorić L, Mikić A, Ćupina B, Luković J, Krstić D, Antanasović S (2014). Digestibility-related histological attributes of vegetative organs of barrel medic (*Medicago truncatula* Gaertn.) cultivars 3:257–64.